The Final Report

Title: Thermographic tools for quality control and damage assessment of Z-pinned composite space structures

Principal Investigator:

Rhys Jones, Ph.D., Professor
Department of Mechanical Engineering
Monash University
P.O. Box 31
Monash, Victoria 3800
Australia
Telephone: +61-3-9905-3809
Facsimile: +61-3-9905-1825
E-mail: rhys.jones@eng.monash.edu.au

Contract Number: FA5209-04-P-0614

AOARD Reference Number: AOARD-44064

AOARD Program Manager: JP Singh, Ph.D

Period of Performance: 21-Sep-04 – 21-Nov-05

Submission Date:

Report Documentation Page

Form Approved
OMB No. 0704-0188

1. REPORT DATE	2. REPORT TYPE	3. DATES COVERED
25 JAN 2007	**FInal**	**21-10-2004 to 11-01-2007**

4. TITLE AND SUBTITLE
Thermographic tools for quality control and damage assessment of Z-pinned composite space structures

5a. CONTRACT NUMBER
FA520904P0614

5b. GRANT NUMBER

5c. PROGRAM ELEMENT NUMBER

6. AUTHOR(S)
Rhys Jones

5d. PROJECT NUMBER

5e. TASK NUMBER

5f. WORK UNIT NUMBER

7. PERFORMING ORGANIZATION NAME(S) AND ADDRESS(ES)
Monash University,P.O. Box 31,Monash Victoria 3800,Australia,AU,3800

8. PERFORMING ORGANIZATION REPORT NUMBER
N/A

9. SPONSORING/MONITORING AGENCY NAME(S) AND ADDRESS(ES)
AOARD, UNIT 45002, APO, AP, 96337-5002

10. SPONSOR/MONITOR'S ACRONYM(S)
AOARD

11. SPONSOR/MONITOR'S REPORT NUMBER(S)
AOARD-044064

12. DISTRIBUTION/AVAILABILITY STATEMENT
Approved for public release; distribution unlimited

13. SUPPLEMENTARY NOTES

14. ABSTRACT
It would appear that lockin thermography could (just) assess the presence and distribution of the z pins in the composite structures. It was also possible to detect thickness variations specimens that were approximately 12 mm thick.

15. SUBJECT TERMS
Composite Structures, Damage Detection, Non-destructive Evaluation, Spacecraft Engineering

16. SECURITY CLASSIFICATION OF:			17. LIMITATION OF ABSTRACT	18. NUMBER OF PAGES	19a. NAME OF RESPONSIBLE PERSON
a. REPORT	b. ABSTRACT	c. THIS PAGE			
unclassified	**unclassified**	**unclassified**	**Same as Report (SAR)**	**84**	

AOARD 04-64: THERMOGRAPHIC INSPECTION USING LOCK-IN AND FLASH THERMOGRAPHY FOR SPACE VEHICLE STRUCTURES

Summary of Lockin Optical Thermography Results for Z-pinned Composite Specimens

Introduction

Lockin thermography in its present form was first developed in the early 1990's [1]. Busse [2] was perhaps the first to use this technique in its present form using a set of remote lamps as the thermal excitation source. Busse performed scans of carbon reinforced polymers using an infrared camera with a focal plane array. Busses experiment indeed showed that lockin thermography could indeed be used to interrogate subsurface features in composite structures. Since Busse's initial work a considerable amount of research has been conducted into the use of thermographic techniques to interrogate composite structures [3-5].

Something about Z-pinned structures

When a structure is periodically heated dispersive waves are induced near the surface of the structure. These thermal waves while technically not waves can be thought of as heavily damped waves. These thermal waves were first investigated by Fourier [6] and later by Angstrom [7]. These thermal waves with present day infra-red technology can be physically observed.

Consider a semi-infinite planner specimen periodically heated uniformly by a remote light source. The light source possesses an angular frequency of ω ($\omega=2\pi f$ where f is the frequency in hertz). In this situation the problem can be reduce to a one-dimensional case.

The equation describing the resulting temperature distribution over the plate can be represented by

$$T(z,t) = T_o e^{-z/\mu} \cos\left(\omega t - \frac{2\pi z}{\lambda_t}\right) \qquad (1)$$

Here z represents the thickness of the plate, λ_t represents the thermal wavelength in the plate, t represents the time and μ is the thermal diffusion length.

The thermal diffusion length can be expressed as

$$\mu = \sqrt{2k / \omega\rho C} = \sqrt{2\alpha / \omega} \tag{2}$$

Where k is the thermal conductivity of the plate, C is the specific heat, ρ is the density and α is the diffusivity of the plate. The thermal wavelength is related to the thermal diffusion length by $\lambda_t = 2\pi\mu$.

In equation 1 the phase angle $\phi(z)$ is directly related to the thickness of the material.

$$\phi(z) = \frac{2\pi z}{\lambda_t} = \frac{z}{\mu} \tag{3}$$

In reference to NDT applications high modulation frequencies can be used to interrogate only a small layer near the surface of the structure. Low modulation frequencies can be used to interrogate structures much deeper but require much longer acquisition times.

Lockin thermography utilizes a sinusoidal thermal stimulus. This stimulus can be introduced internally via the thermo-elastic effect or external stimulus such as a set of lamps. The use of lamps usually refers to optical lockin thermography. Lockin thermography can provide both amplitude and phase images. The phase in this instance refers to the measured phase difference between the lockin signal from the lamps and the thermal signal from the infrared camera. The phase image is particularly useful as it generally is invariant of non-uniform heating. This technique usually provides better depth information than does the pulse phase technique. This increased depth penetration results from only interrogating with one frequency at a time, unlike the pulse phase technique which excites multiple frequencies simultaneously. However, multiple measurements are required to scan the frequency spectrum to achieve the greatest phase contrasts.

A thermal impulse can induce a thermal wave into a structure. The term wave is not strictly correct but the heat impulse can be considered to be a heavily damped wave. The wave introduced into the structure quickly attenuates, thus measurements of phase can become difficult as the signal becomes weak after one to two periods. Measurement of the depth can be made using the magnitude of the wave form or the period. Typically the depth range is that of the diffusion length μ which is given by:

$$\mu = \sqrt{\frac{2k}{\omega\rho c}} \tag{4}$$

Where k is the thermal conductivity, ρ is the density, c is the specific heat and ω is the angular frequency.

In the case of phase measurements a depth range of up to two times the diffusion length can be achieved [8, 9]. In some of Busse's [10] earlier work he indicates a maximum penetration depth of 1.8μ.

For general image processing purposes the following equations maybe used to extract the phase, magnitude and average thermal images.

$$\phi = Tan^{-1}\frac{S_3 - S_1}{S_4 - S_2} \tag{5}$$

$$A = \sqrt{(S_3 - S_1)^2 + (S_4 - S_2)^2} \tag{6}$$

$$T = \frac{S_1 + S_2 + S_3 + S_4}{4} \tag{7}$$

Here S_1, S_2, S_3 and S_4 represent magnitudes at four equi-distant time intervals measured with reference to a sinusoidal lockin signal with zero phase [8].

Equations 5-7 provide a convenient method of evaluating the phase and amplitude images. However, in the present analysis another approach based on the Fourier transform (equation 8) has been used. The advantage of this approach means that more data can be analysed to minimise the influence of background noise.

$$F(u) = \frac{1}{N}\sum_{n=0}^{N-1} f(x)\exp\left(\frac{-j2\pi ux}{N}\right) = \mathrm{Re}(u) + j\,\mathrm{Im}(u) \tag{8}$$

$$\Phi(u) = \tan^{-1}\left(\frac{\mathrm{Im}(u)}{\mathrm{Re}(u)}\right) \tag{9}$$

Methodology

For the present investigation a JADE mid wavelength infrared (MWIR) radiometric system was used that includes a C9906 Detector with 320*240 elements (30μm pitch). The camera uses a $Hg_xCd_{1-x}Te$ (MCT) detector array with a spectral response within 3μm to 5μm. The detector array uses a Stirling cooler and is thermal sensitivity down to < 25mK. This camera possesses further functionality with adjustable frame rates in the range of 1Hz to 200Hz for a 320*240 image and up to 10 KHz for a 320*2 image.

The camera was set up to perform a single sided scan of the test subject as shown in Figure 1. Four 750 Watt lamps were used and their output controlled by a Hameg HM8131-2 function generator. The lamps were angled to provide even heating over the surface of the sample. The samples themselves were coated with RS 496-782 Matt black paint with an emissivity of 98%.

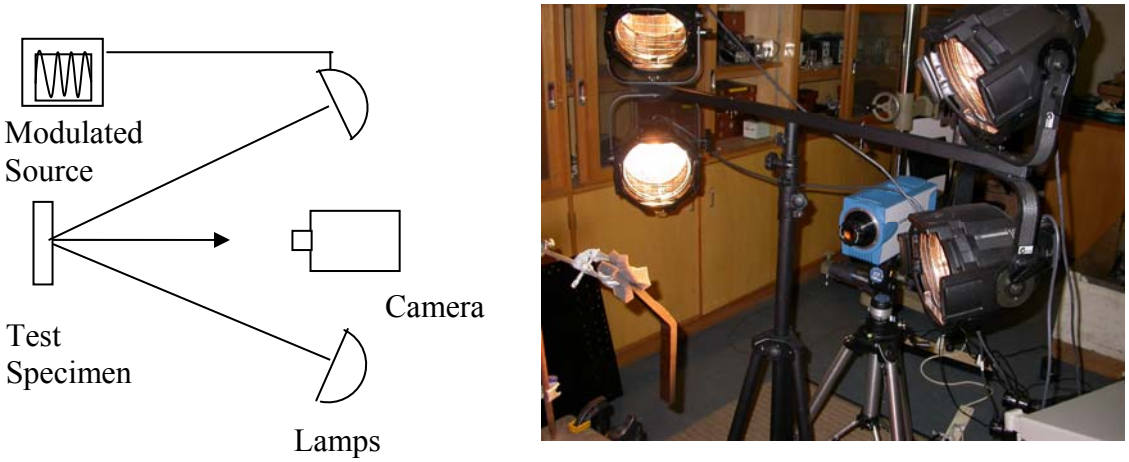

Figure 1 a) Schematic representation of the experimental setup b) Image of the actual experimental arrangement.

Three modulation frequencies were independently applied to each of the specimens investigated 0.5Hz, 0.05Hz and 0.005Hz. The voltage was controlled such that the maximum temperature of the specimens did not exceed 60 degrees Celsius. Each lamp was approximately outputting between 20-40% of its maximum potential output. The lamps themselves were positioned approximately 1 meter from the specimens surface. The infrared camera was positioned behind the lamps at a distance of approximately 1meter.

Three small 135 degree thin angled specimens, 5 135 degree wide angled specimens and 4 large flat specimens were tested. For each of these specimens three modulation frequencies as mention earlier were used to interrogate the front surface and then again on the reverse side of the specimens. Amplitude and phase images were obtained for all the samples tested.

Results

Sample: H166-A2

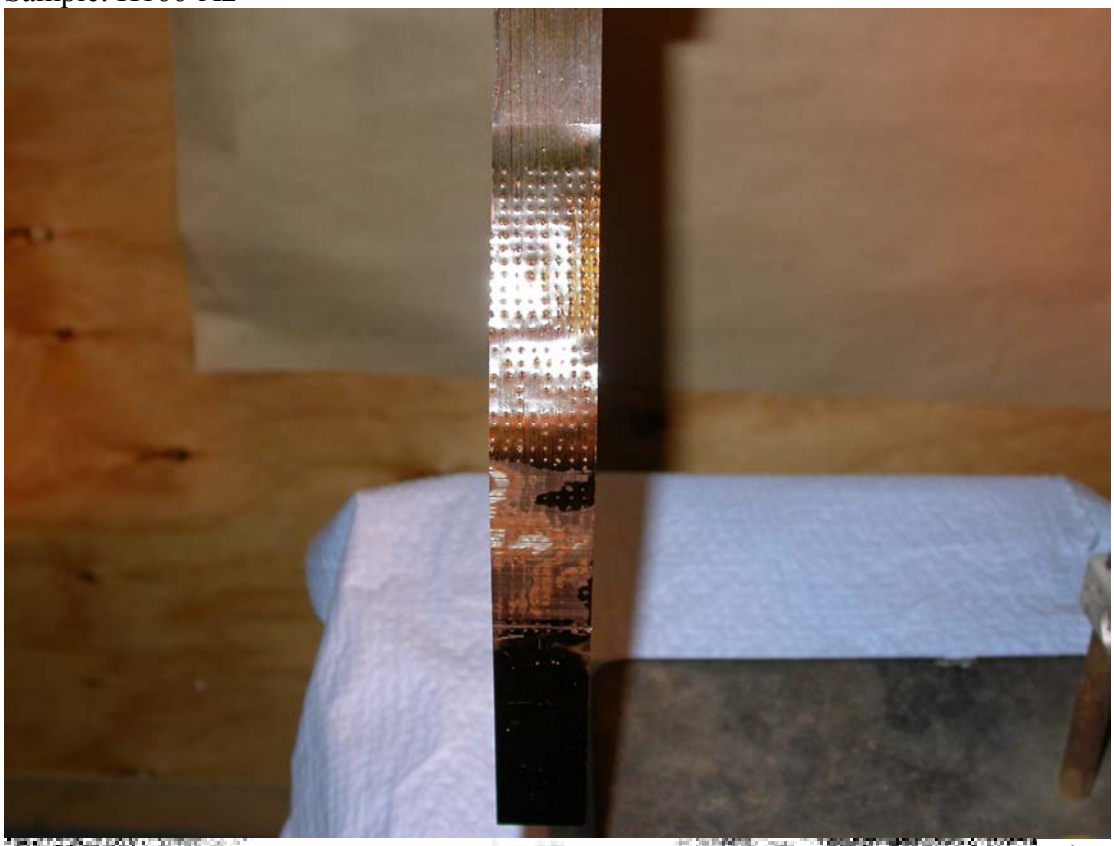

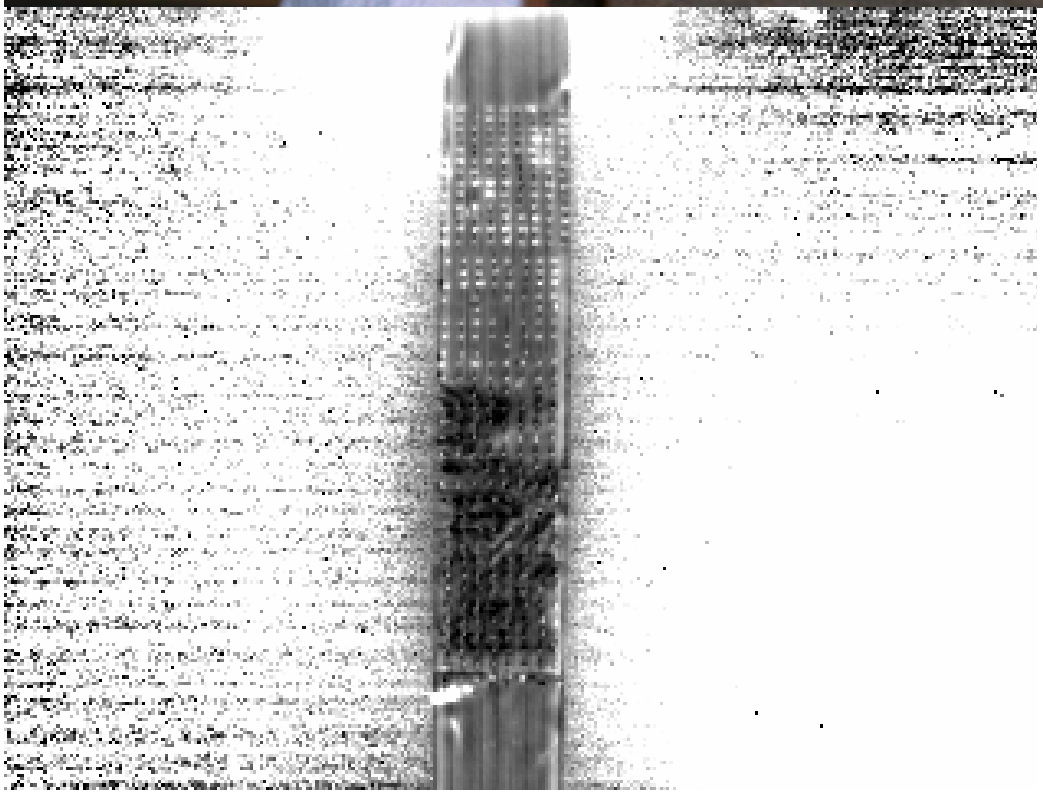

Phase
Frequency 0.5Hz
Periods 20

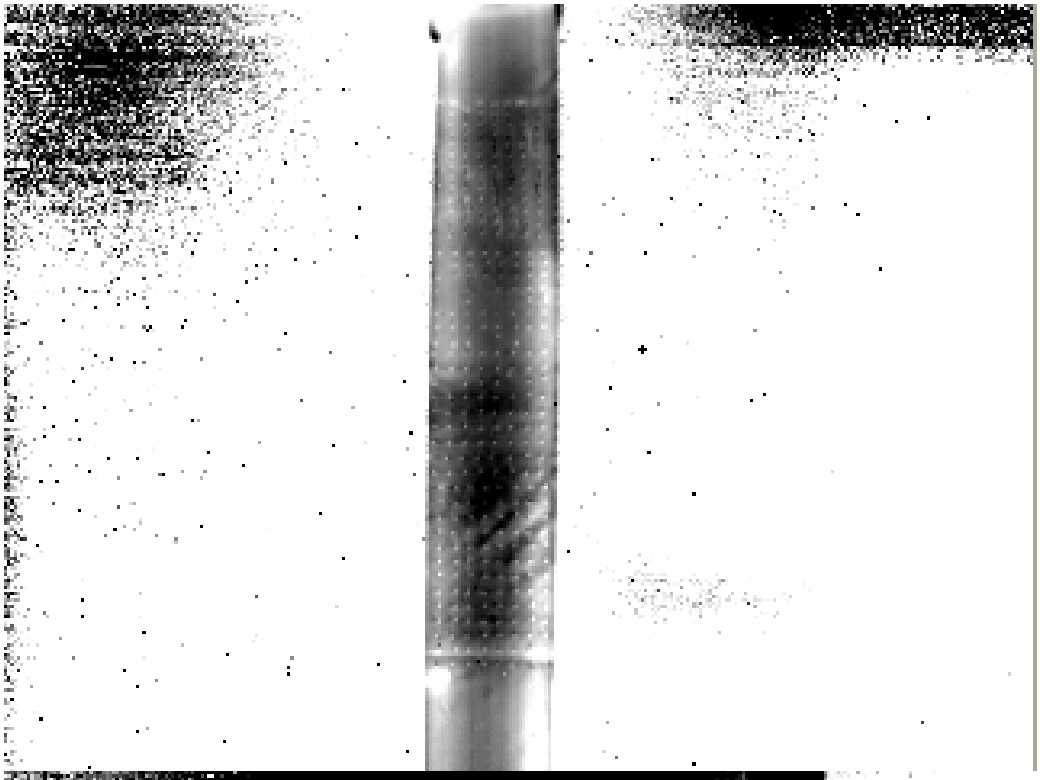

Phase
Frequency
0.05Hz
Periods 5

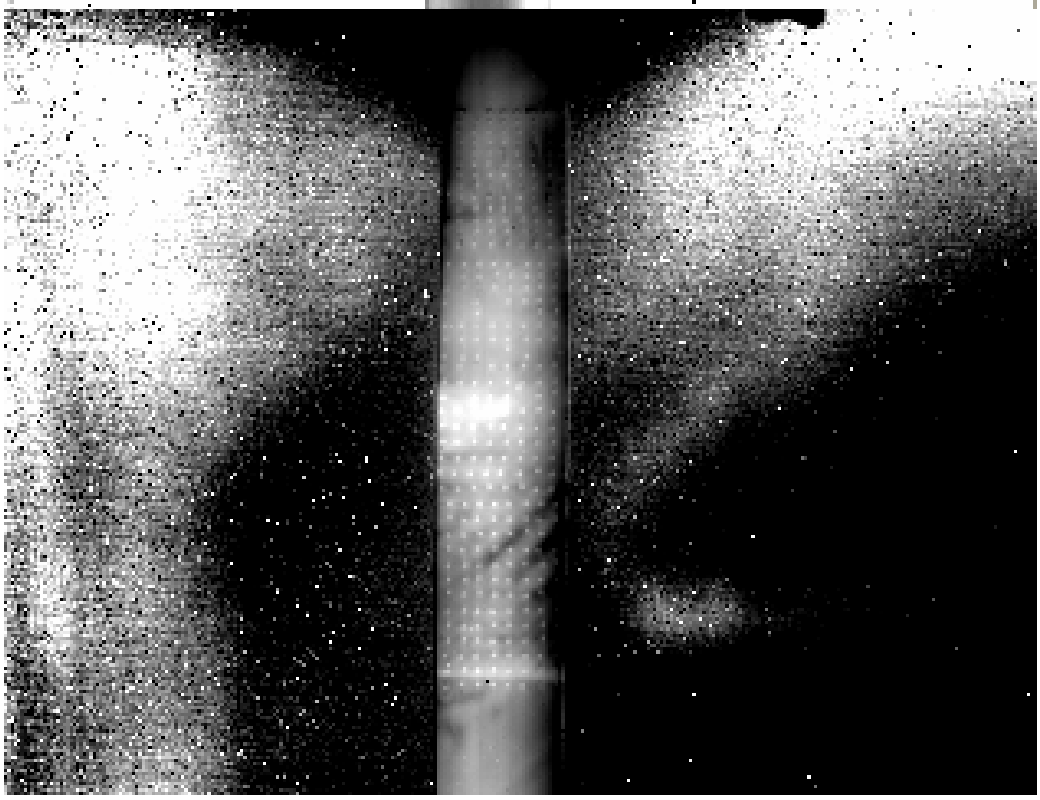

Phase
Frequency
0.005Hz
Periods 2

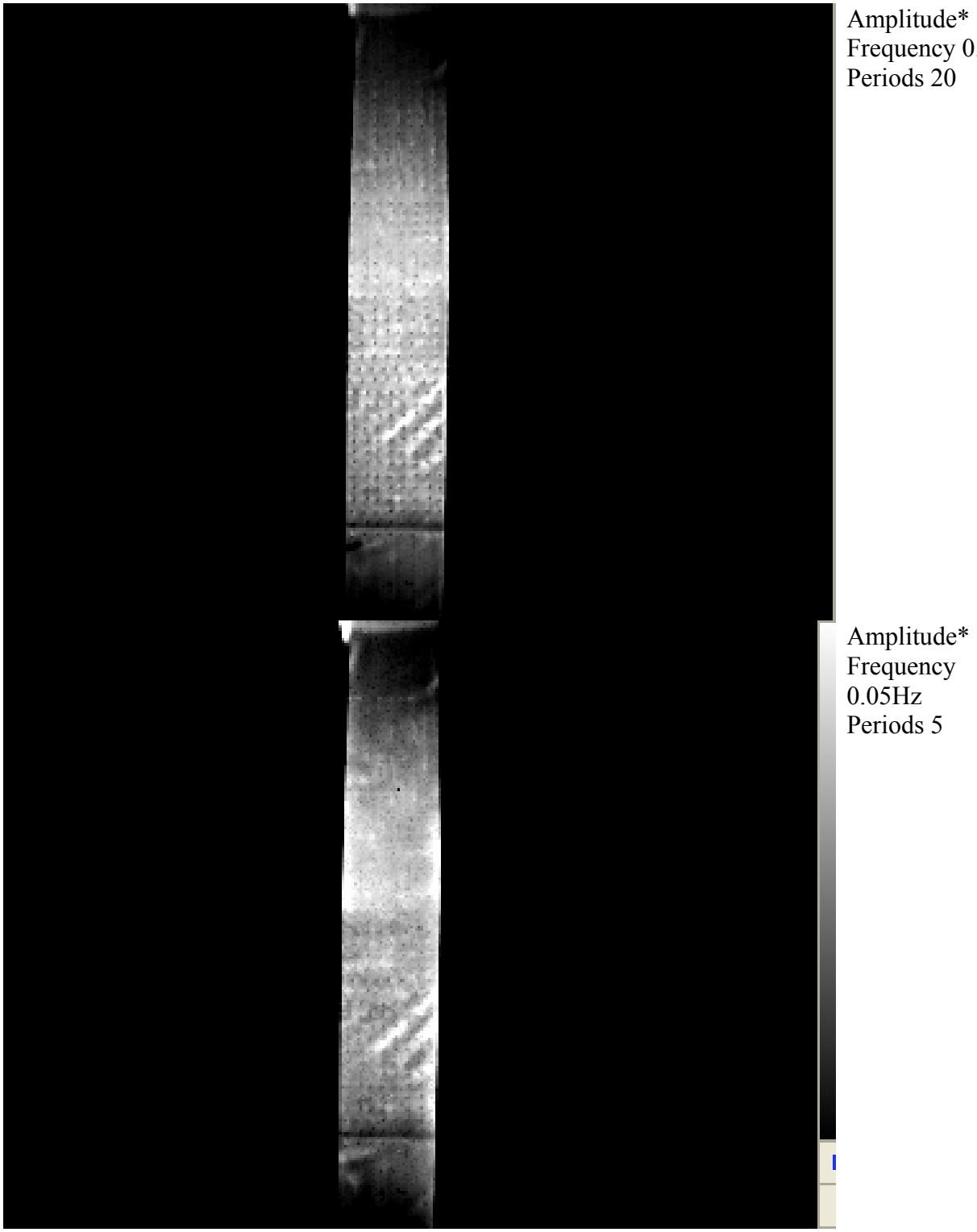
Amplitude*
Frequency 0.5Hz
Periods 20
Amplitude*
Frequency
0.05Hz
Periods 5

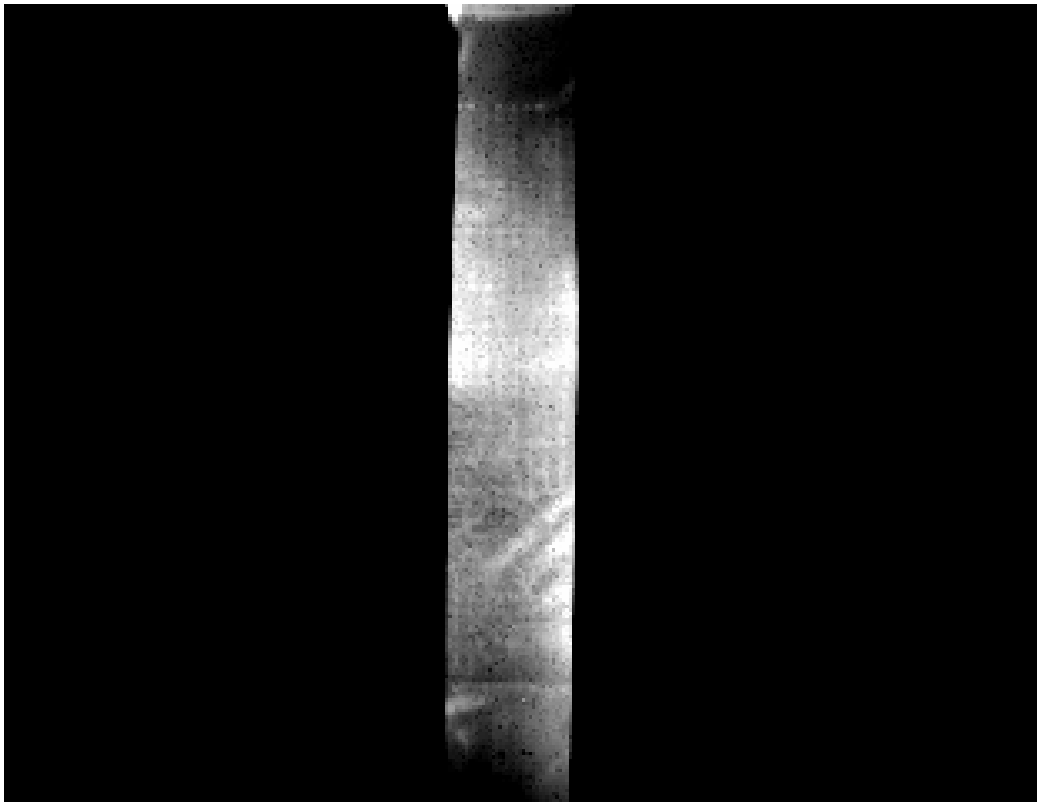

Amplitude*
Frequency
0.005Hz
Periods 2

Sample: H166-A1

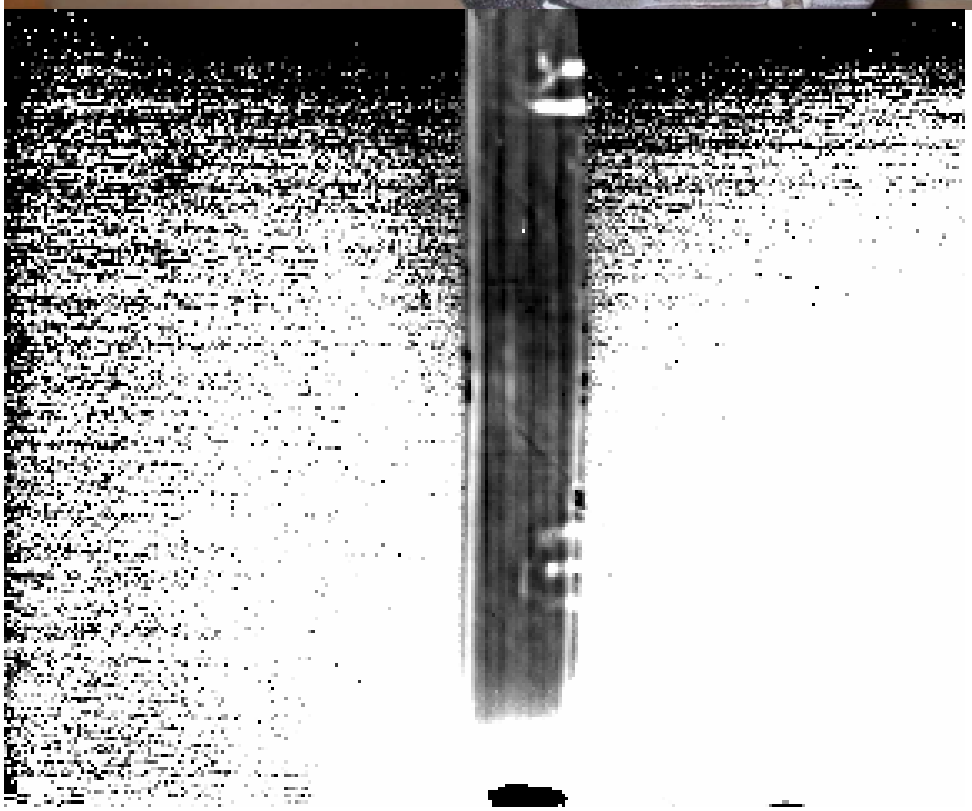

Phase
Frequency 0.5Hz
Periods 20

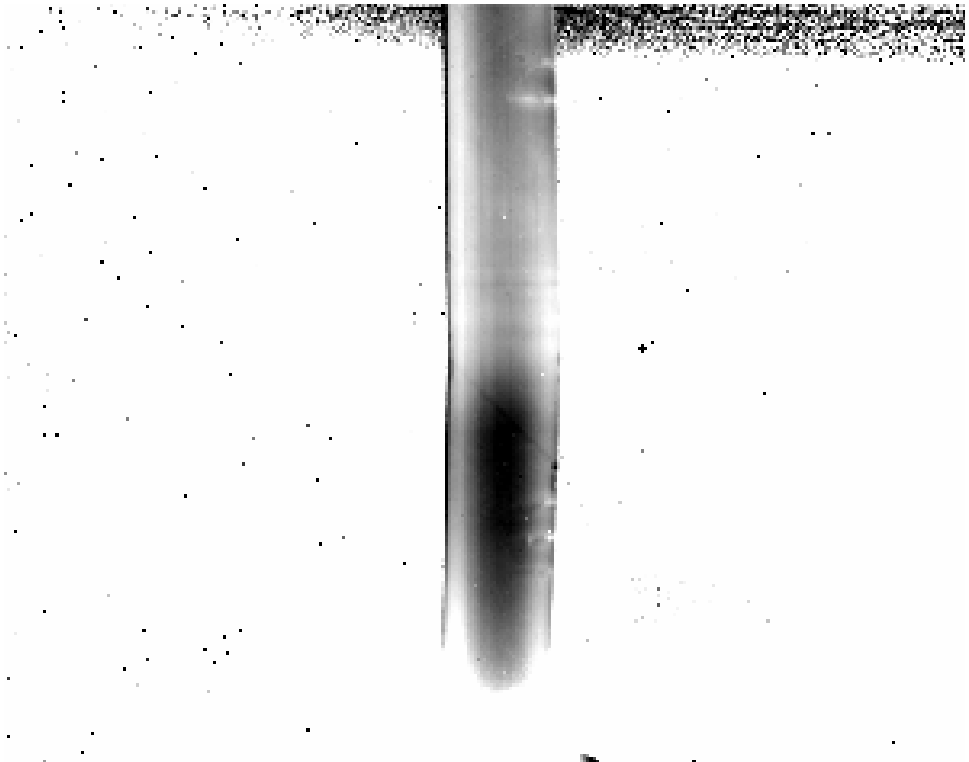

Phase
Frequency 0.05Hz
Periods 5

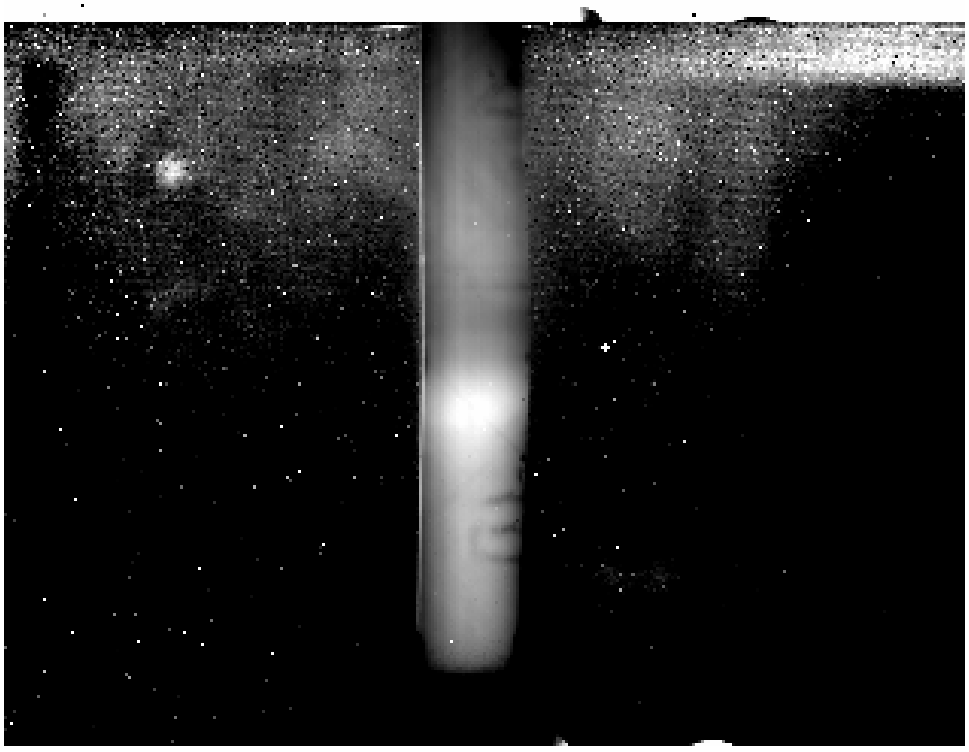

Phase
Frequency 0.005Hz
Periods 2

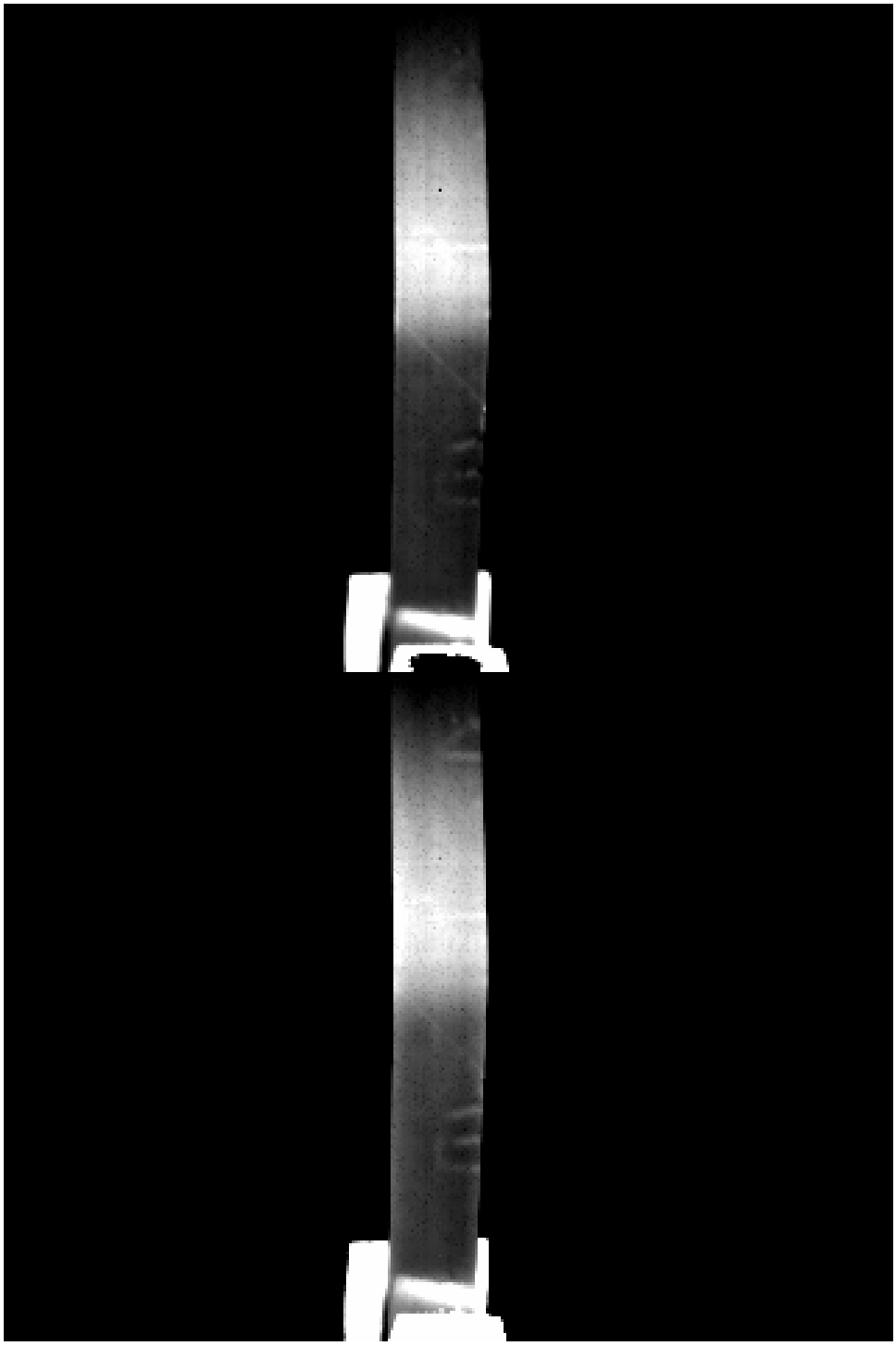

Amplitude*
Frequency 0.5Hz
Periods 20

Amplitude*
Frequency 0.05Hz
Periods 5

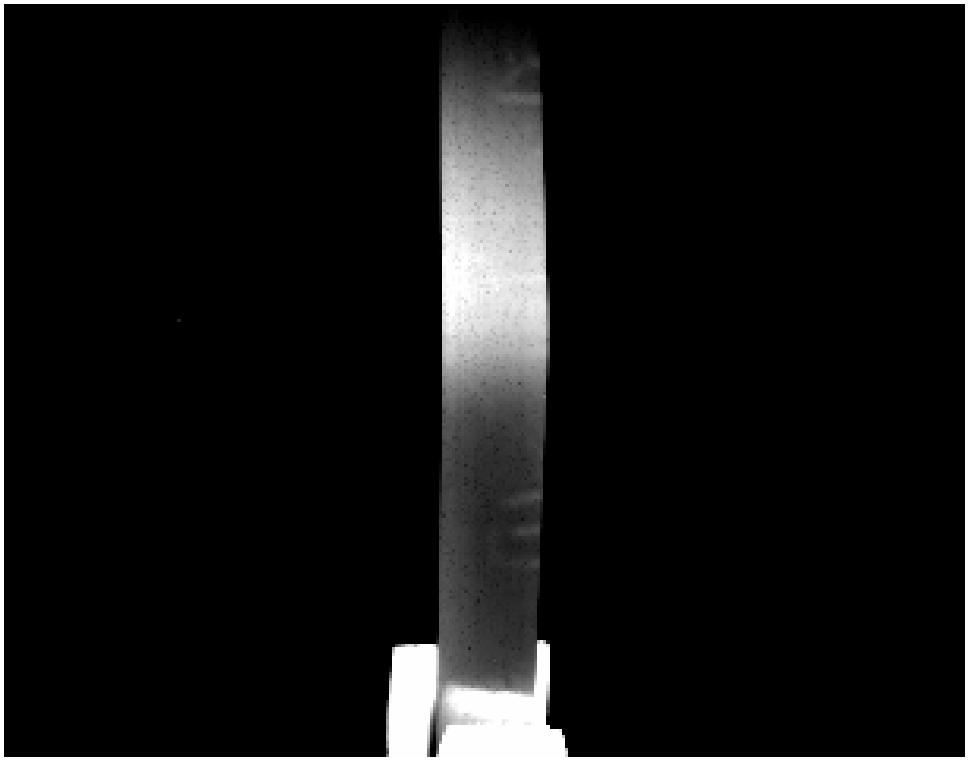

Amplitude*
Frequency 0.005Hz
Periods 2

Sample: H166-A6-A7-A8

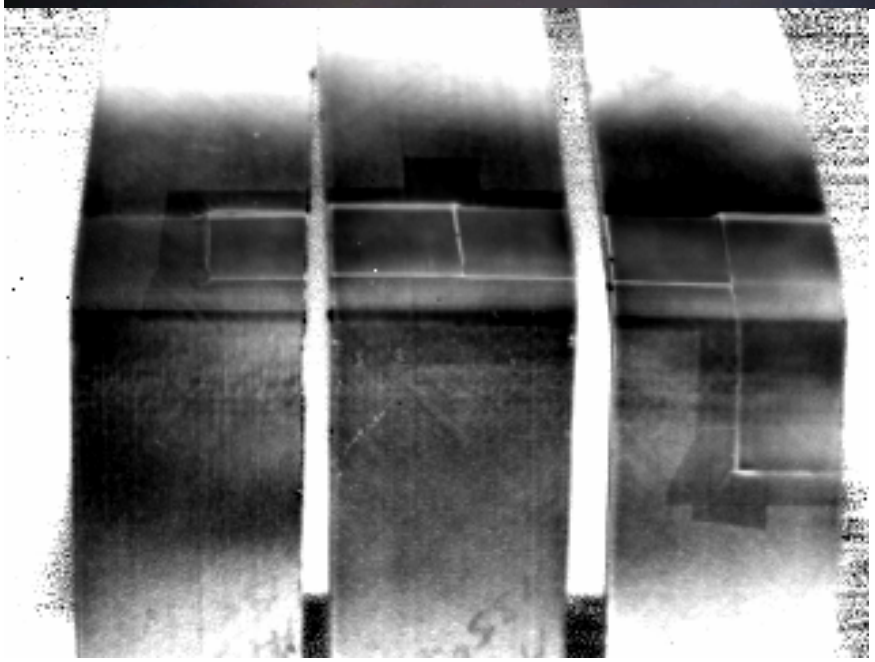

Phase
Frequency 0.5Hz
Periods 20

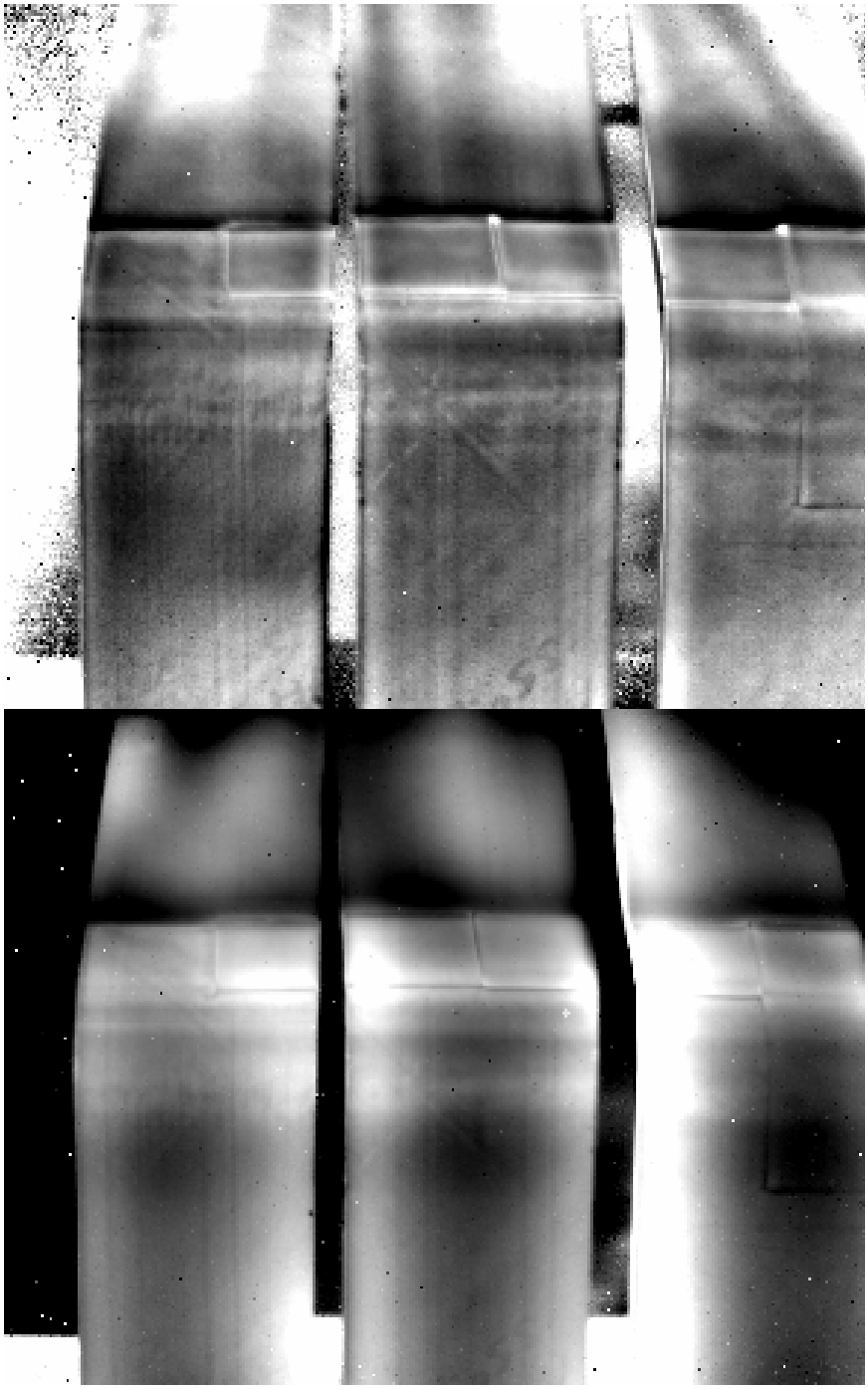

Phase
Frequency 0.05Hz
Periods 5

Phase
Frequency 0.005Hz
Periods 2

Amplitude*
Frequency 0.5Hz
Periods 20

Amplitude*
Frequency 0.05Hz
Periods 5

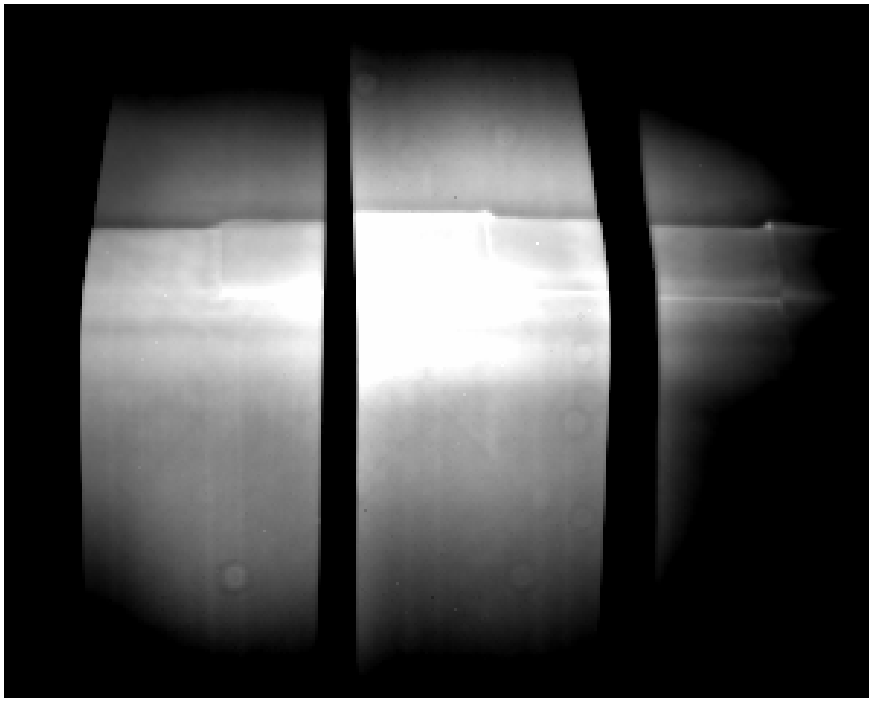

Amplitude*
Frequency 0.005Hz
Periods 2

Sample: H166-A6-A7-A8 Rear

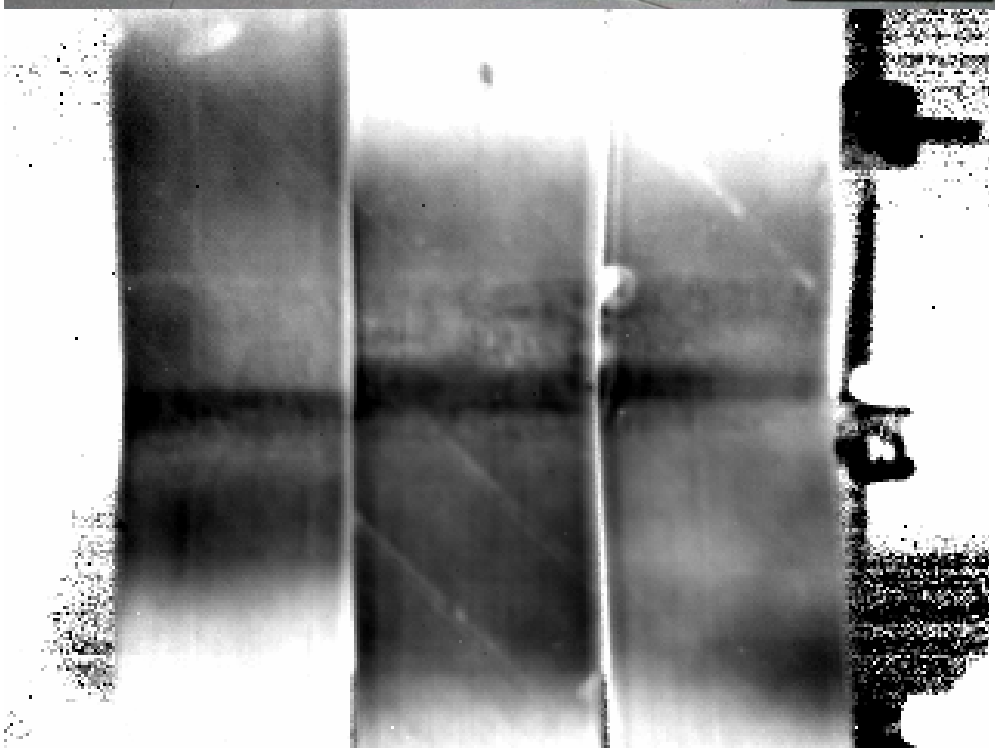

Phase
Frequency 0.5Hz
Periods 20

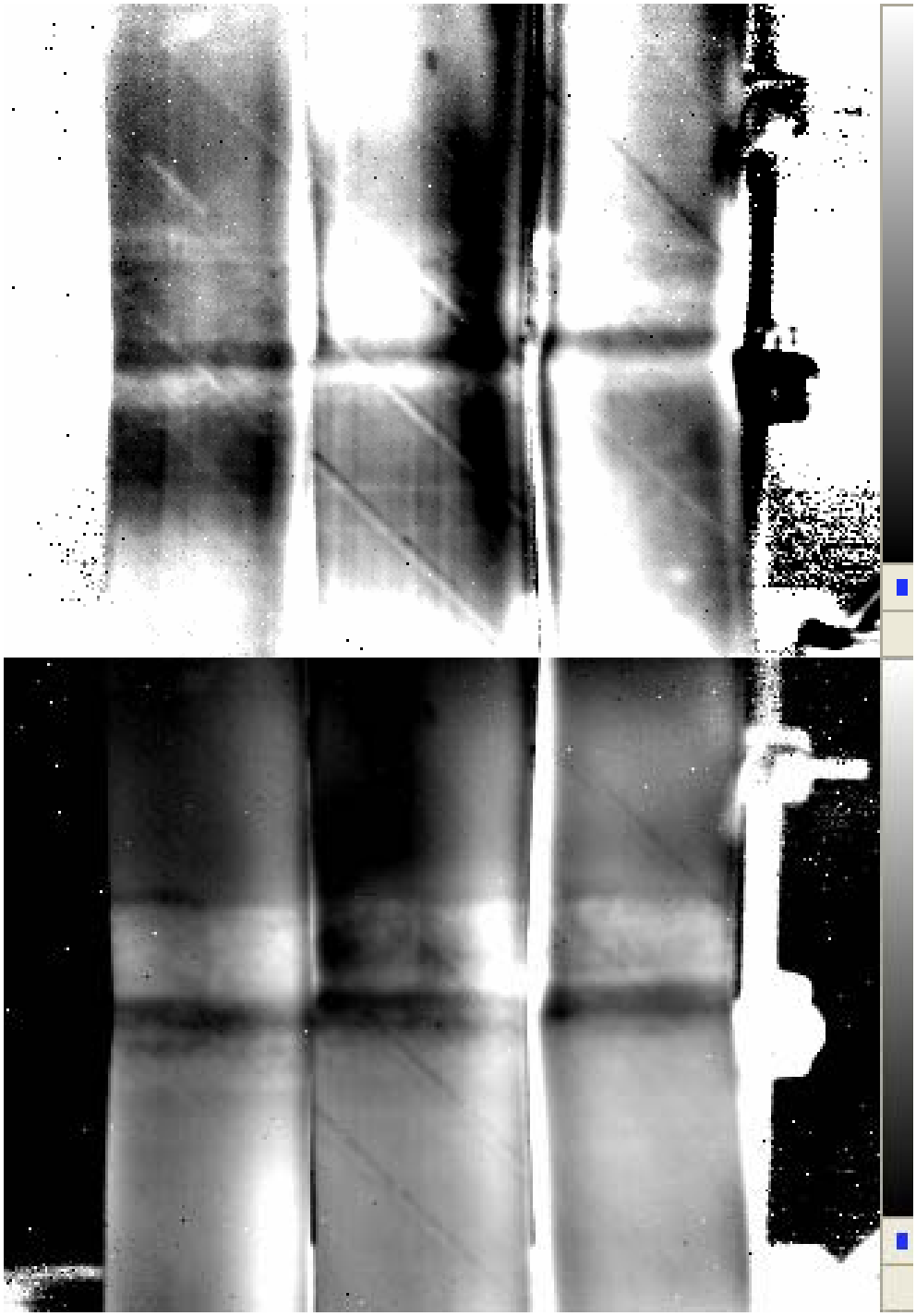

Phase
Frequency 0.05Hz
Periods 5

Phase
Frequency 0.005Hz
Periods 2

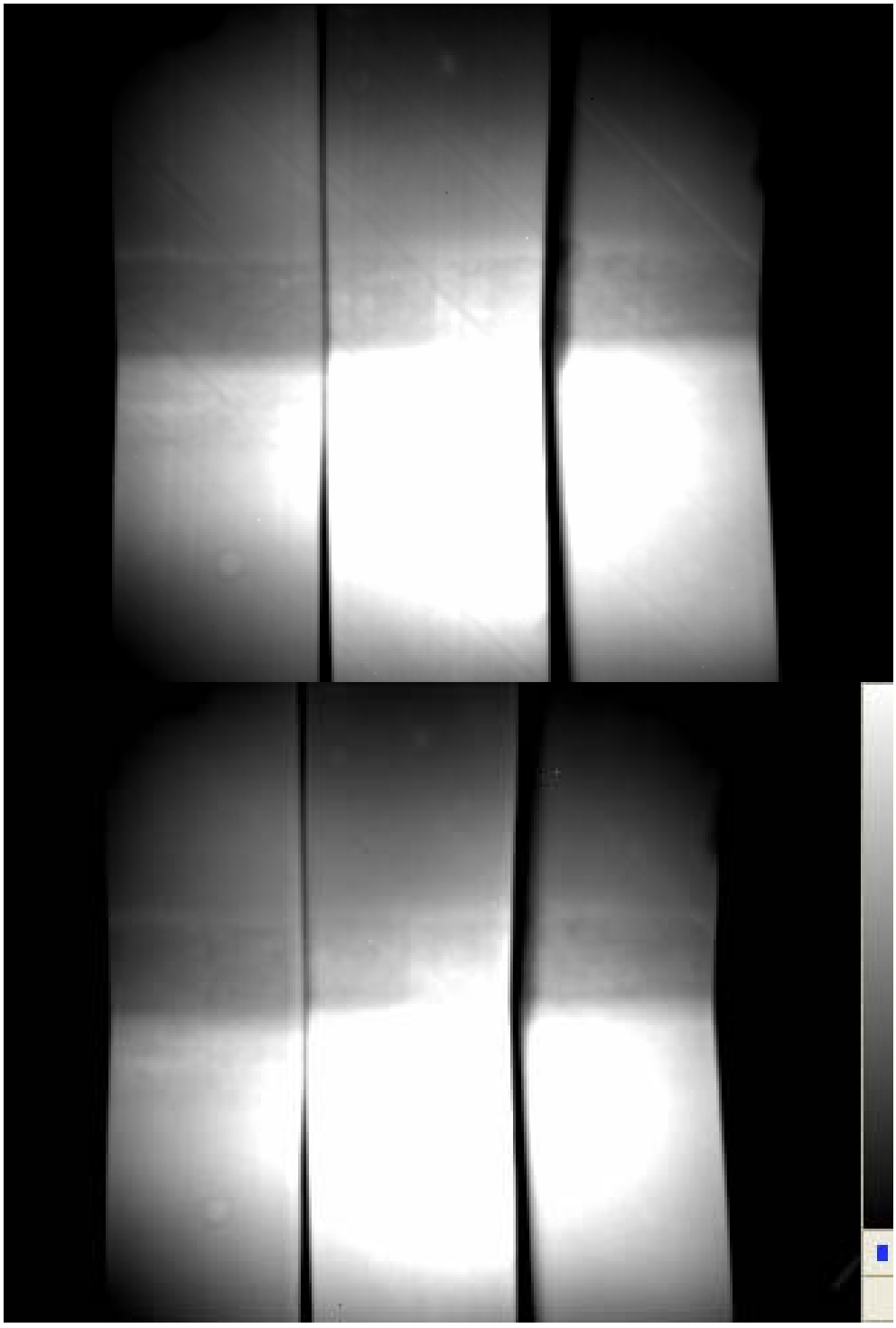

Amplitude*
Frequency 0.5Hz
Periods 20

Amplitude*
Frequency 0.05Hz
Periods 5

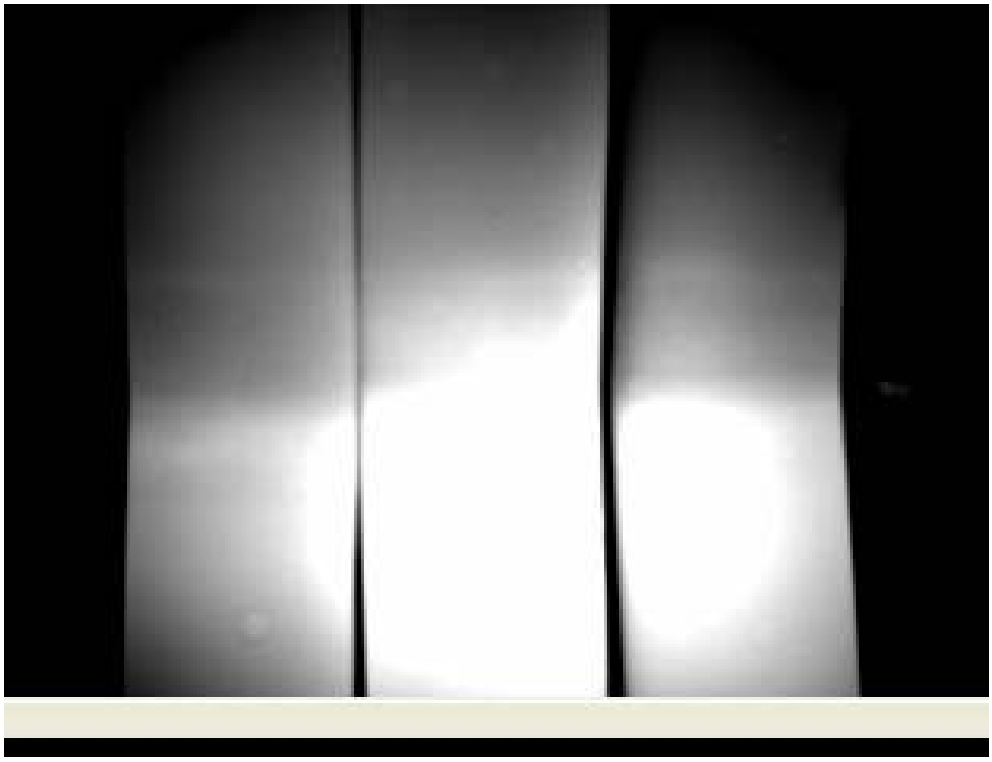

Amplitude*
Frequency 0.005Hz
Periods 2

Sample: H166-B1-B2-B3-B4

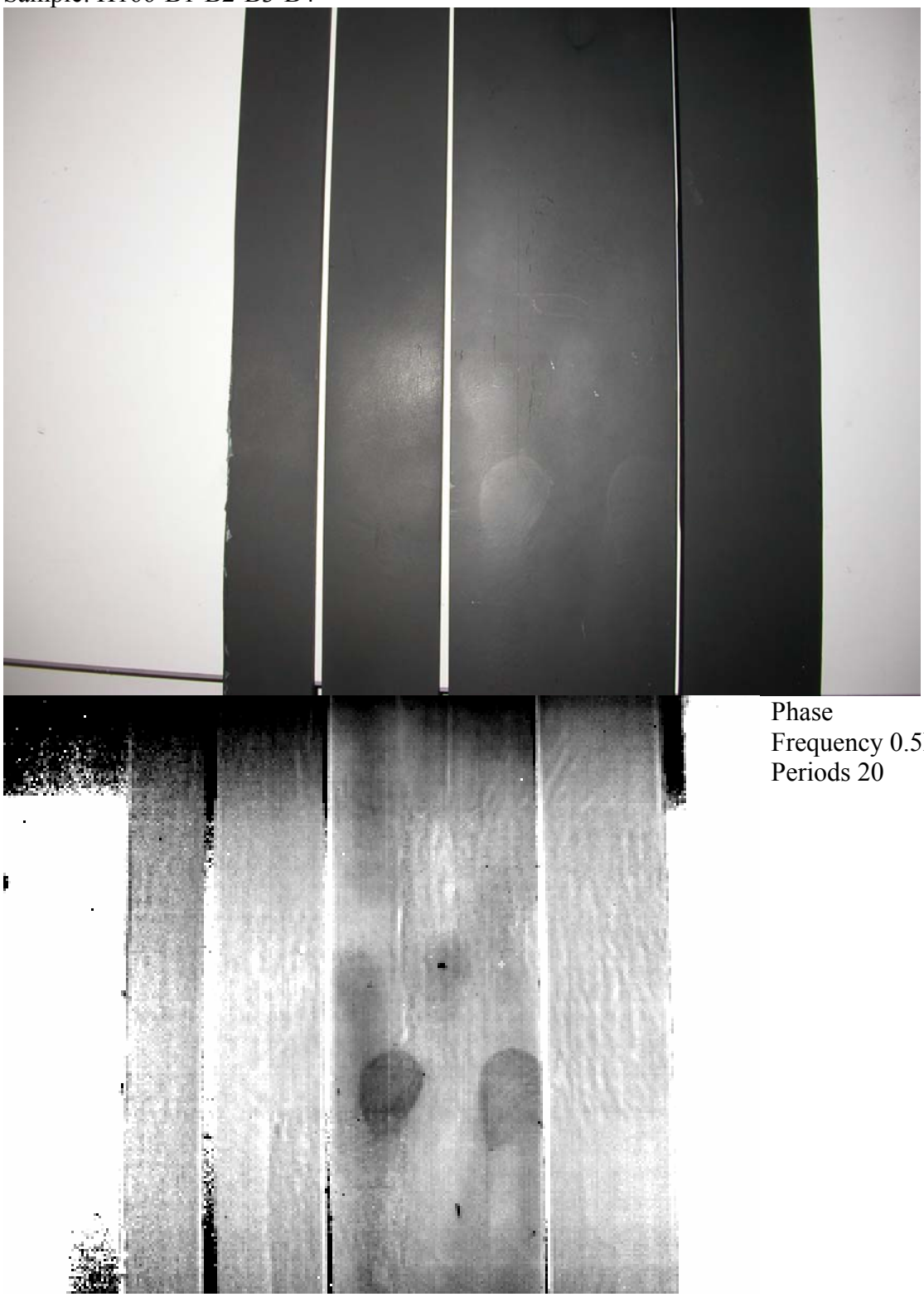

Phase
Frequency 0.5Hz
Periods 20

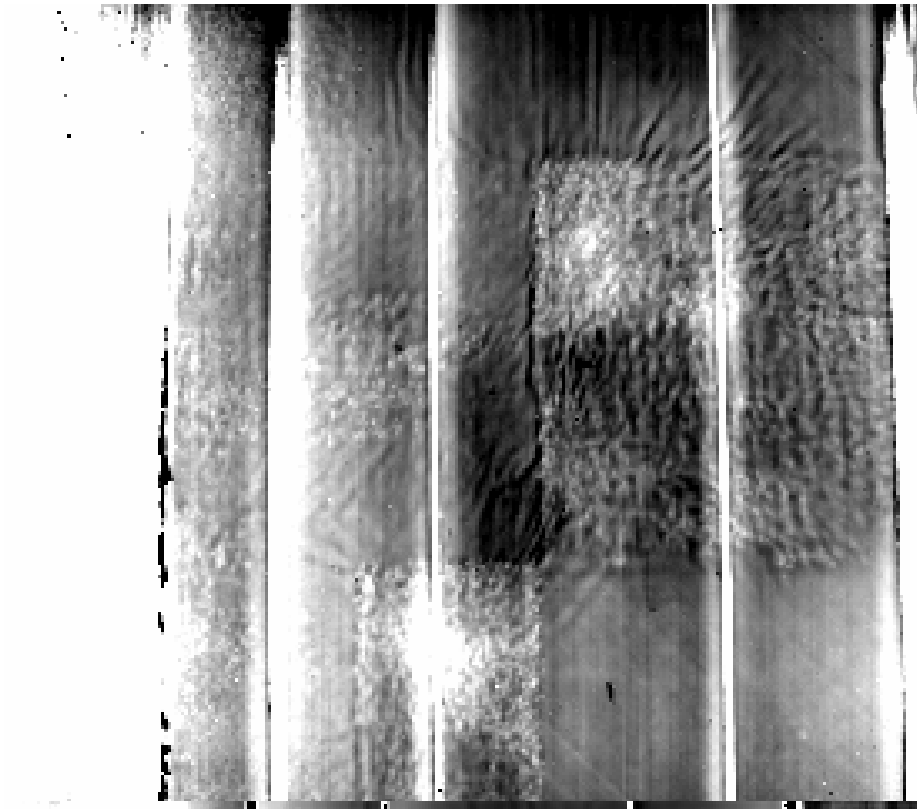

Phase
Frequency 0.05Hz
Periods 5

Z pin distribution can be determined

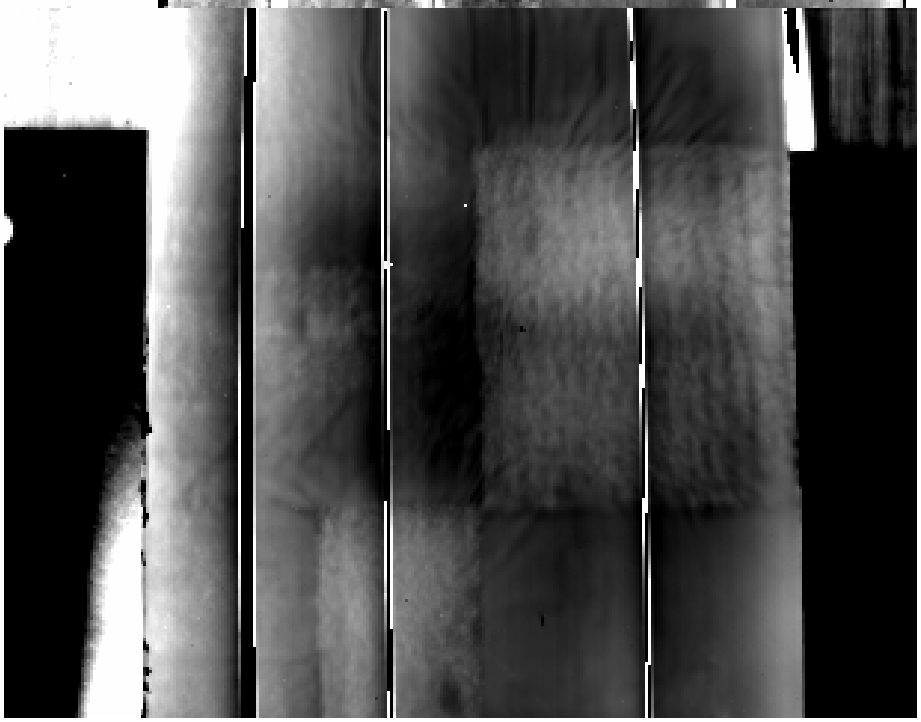

Phase
Frequency 0.005Hz
Periods 2

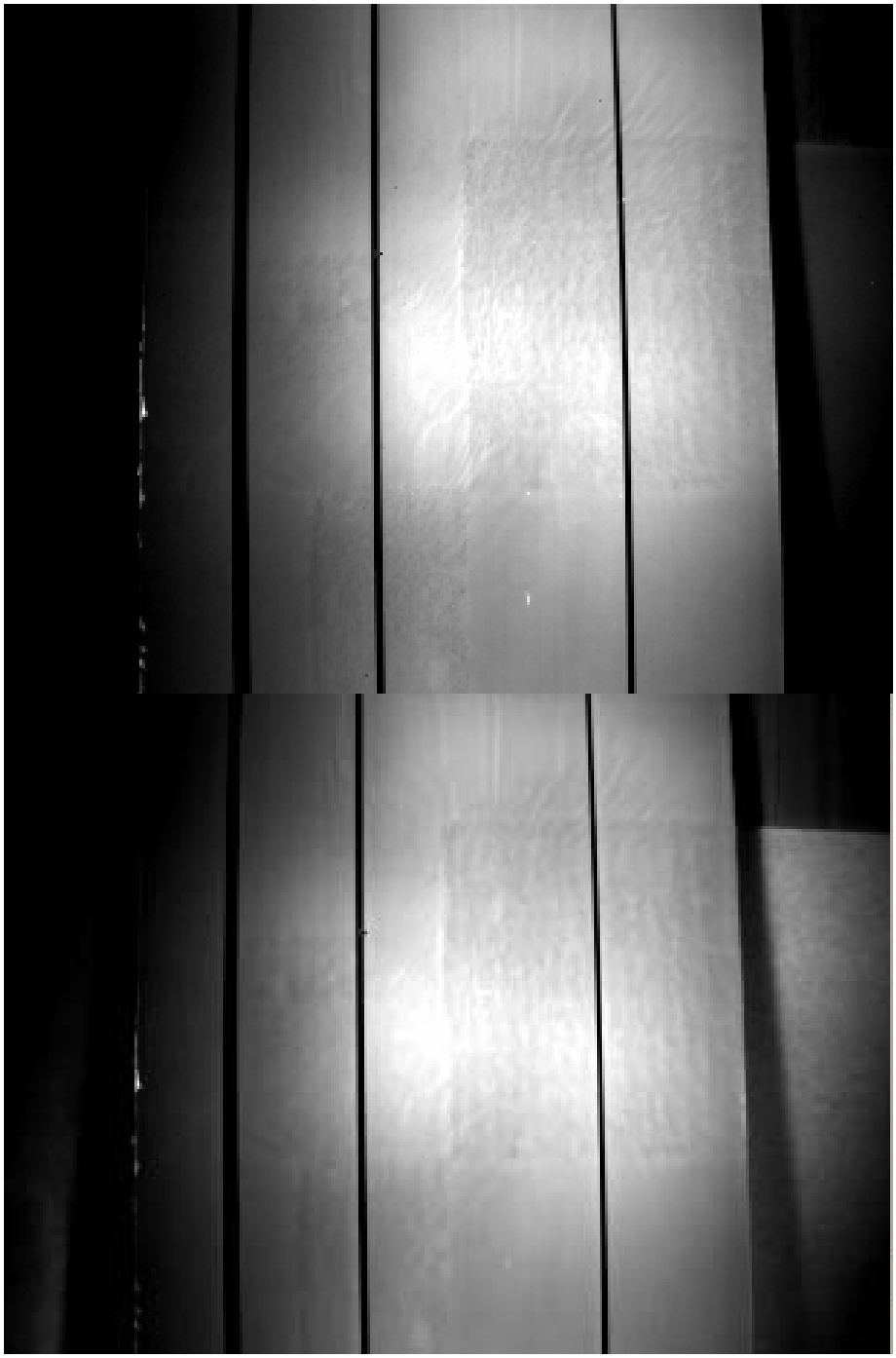

Amplitude*
Frequency 0.5Hz
Periods 20

Amplitude*
Frequency 0.05Hz
Periods 5

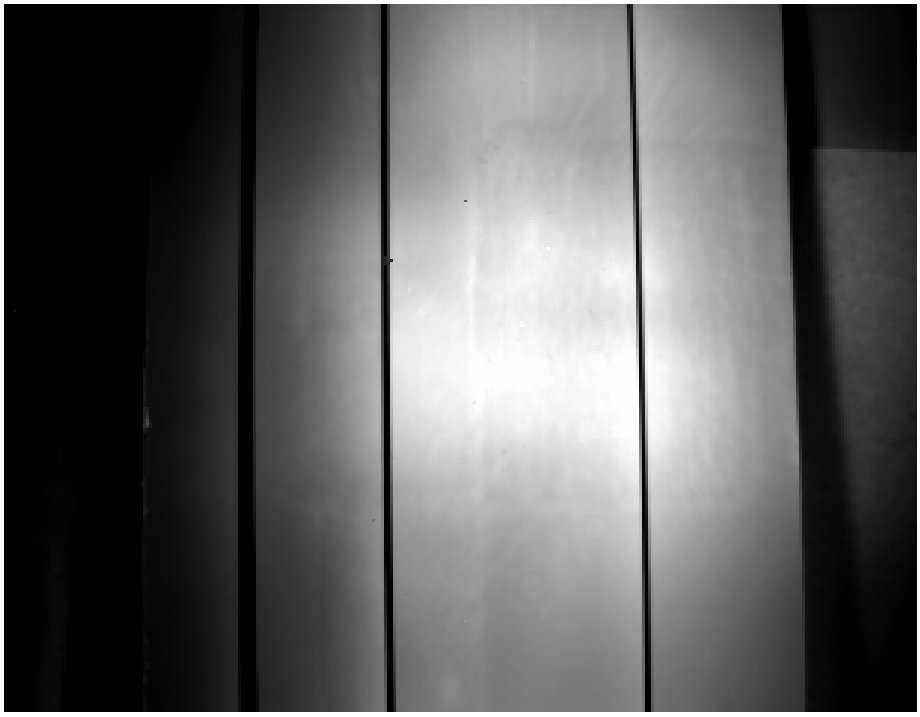

Amplitude*
Frequency 0.005Hz
Periods 2

Sample: H166-B1-B2-B3-B4 Rear

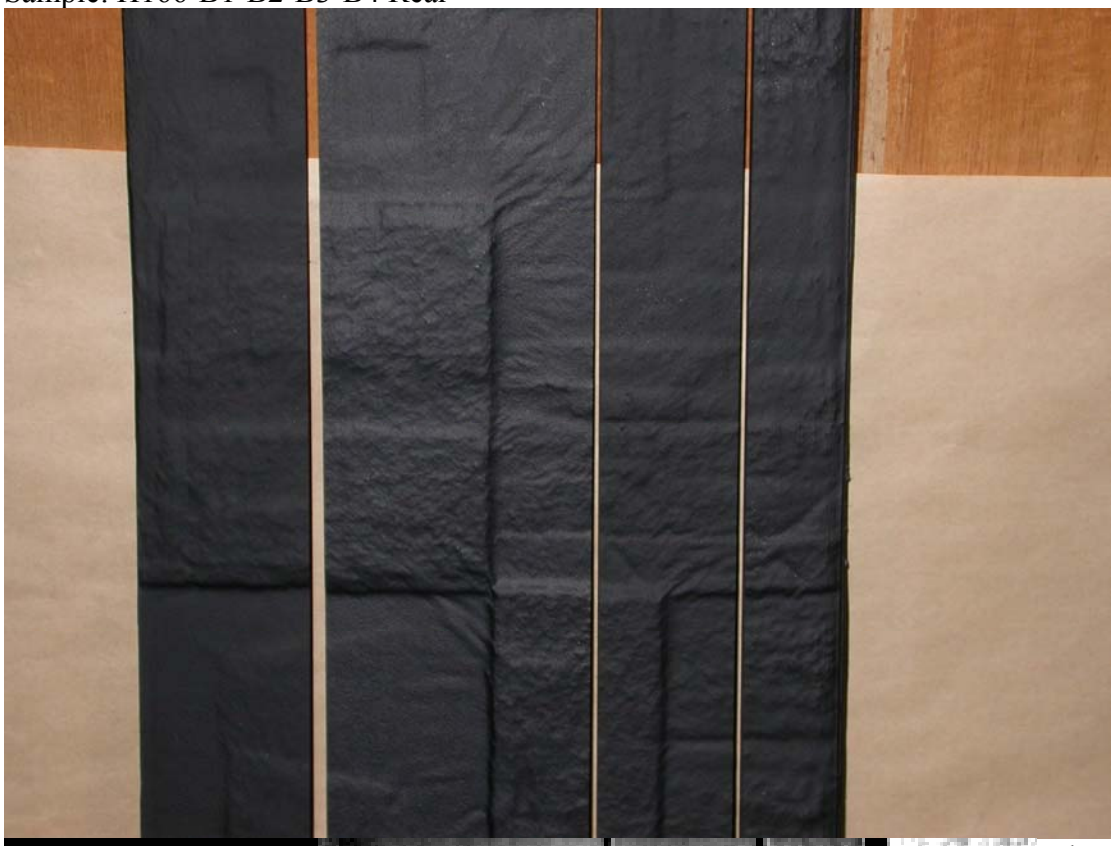

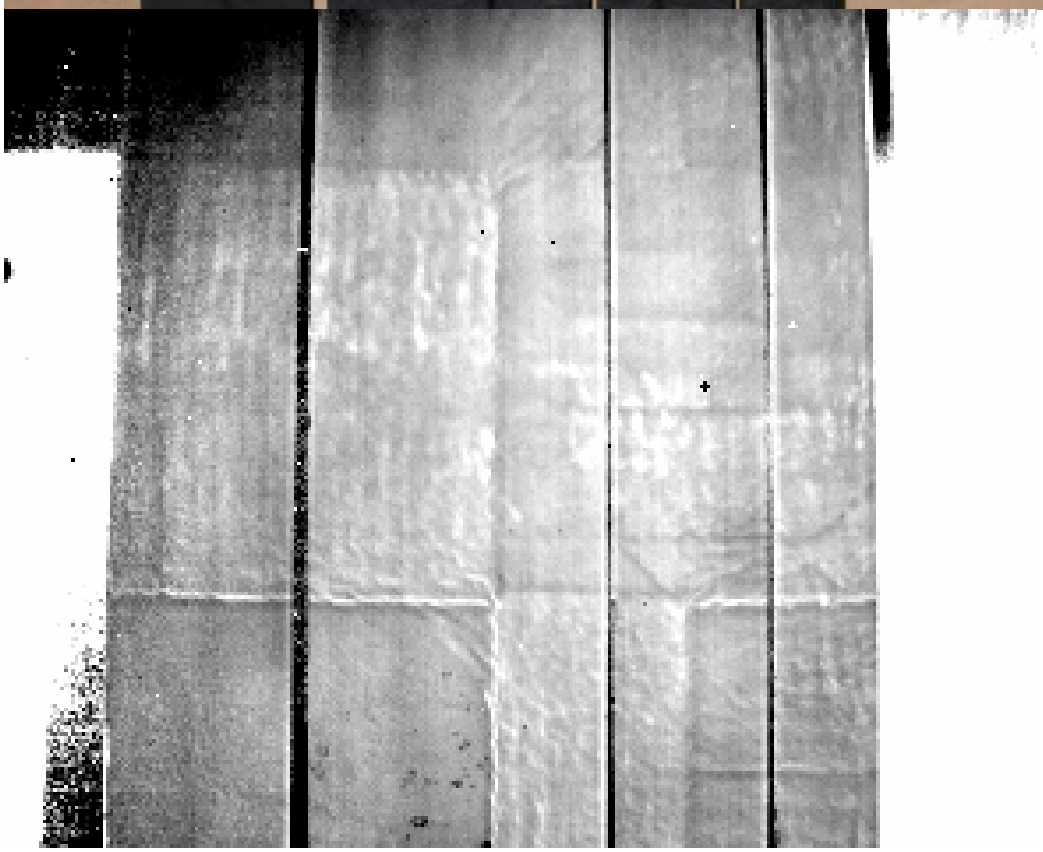

Phase
Frequency
0.5Hz
Periods 20

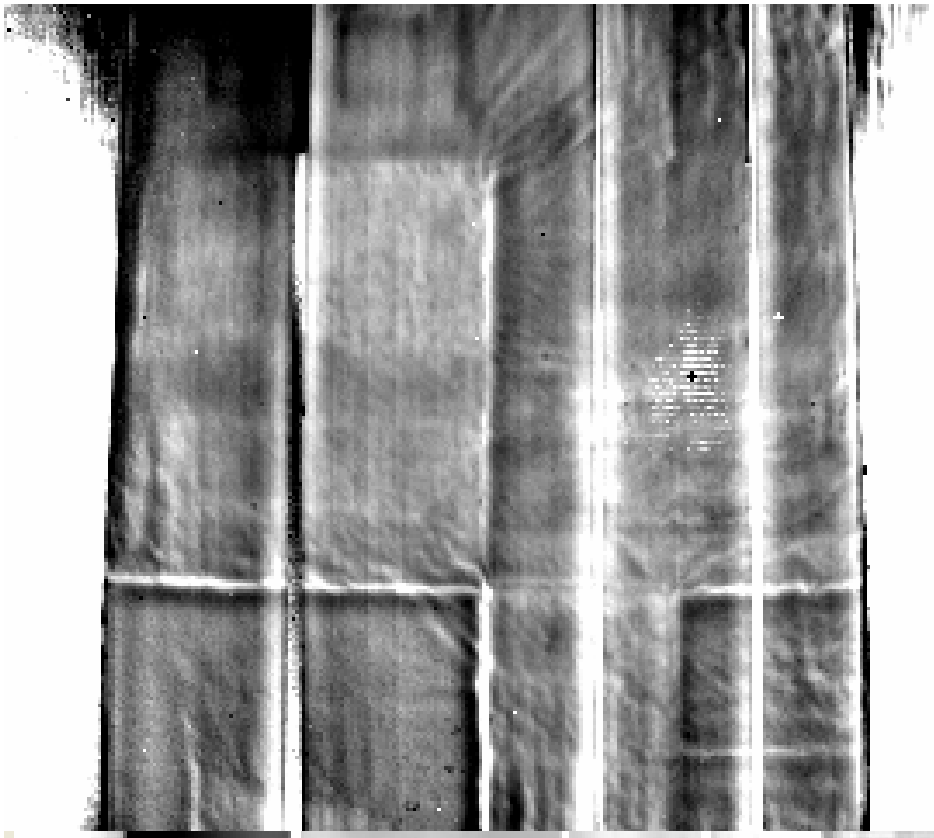

Phase
Frequency
0.05Hz
Periods 5

A clear picture but z pins cannot be seen well

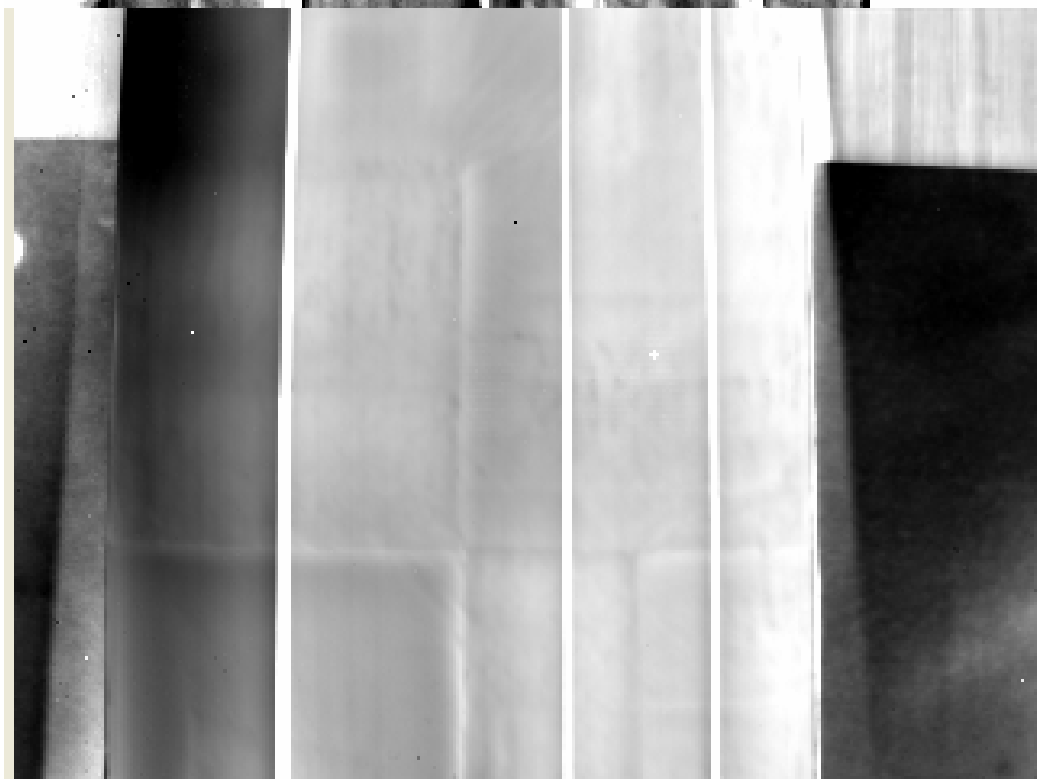

Phase
Frequency
0.005Hz
Periods 2

Amplitude*
Frequency
0.5Hz
Periods 20

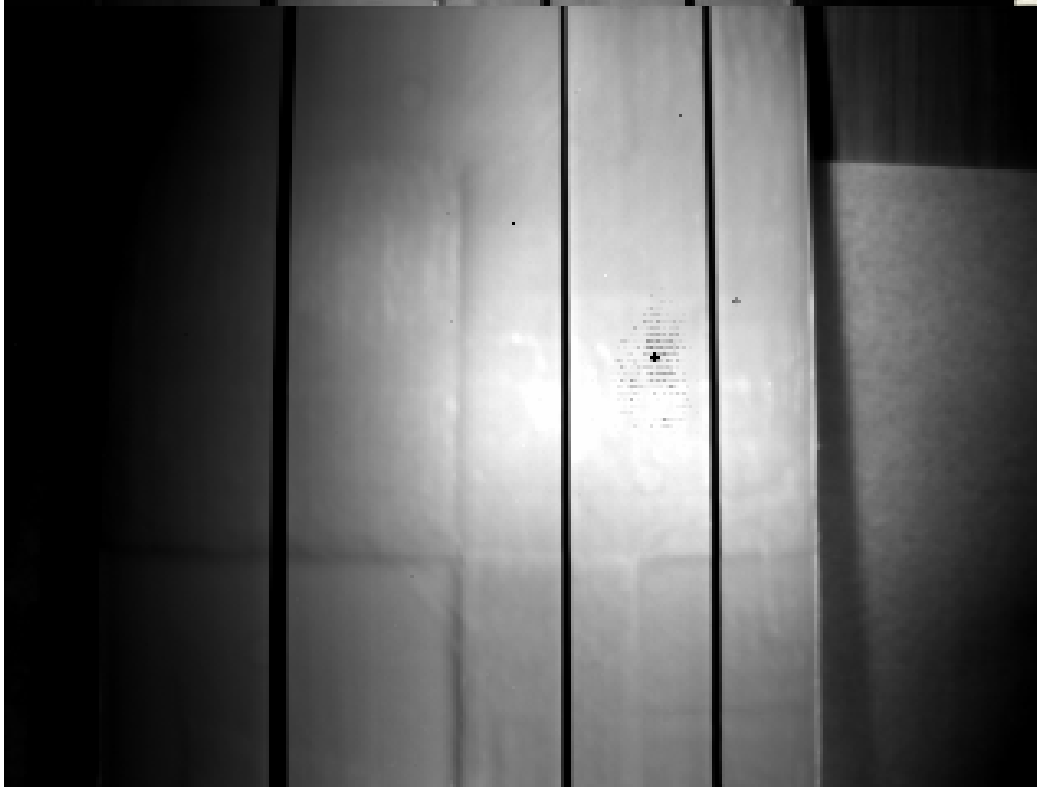

Amplitude*
Frequency
0.05Hz
Periods 5

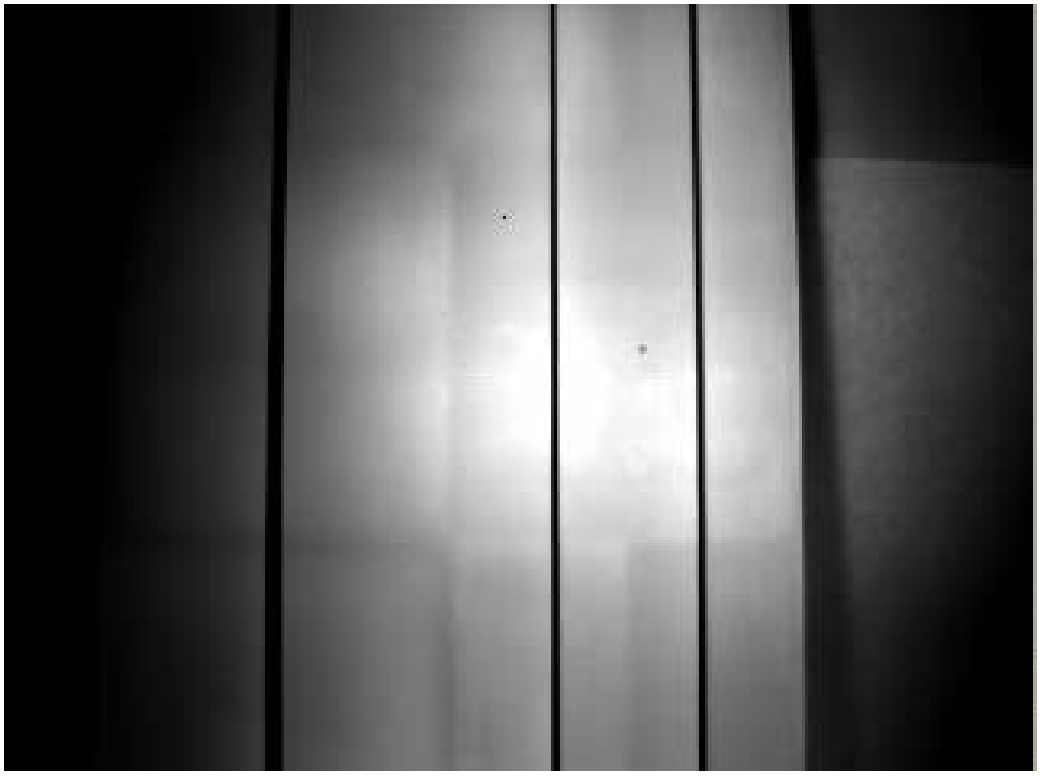

Amplitude*
Frequency
0.005Hz
Periods 2

Sample: H166-A1-A2-A3-A4-A5

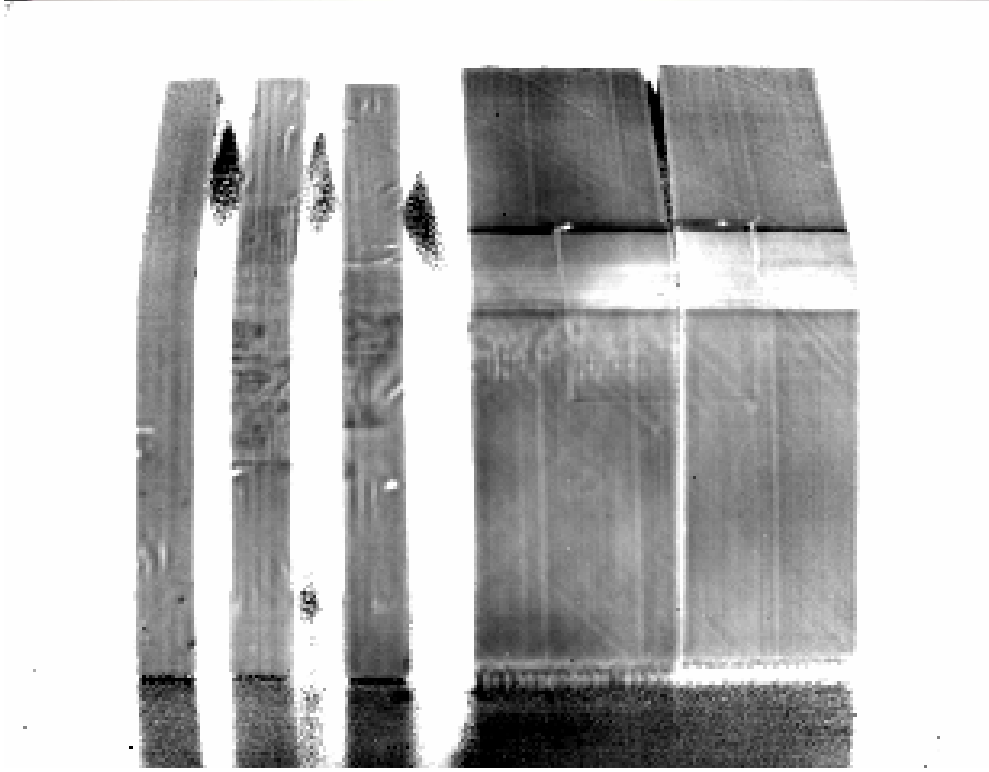

Phase
Frequency 0.5Hz
Periods 20

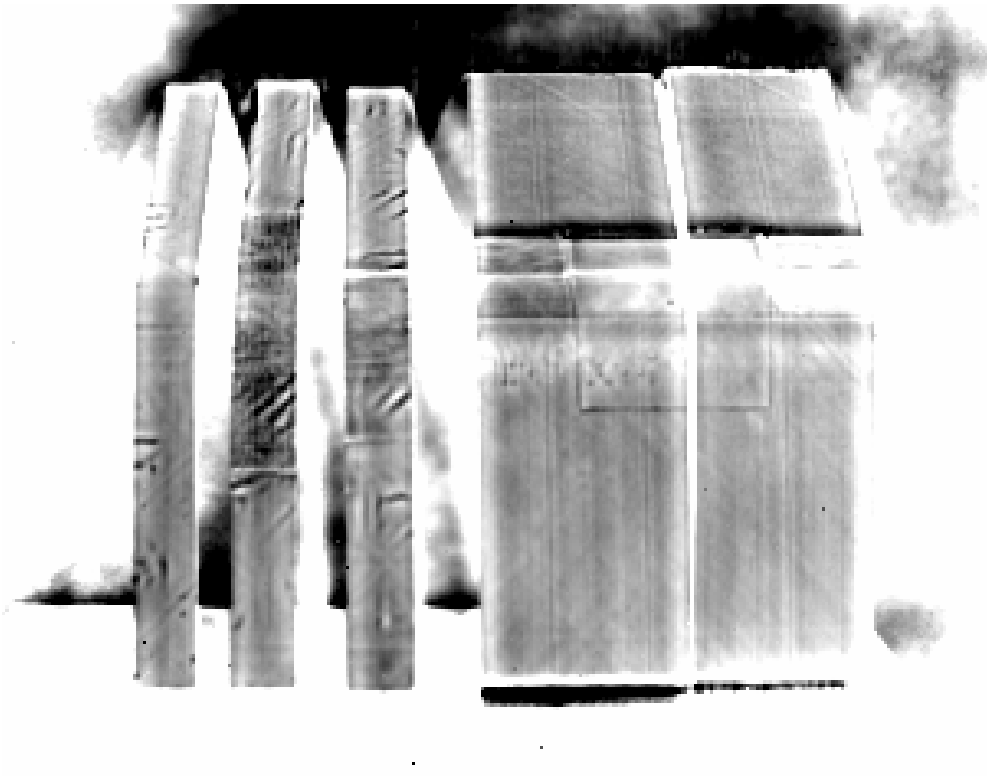

Phase
Frequency 0.05Hz
Periods 5

Sub surface damage can be clearly seen

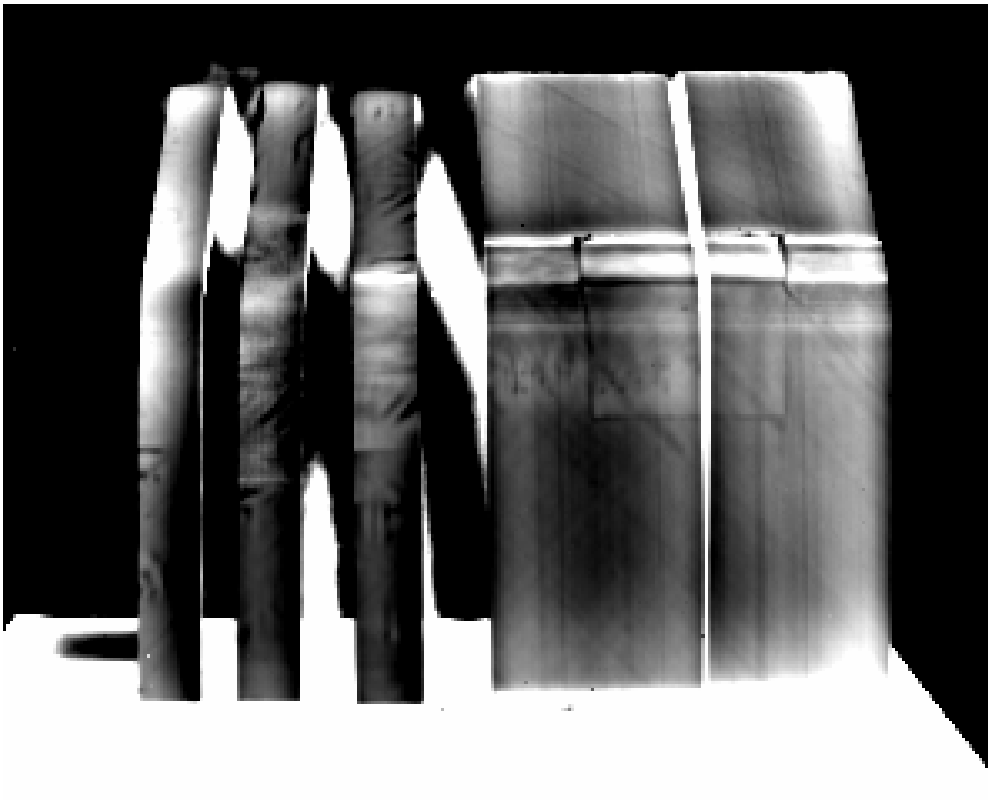

Phase
Frequency 0.005Hz
Periods 2

Amplitude*
Frequency 0.5Hz
Periods 20

Amplitude*
Frequency 0.05Hz
Periods 5

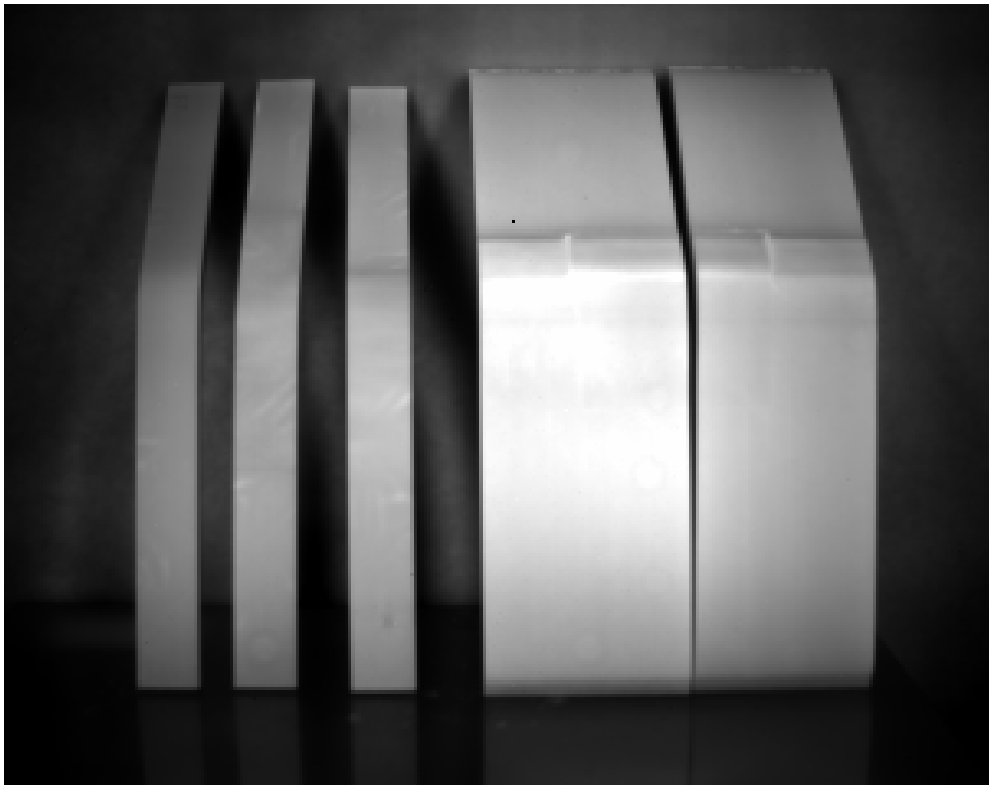

Amplitude*
Frequency 0.005Hz
Periods 2

Sample: H166-A1-A2-A3

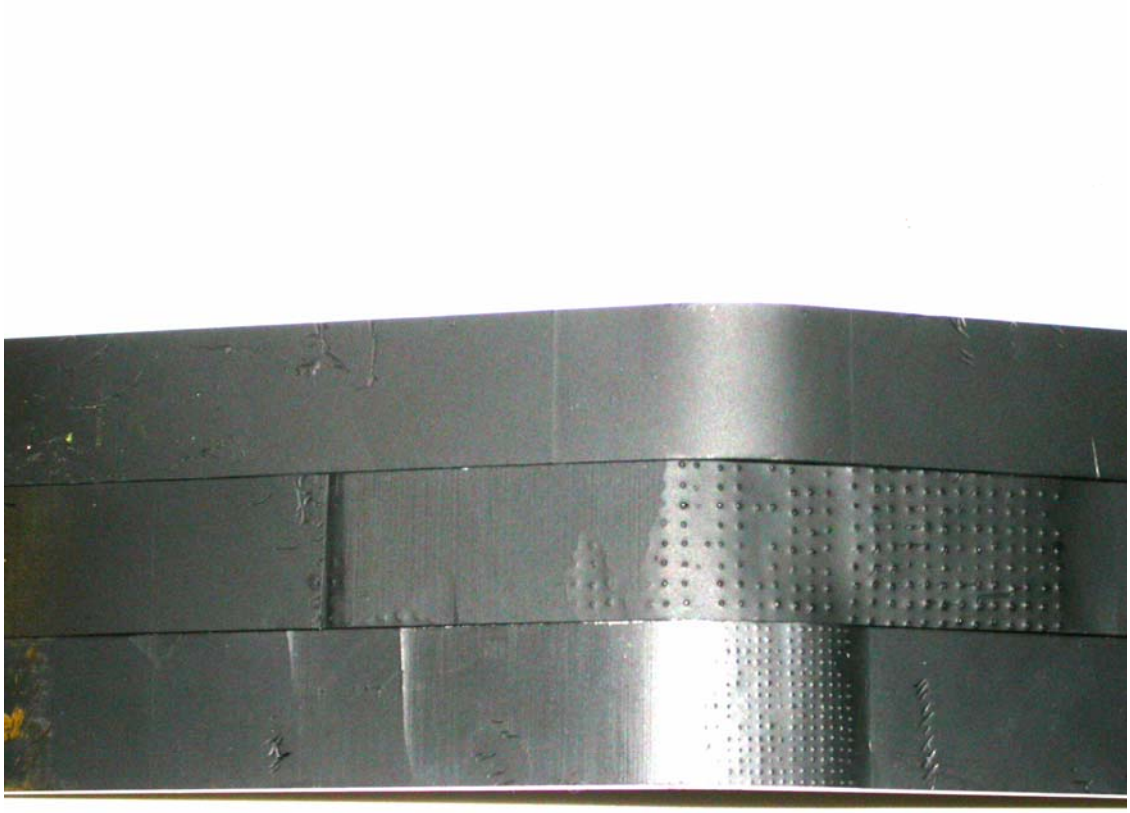

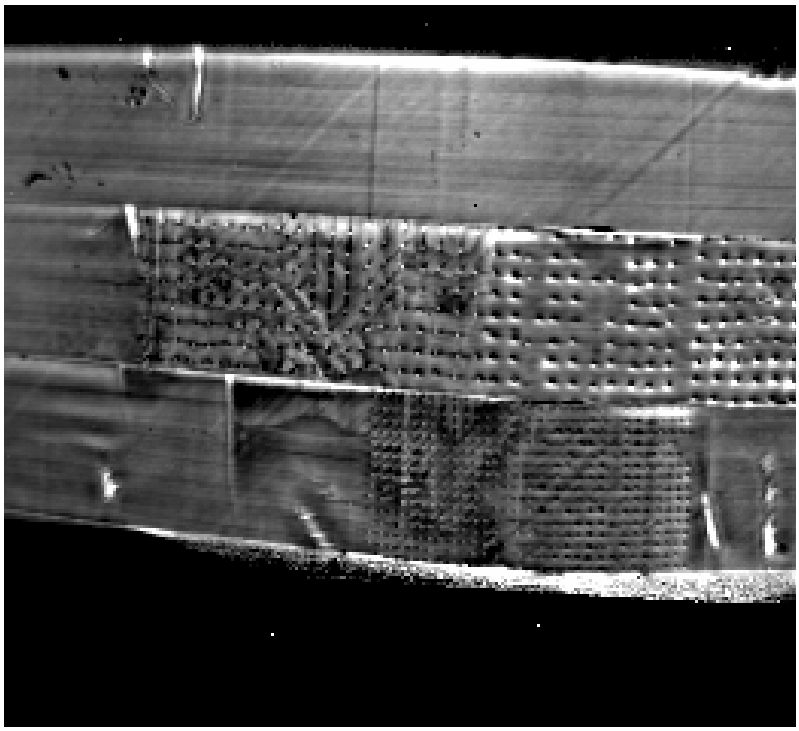

Phase
Frequency 0.5Hz
Periods 20

The distribution of the z-pins is clear, as is the surface and subsurface damage.

Non visible pins can be seen.

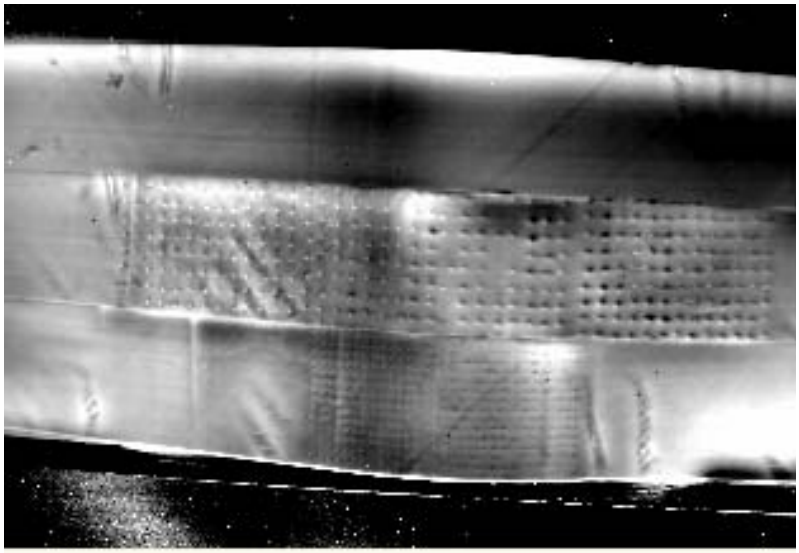

Phase
Frequency 0.05Hz
Periods 5

The distribution of the z-pins is clear, as is the surface and subsurface damage.

Non visible pins can be seen.

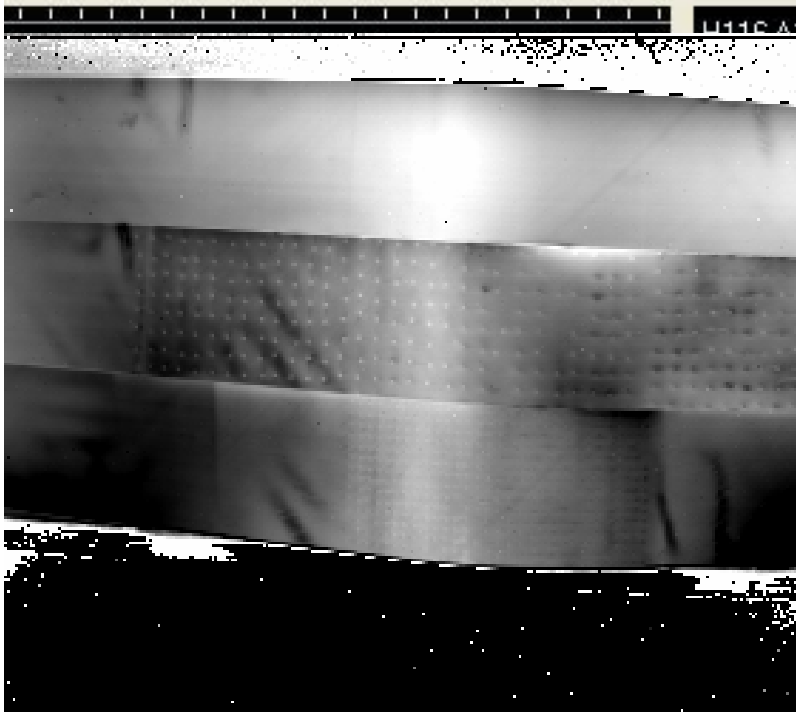

Phase
Frequency 0.005Hz
Periods 2

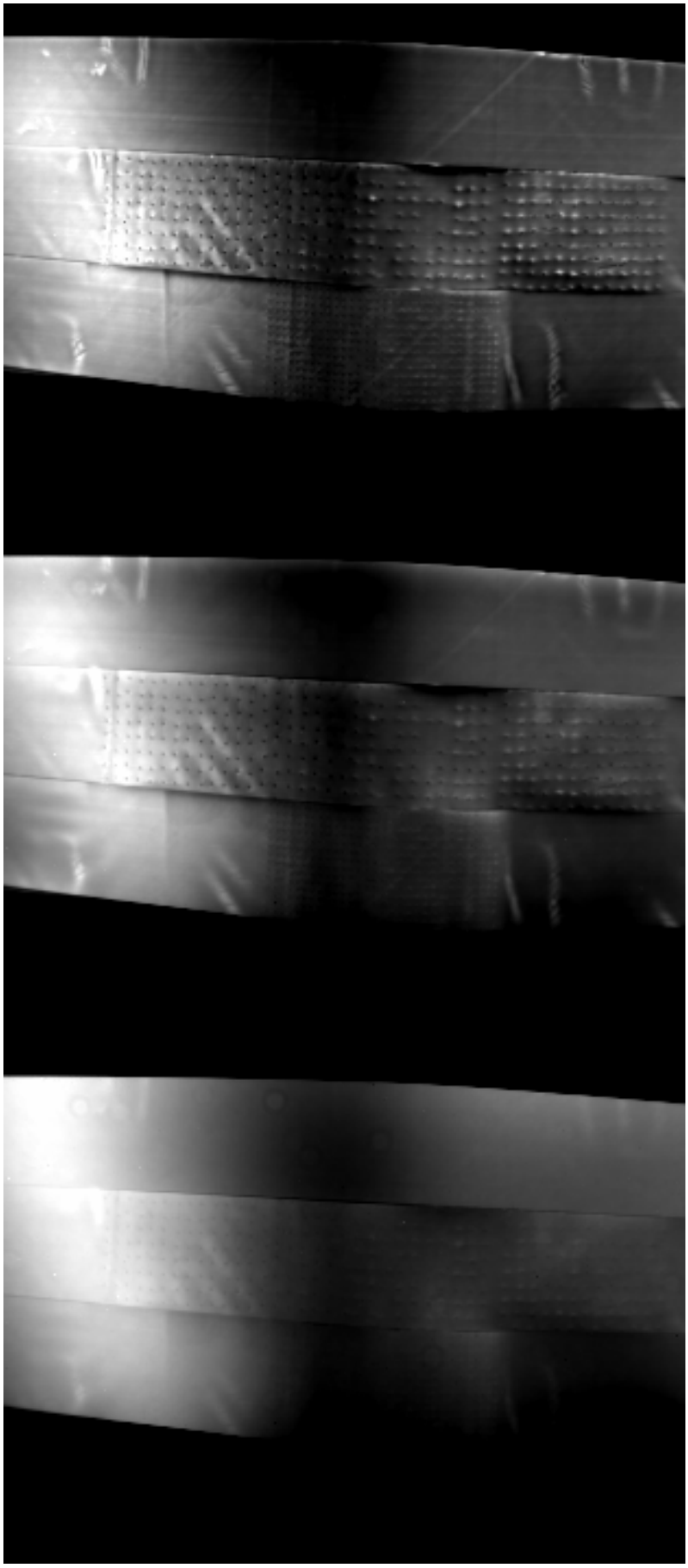

Amplitude*
Frequency 0.5Hz
Periods 20

Amplitude*
Frequency 0.05Hz
Periods 5

Amplitude*
Frequency 0.005Hz
Periods 2

Sample: H166-A1-A2-A3

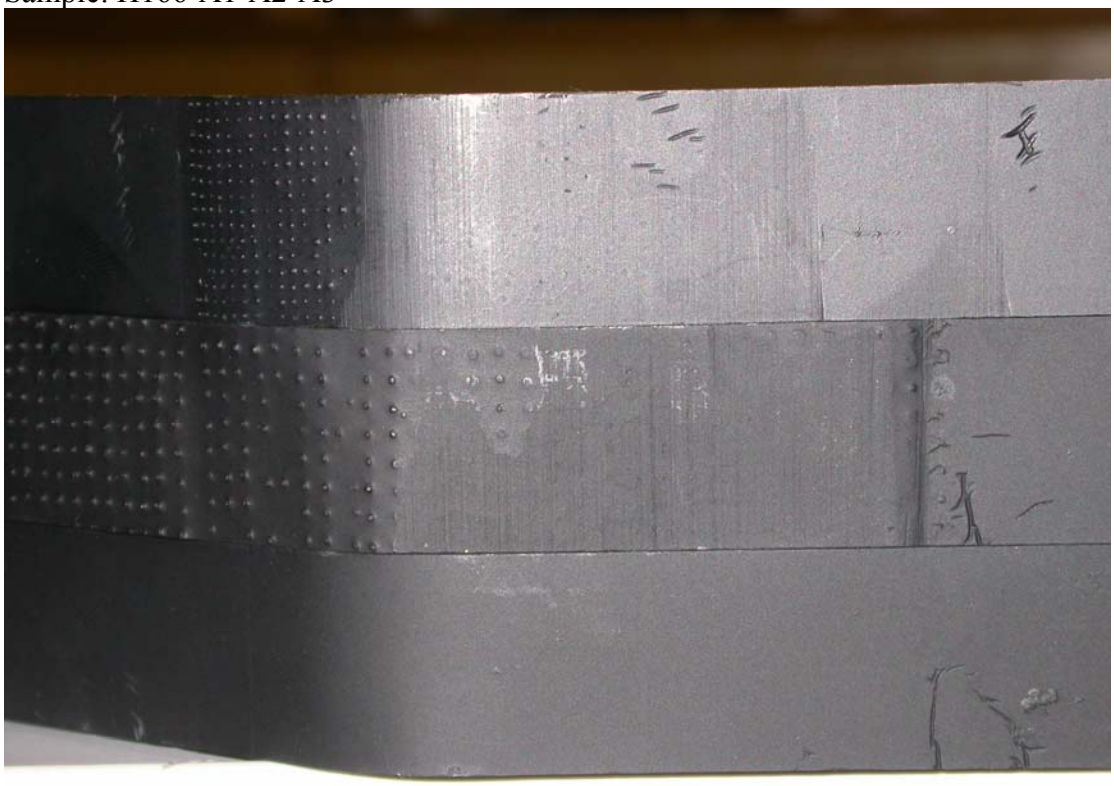

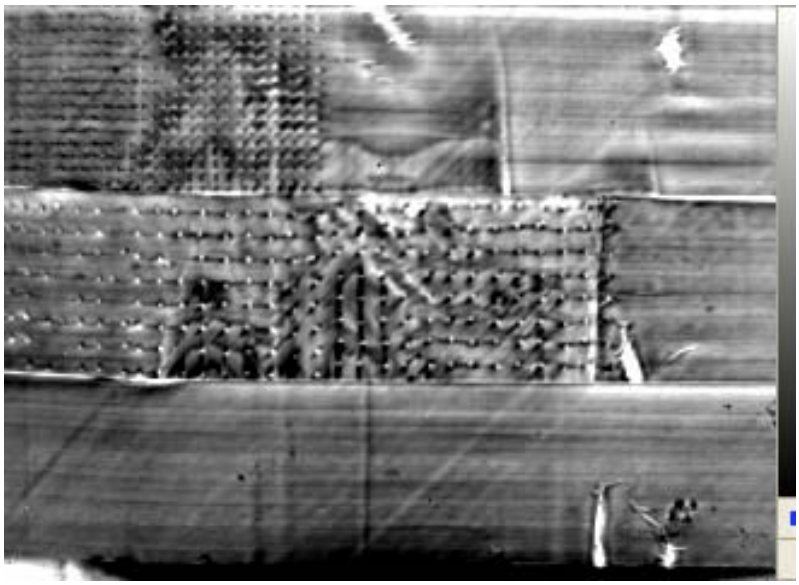

Phase
Frequency 0.5Hz
Periods 20

The distribution of the z-pins is clear, as is the surface and subsurface damage.

Non visible pins can be seen.

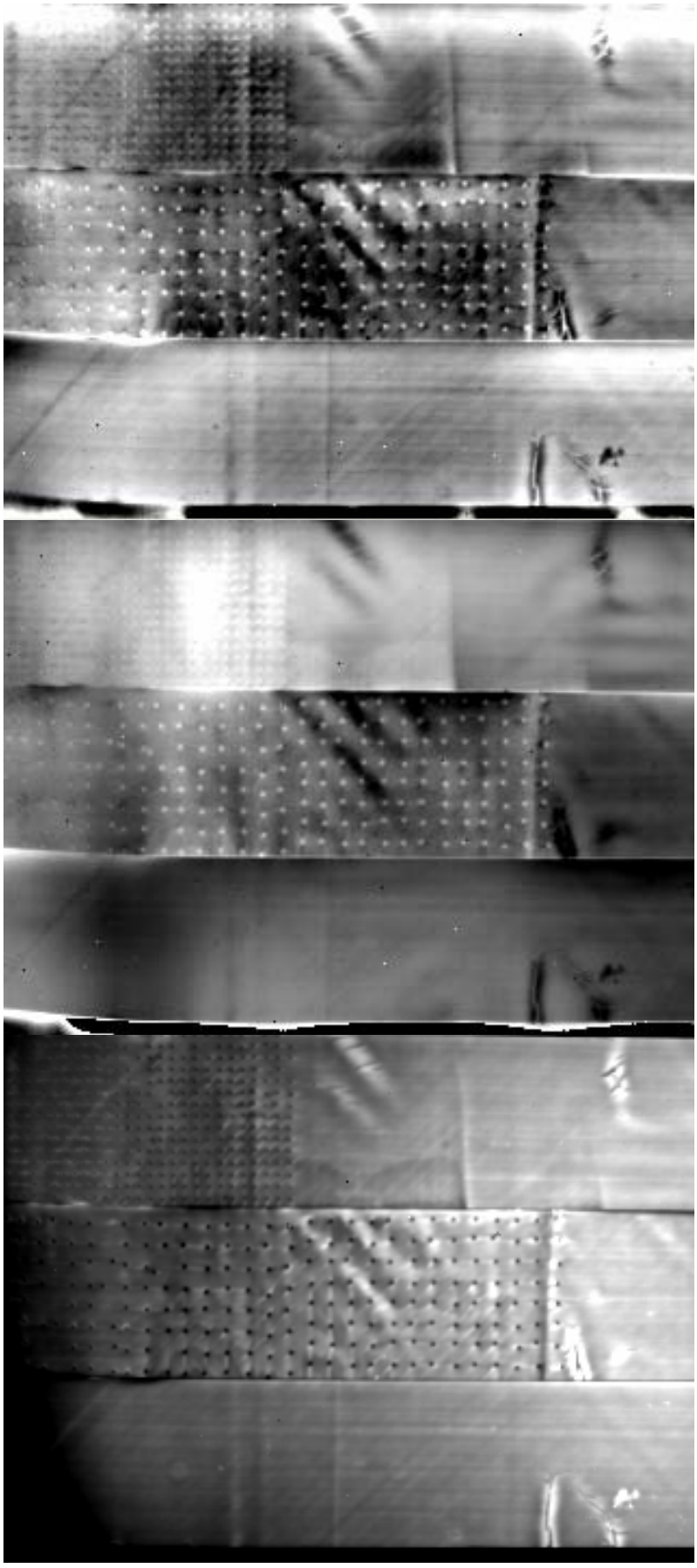

Phase
Frequency 0.05Hz
Periods 5

Phase
Frequency 0.005Hz
Periods 2

Amplitude*
Frequency 0.5Hz
Periods 20

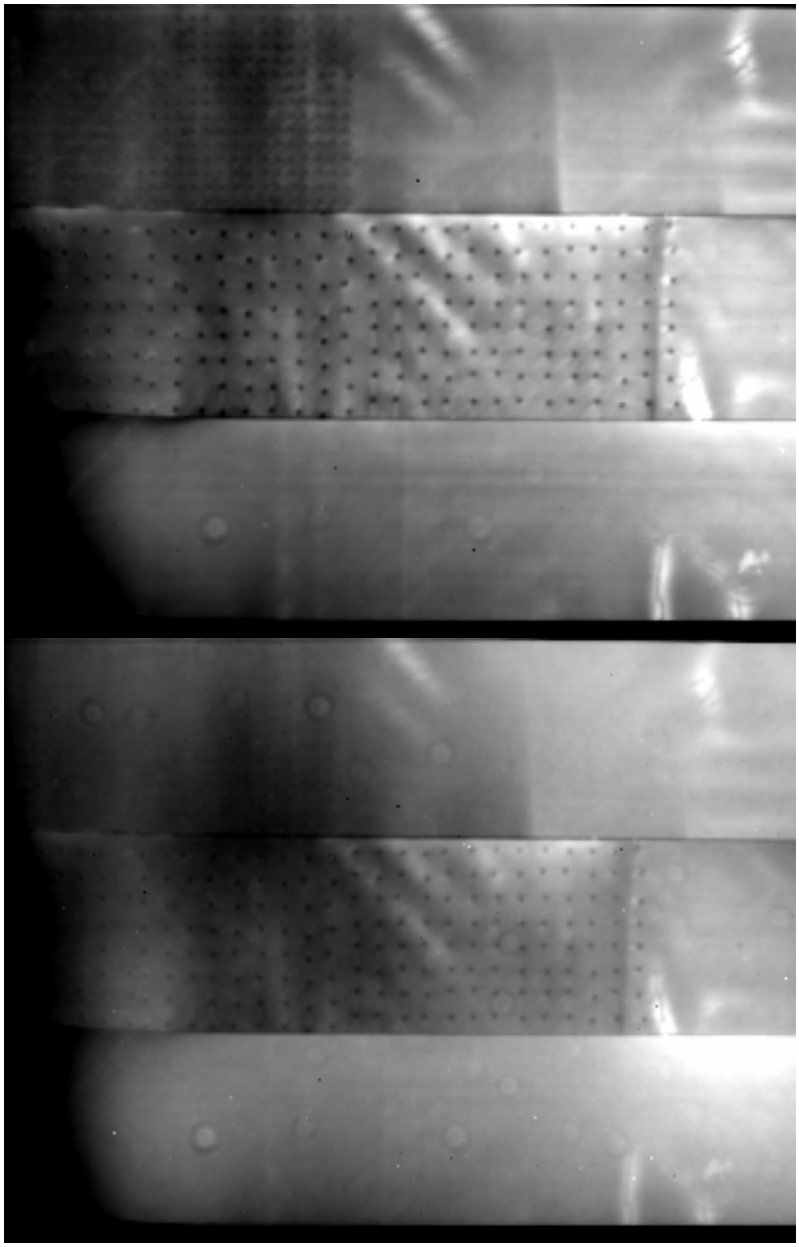

Amplitude*
Frequency 0.05Hz
Periods 5

Amplitude*
Frequency 0.005Hz
Periods 2

Sample: H166-A1-A2-A3

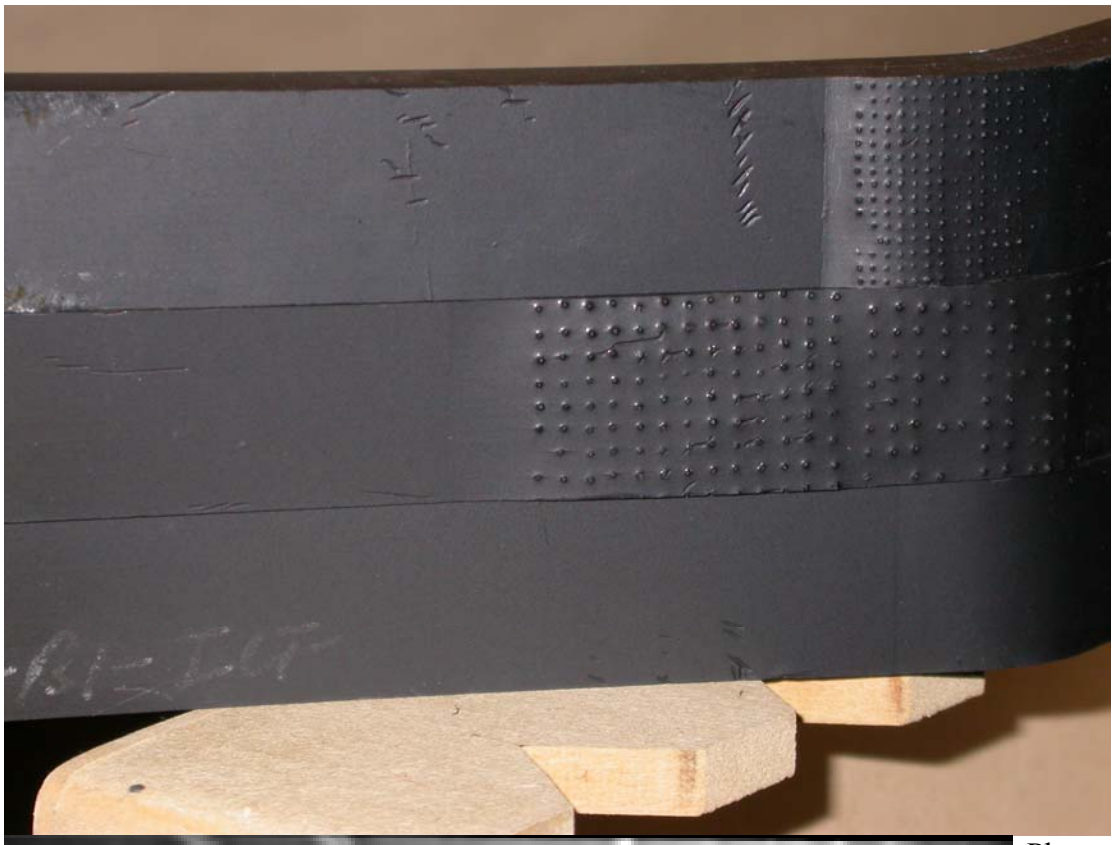

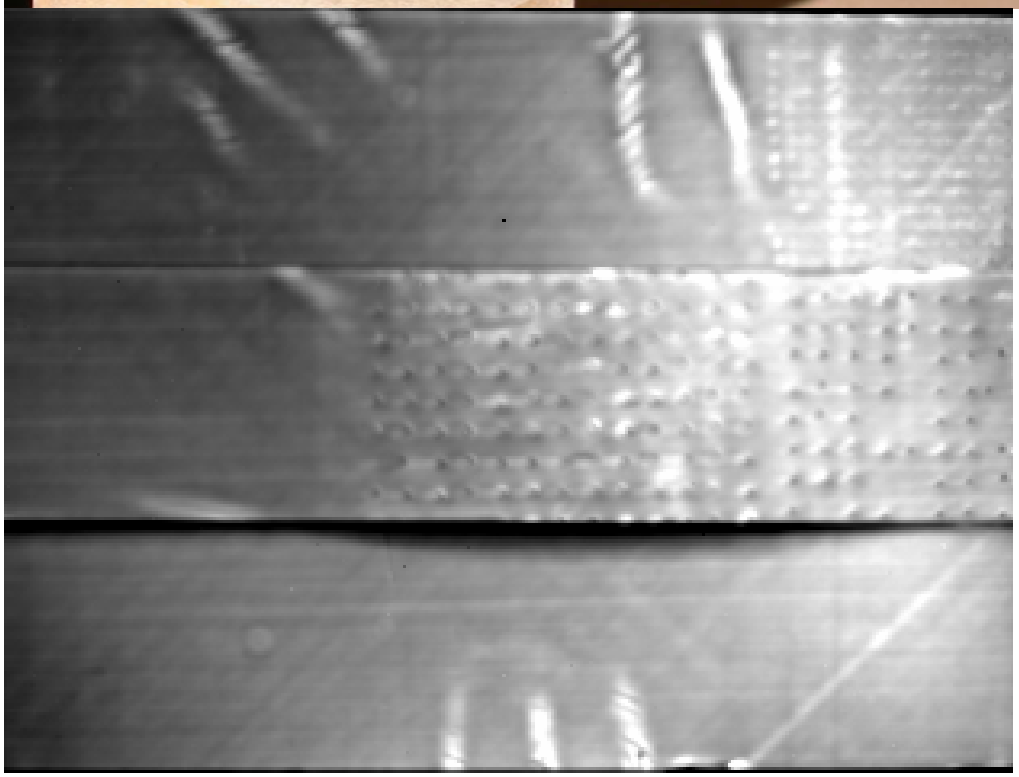

Phase
Frequency 0.5Hz
Periods 20

The distribution of the z-pins is relatively clear, as is the surface and subsurface damage

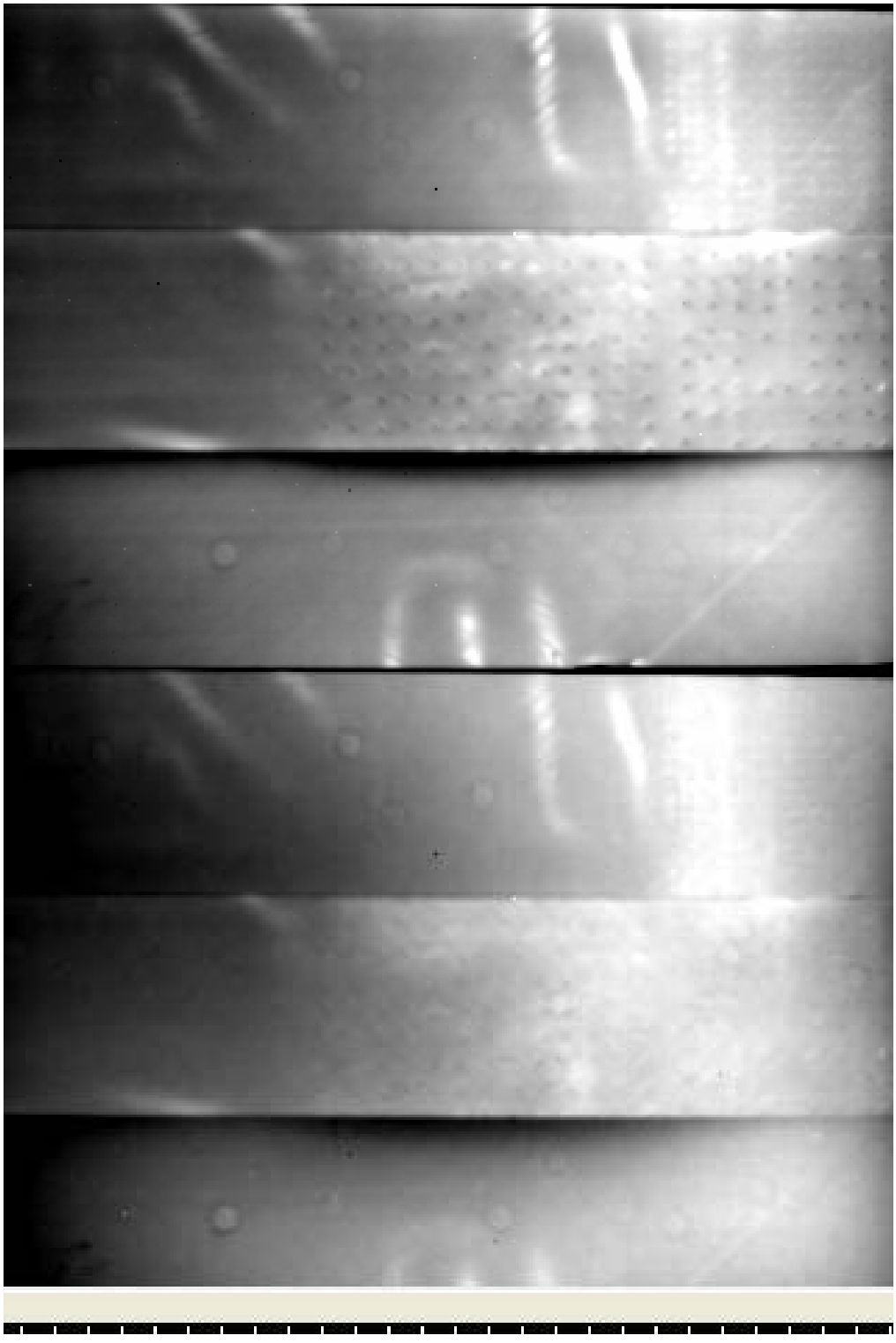

Phase
Frequency 0.05Hz
Periods 5

Phase
Frequency 0.005Hz
Periods 2

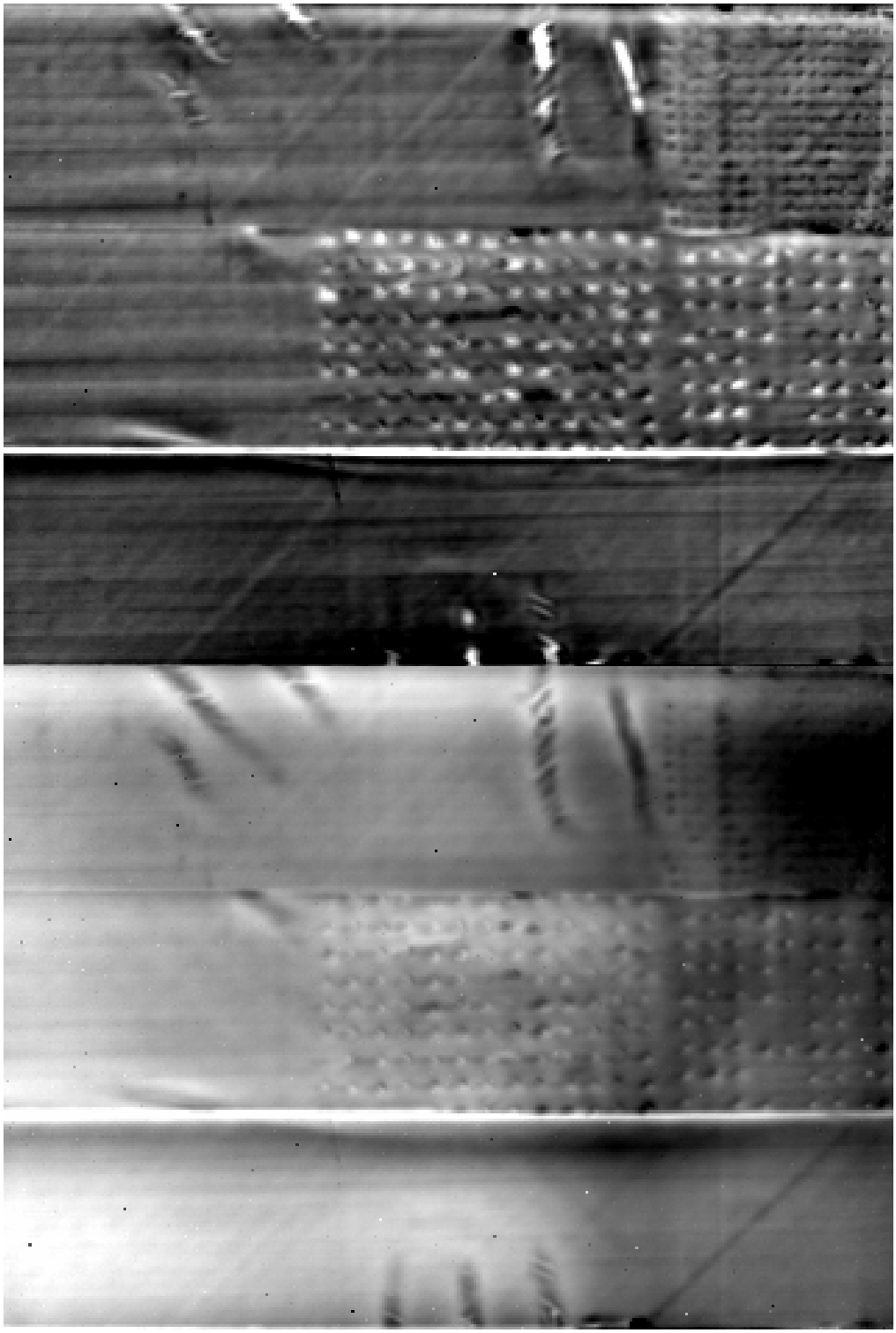

Amplitude*
Frequency 0.5Hz
Periods 20

The distribution of the z-pins is clear, as is the surface and subsurface damage.

Amplitude*
Frequency 0.05Hz
Periods 5

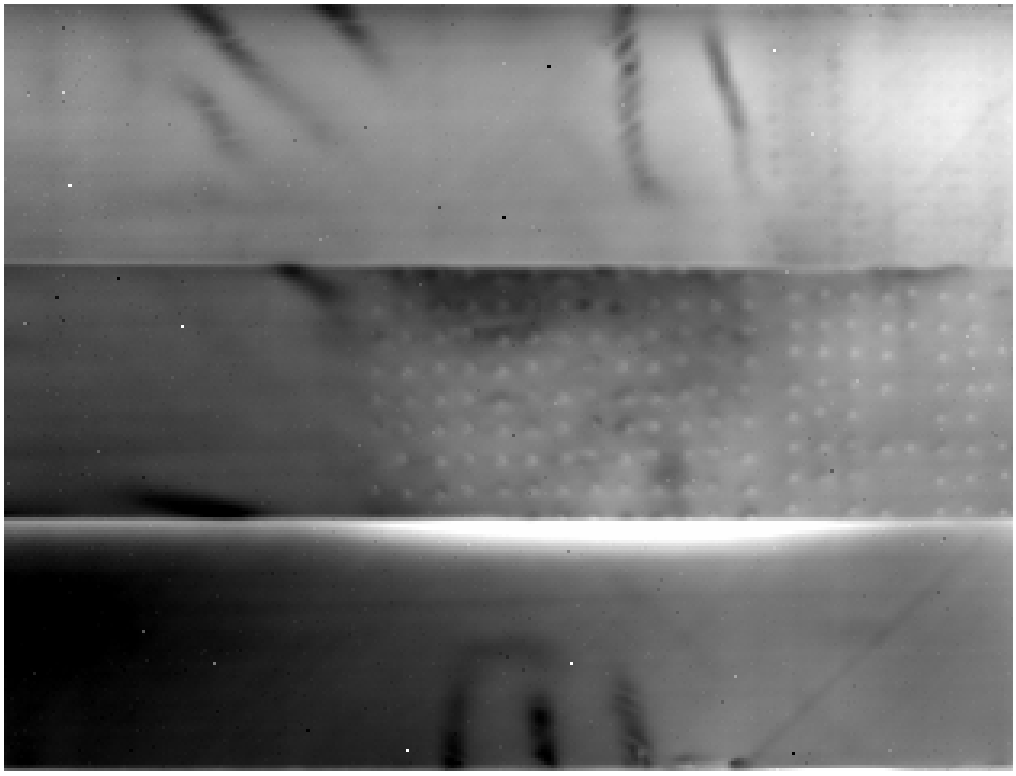

Amplitude*
Frequency 0.005Hz
Periods 2

Sample: H166-A4

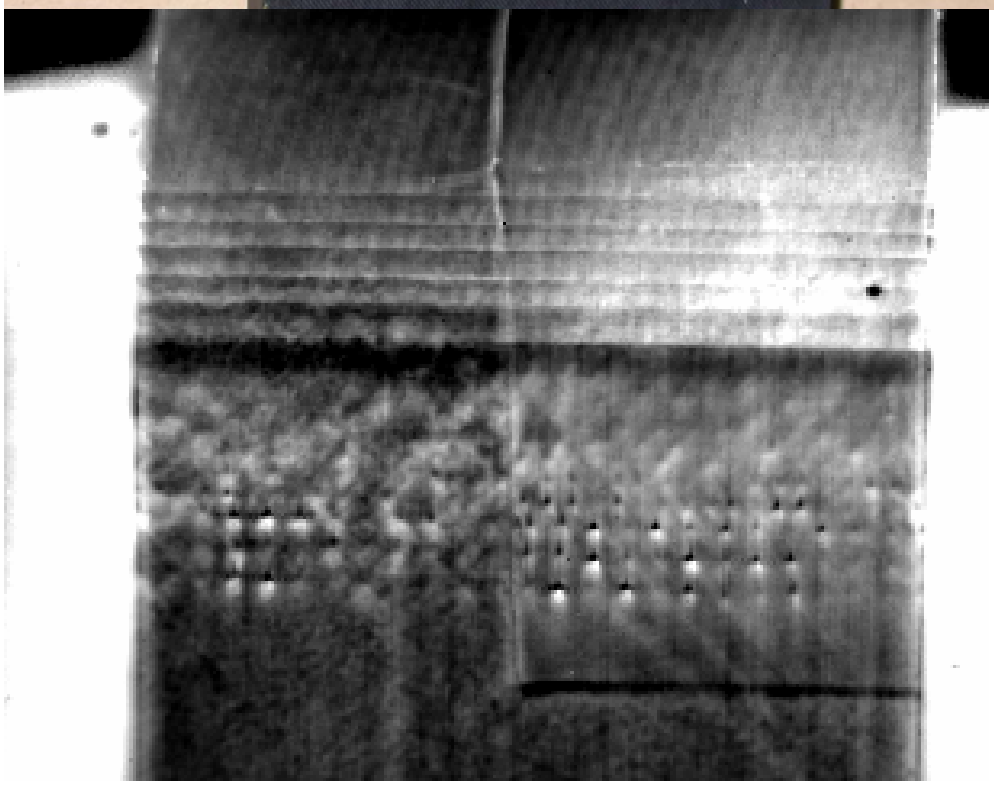

Phase
Frequency 0.5Hz
Periods 20

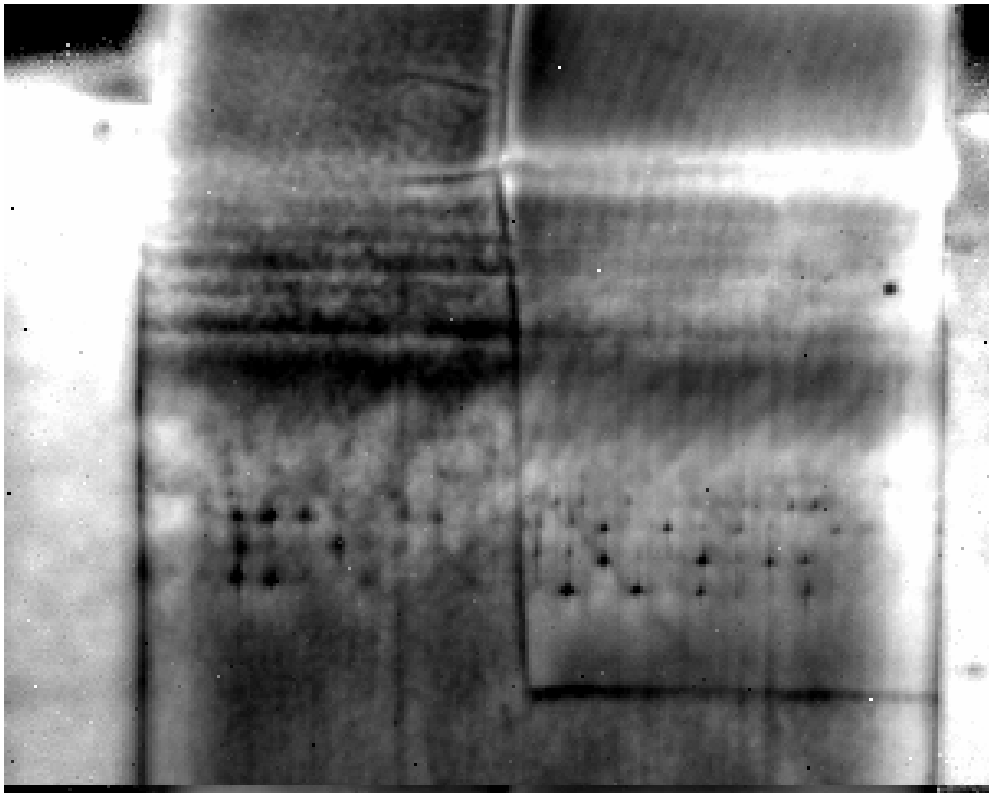

Phase
Frequency 0.05Hz
Periods 5

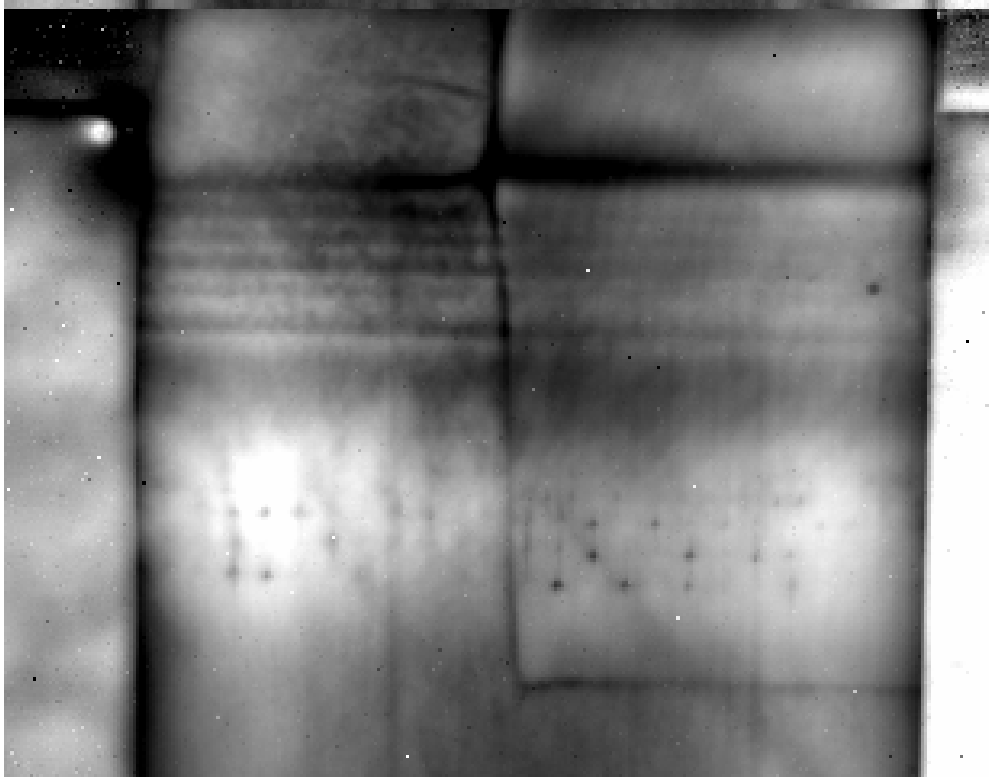

Phase
Frequency 0.005Hz
Periods 2

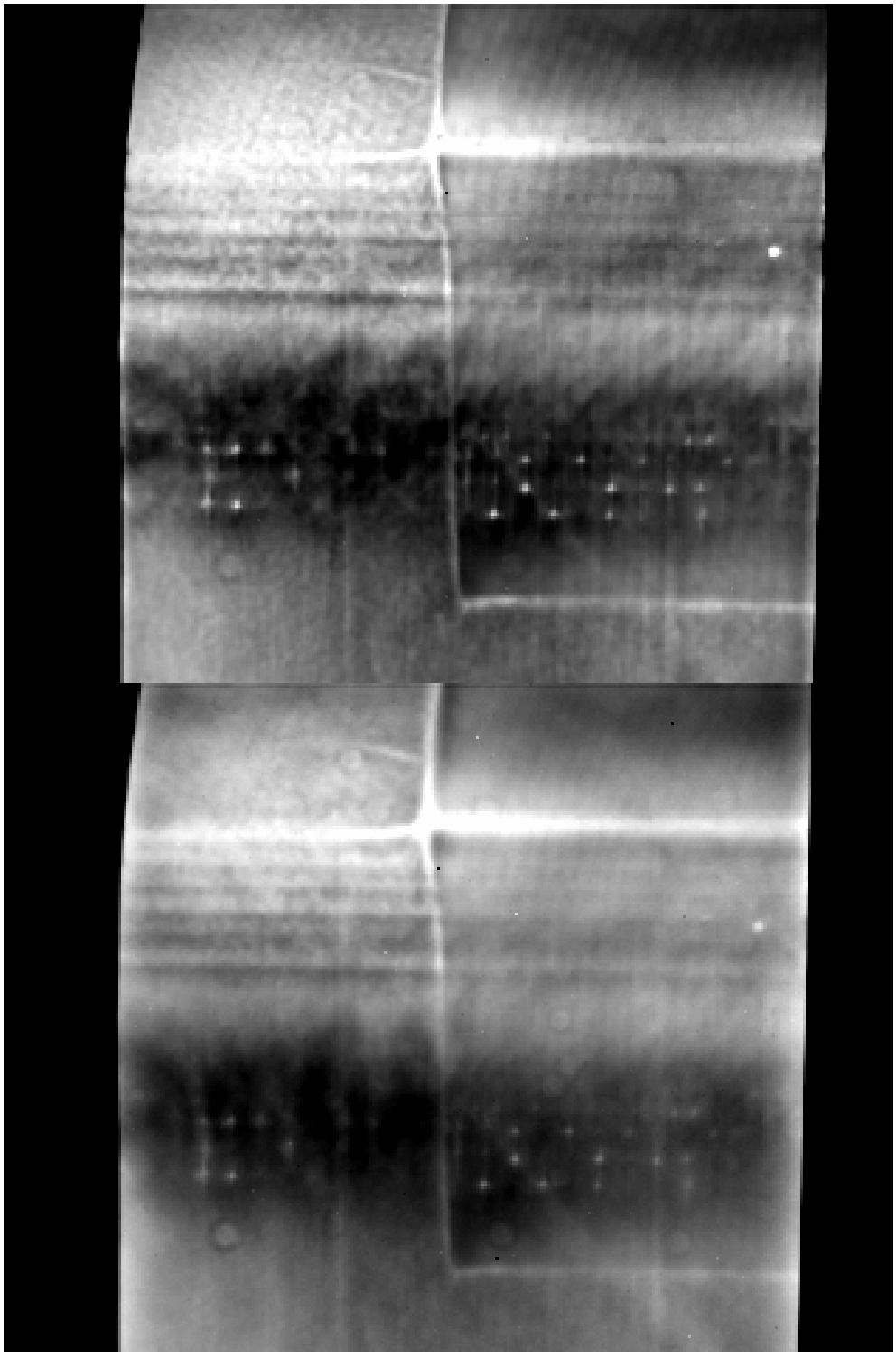

Amplitude*
Frequency 0.5Hz
Periods 20

Amplitude*
Frequency 0.05Hz
Periods 5

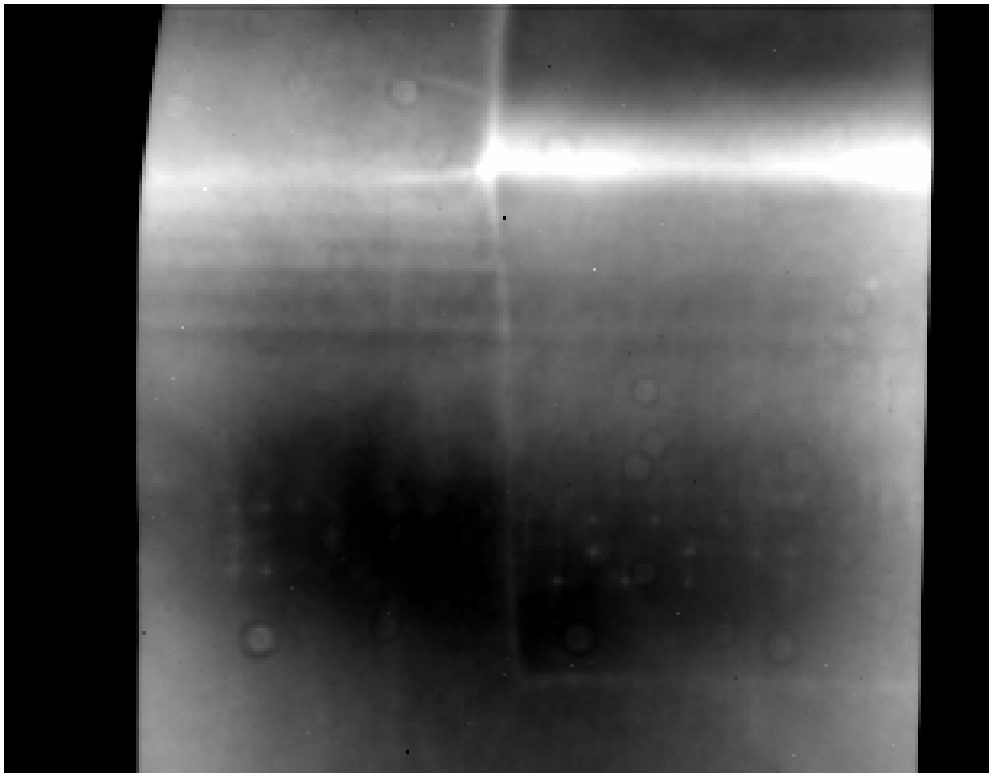

Amplitude*
Frequency 0.005Hz
Periods 2

Sample: H166-A5

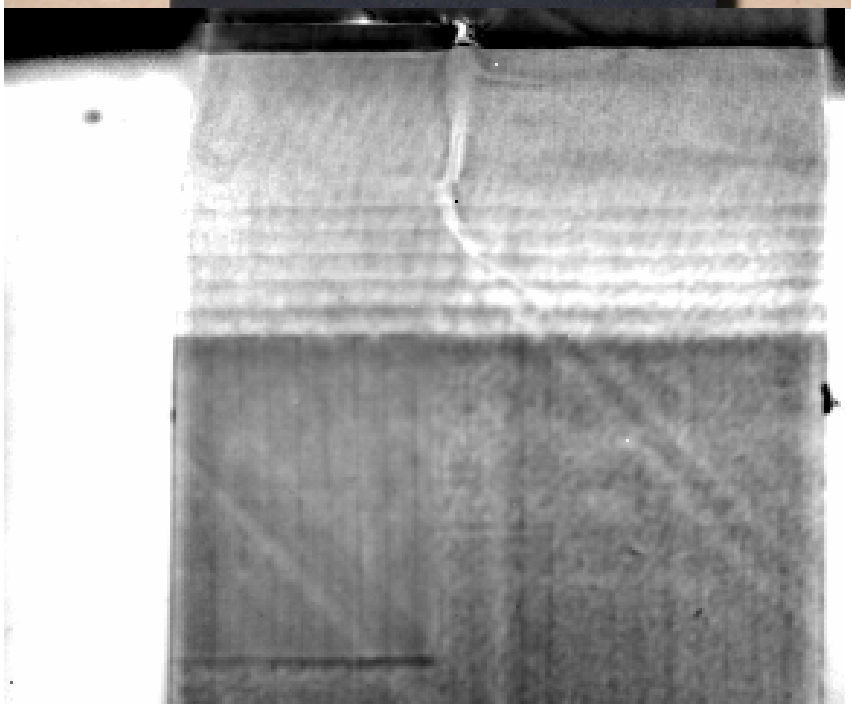

Phase
Frequency 0.5Hz
Periods 20

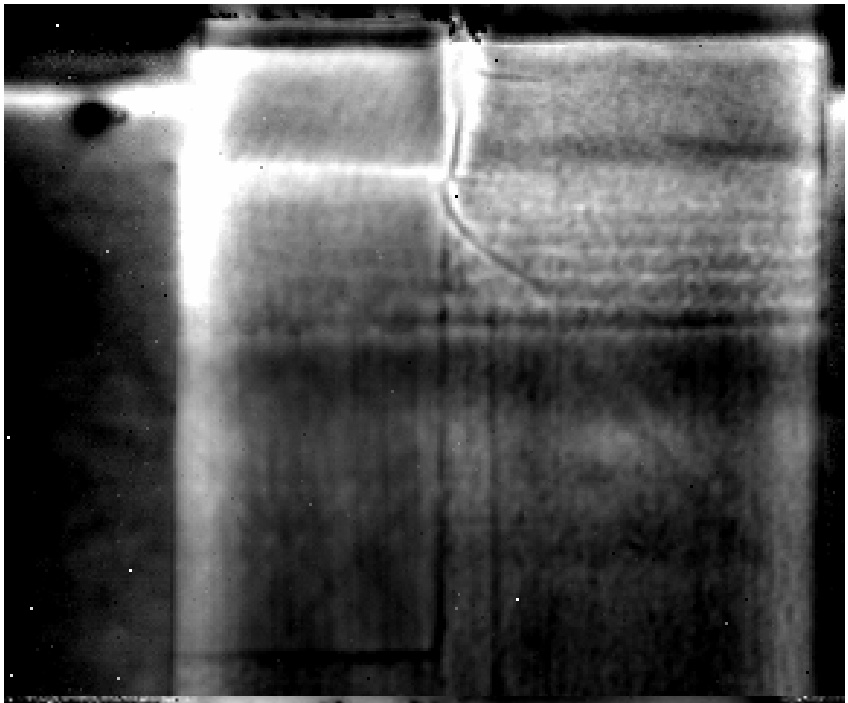

Phase
Frequency 0.05Hz
Periods 5

Note the presence of the embedded optical fibre.

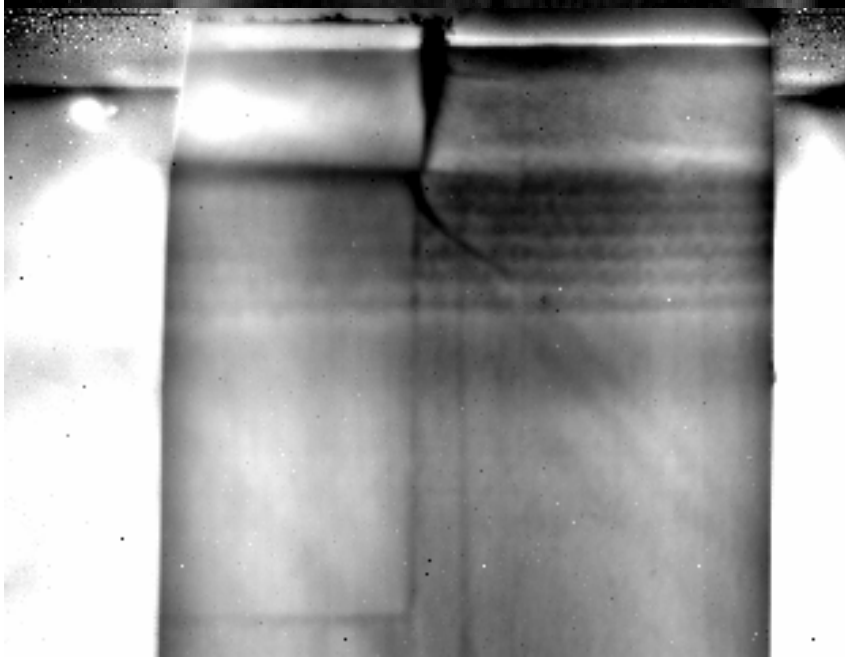

Phase
Frequency 0.005Hz
Periods 2

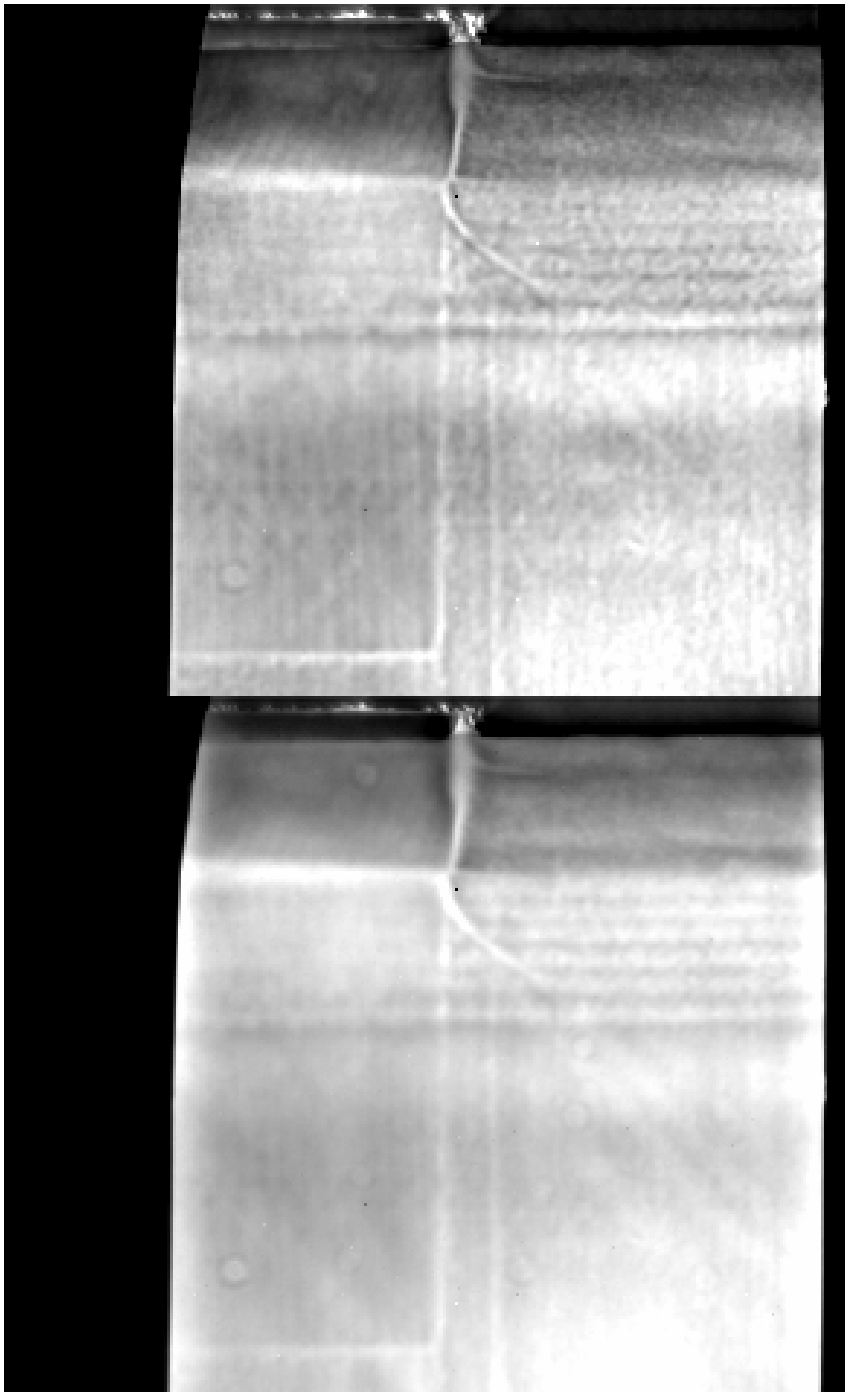

Amplitude*
Frequency 0.5Hz
Periods 20

Amplitude*
Frequency 0.05Hz
Periods 5

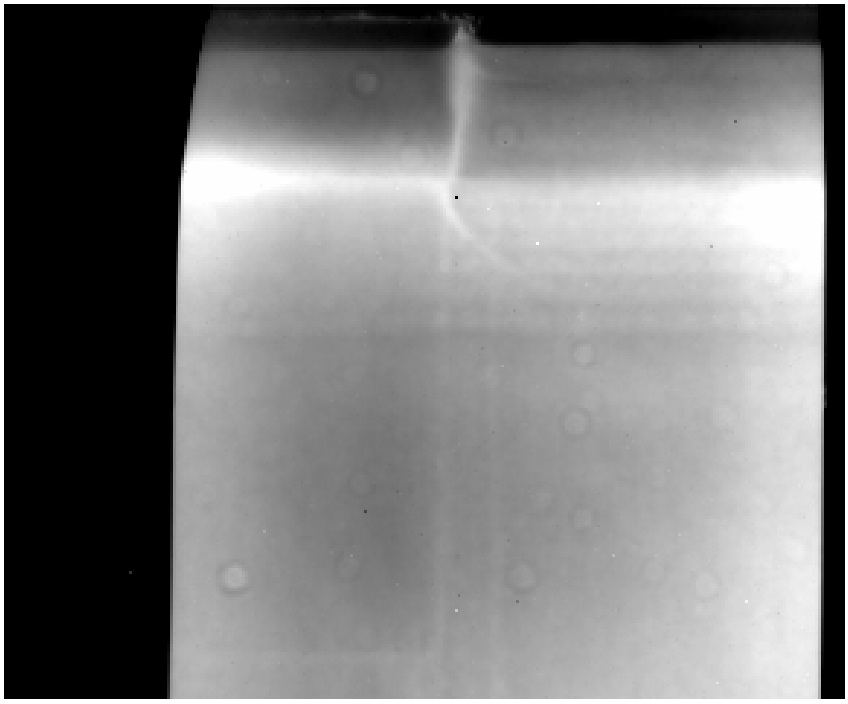

Amplitude*
Frequency 0.005Hz
Periods 2

*Note that the amplitude is measured in an arbitrary unit and not MPa as specified in the images

Discussion

After an exhaustive investigation it would appear that only limited detection of z pins in the supplied composite specimens was possible.

Samples H166-A2 and H166-A3 revealed that detection of the pins was possible only if they were located just below the surface. Examining the images with respect to H166-A2 and H166-A3 one can see areas where the z pins are revealed where they were not visible in the photograph.

Thermographic inspection of other samples has not always revealed the presence of z pins. These observations appear to be consistent with the widely held belief that the radius of the smallest detectable defect should be at least one to two times larger than its depth under the surface [11]. This empirical rule of thumb was developed in relation to observations in pulse or flash thermography for homogeneous isotropic materials. In the present analysis it would appear that the dispersive nature of the composite matrix inhibits the ability to image small structural features. The diameter of the z pins are relatively small and thus z pins any further than the thickness of a ply below the surface become undetectable with this technique.

Examining results of specimens H166-A6-A7-A8 and H166-B1-B2-B3-B4 where images were taken from the flat sides, it is possible to make some observations. For lower frequencies of the order of 0.005Hz the thickness variations of the back surface were visible. These measurements indicate that the present thermographic technique is able to resolve a 2mm variation in a 12mm thick composite specimen.

Conclusion

It would appear that lockin thermography could (just) assess the presence and distribution of the z pins in the present composite structures. It was also possible to detect thickness variations specimens that were approximately 12 mm thick.

Reference:

1. X. Maldague, F. Galmiche, and A. Ziadi, "Advances in Pulsed Phase Thermography," *Infrared Physics and Technology*, Vol. 43, No. 3-5, pp. 175, 2002.
2. G. Busse, D. Wu, and W. Karpen, "Thermal Wave Imaging with Phase Sensitive Modulated Thermography," *Journal of Applied Physics*, Vol. 71, No. 8, pp. 3962-3965, 1992.
3. C. Meola, G. M. Carlomagno, and L. Giorleo, "Geometrical Limitations to Detection of Defects in Composites by Means of Infrared Thermography," *Journal of Nondestructive Evaluation*, Vol. 23, No. 4, pp. 125, 2004.
4. B. S. Wong, C. G. Tui, W. Bai, P. H. Tan, B. S. Low, and K. S. Tan, "Thermographic Evaluation of Defects in Composite Materials," *Insight: Non-Destructive Testing and Condition Monitoring*, Vol. 41, No. 8, pp. 504, 1999.

5. A. Dillenz, G. Busse, and D. Wu, "Ultrasound Lockin Thermography: Feasibilities and Limitations," *Proceedings of the SPIE - The International Society for Optical Engineering*, Vol. 3827, pp. 10, 1999.
6. J. Fourier, "Theorie Du Mouvement De La Chaleur Dans Les Corps Solides 1ere Partie," *Momoires de l'Academie des Sciences*, Vol. 4, pp. 185-555, 1824.
7. A. J. Angstrom, "New Method of Determining the Thermal Conductibility of Bodies," *Phil. Mag.*, Vol. 25, pp. 130-142, 1863.
8. G. Busse, "Nondestructive Evaluation of Polymer Materials," *NDT & E International*, Vol. 27, No. 5, pp. 253, 1994.
9. G. Busse, "Imaging with the Optoacoustic Effect," Vol. 12, No. 3, pp. 149, 1980.
10. G. Busse, "Optoacoustic Phase Angle Measurement for Probing a Metal," *Applied Physics Letters*, Vol. 35, No. 10, pp. 759, 1979.
11. X. Maldague, "Introduction to NDT by Active Infrared Thermography," *Materials Evaluation*, Vol. 6, No. 9, pp. 1060 -1073, 2002.

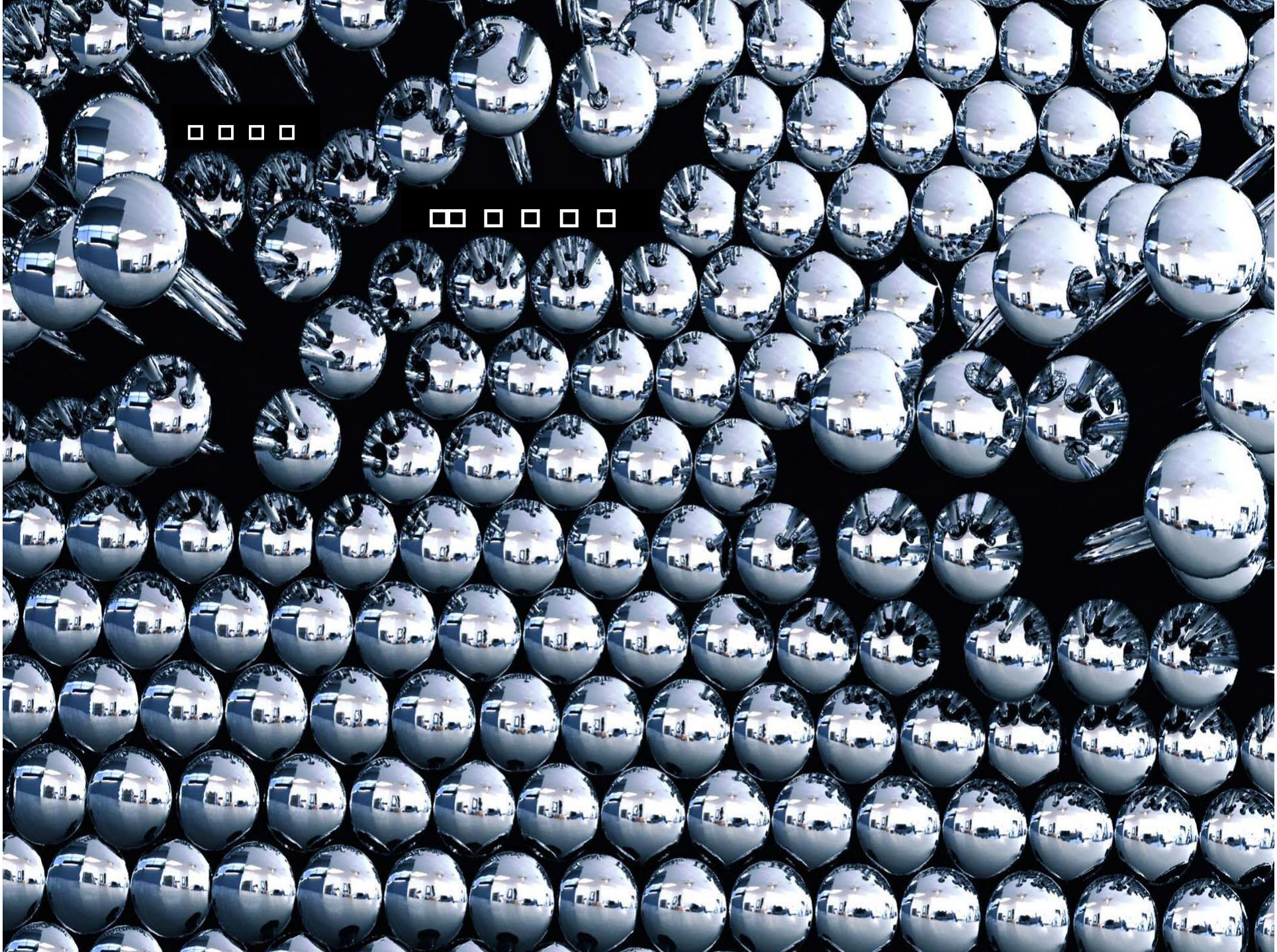

[illegible]

- Research Partners
  - Monash University
  - Co-operative Research Council – Advanced Composites Structures
- Supervisors
  - Professor R. Jones [Monash]
  - Dr M. Bannister [CRC-ACS]
- Research Task
  - In fulfillment of PhD [Mechanical Eng]

□ □ □ □ □ □ □□ □□□ □ □□□ □ □□□ □

- INTRODUCTION
- RESEARCH JUSTIFICATION
- METHODOLOGY
- RESULTS
- CONCLUSIONS
- FUTURE WORK

- Infrared Thermography (IRT) is a thermal Non-Destructive Inspection Technique.
- It is used primarily in thin structures.
- Hence its applicability in inspecting CFRP.
- It can be used to detect typical composite sub-surface defect types and characteristics.
- Advantage of broad area scanning for defects, delaminations and material disbonding.

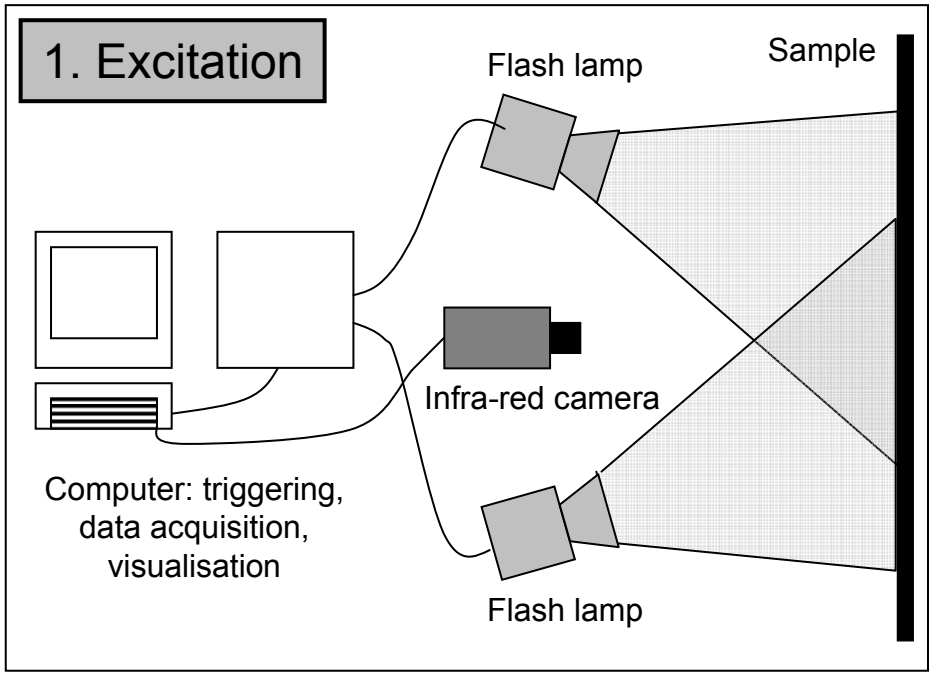
1. Excitation
Flash lamp
Sample
Infra-red camera
Computer: triggering,
data acquisition,
visualisation
Flash lamp

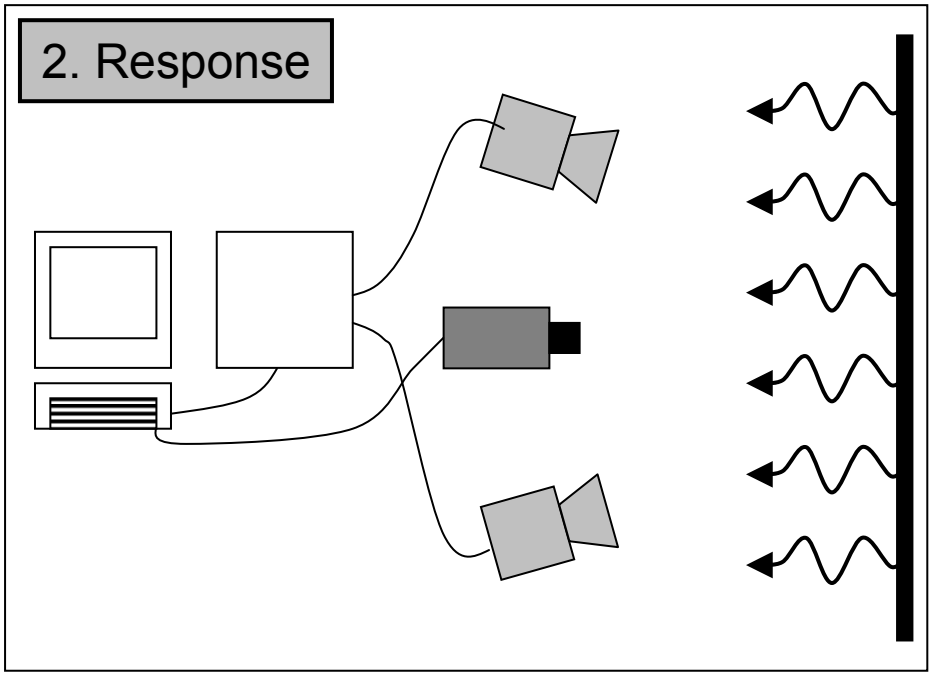
2. Response

- Direction of arrows represent passage of thermal energy.
- Thermal impedance alters surface temperature contrast.

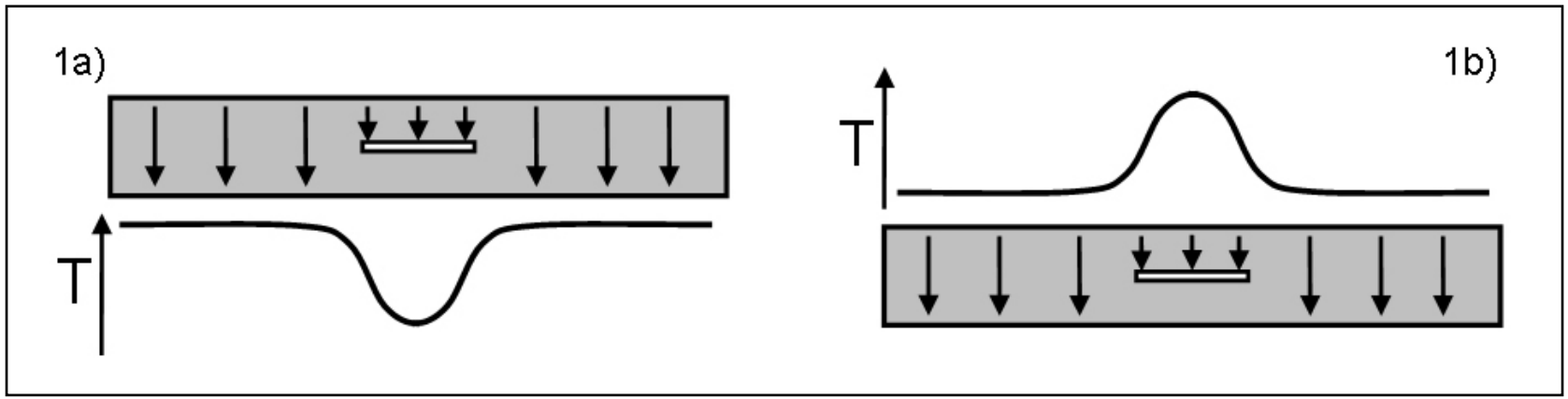

0.315"
0.222"
0.090"
E1F3 No 1

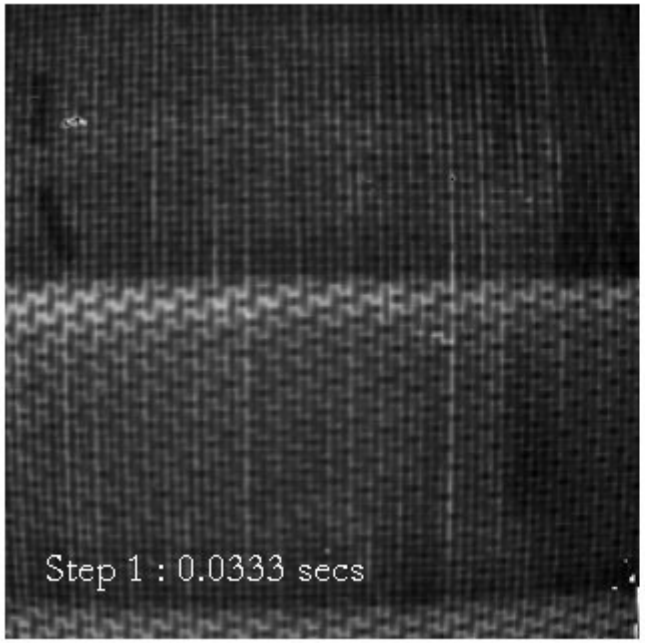
Step 1 : 0.0333 secs

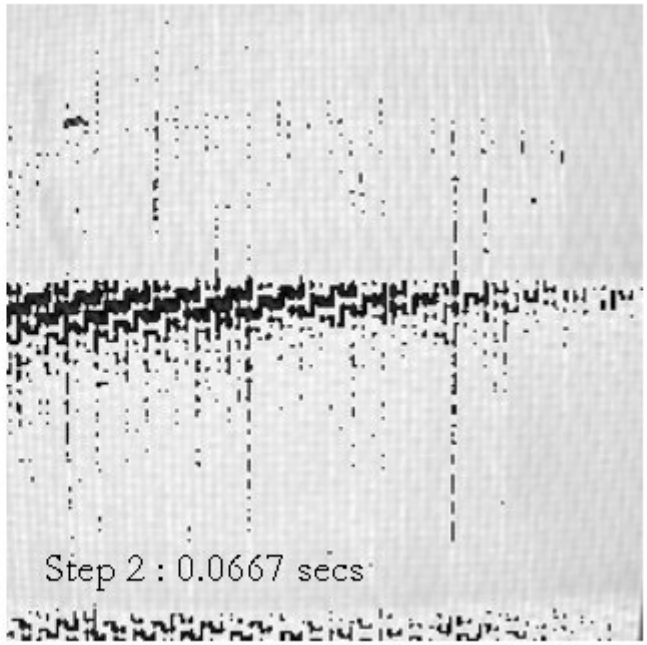
Step 2 : 0.0667 secs

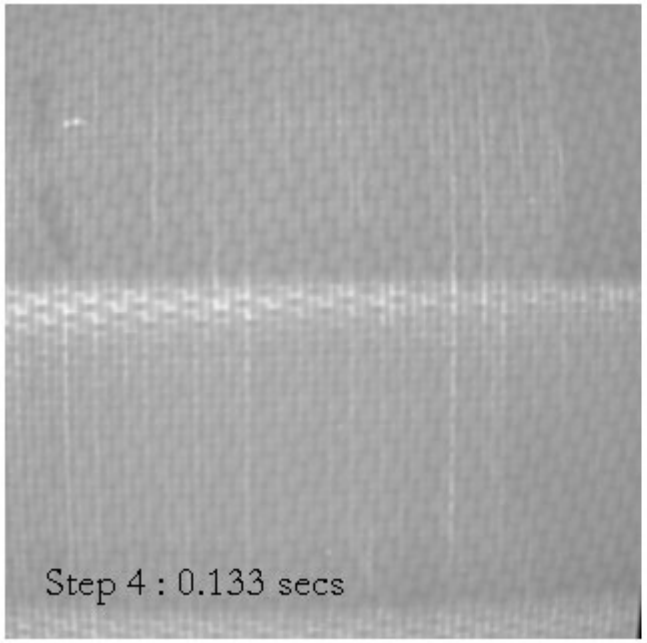
Step 4 : 0.133 secs

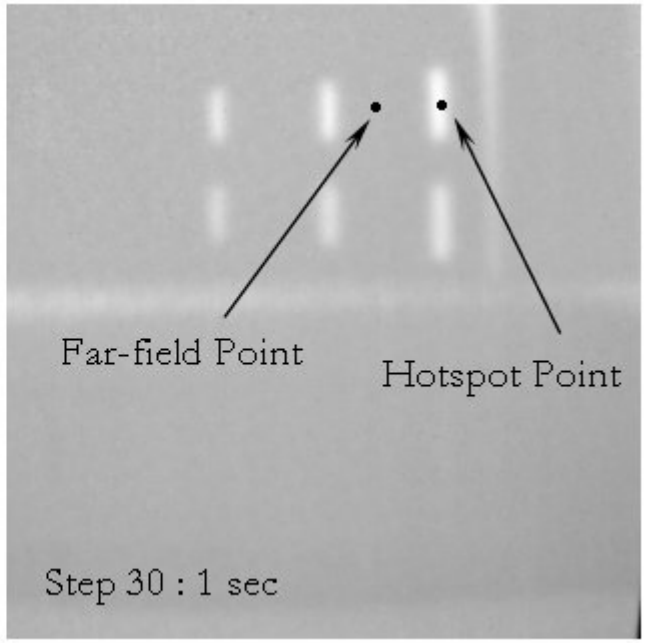
Far-field Point
Hotspot Point
Step 30 : 1 sec

- IRT provides a cost-effective flexible NDI scanning technique.
- Extensive experimental and 2D numerical work completed on flat panel cases.
- Response characteristics and trends obtained for these cases.
- Adequate 3-dimensional finite element analysis has not been performed.
- Numerical relationships are limited to 2-D normal delamination/disbond configurations.
- The investigation of 3D thermal mechanisms is limited due to lack of 3D numerical work.

- Project concerns the development of a numerical process that can predict defect detectability through FEA.
- Important given the increasing use of complex structures in aerospace components.
- The need to establish FE relationships is required to predict damage parameters.
- There exist many types of thermography. This project is focused on only one; flash thermography.

- FE Feasibility Study
- Precursor
  - Calibration Study
  - FBH Validation
- Numerical Method [Delams]

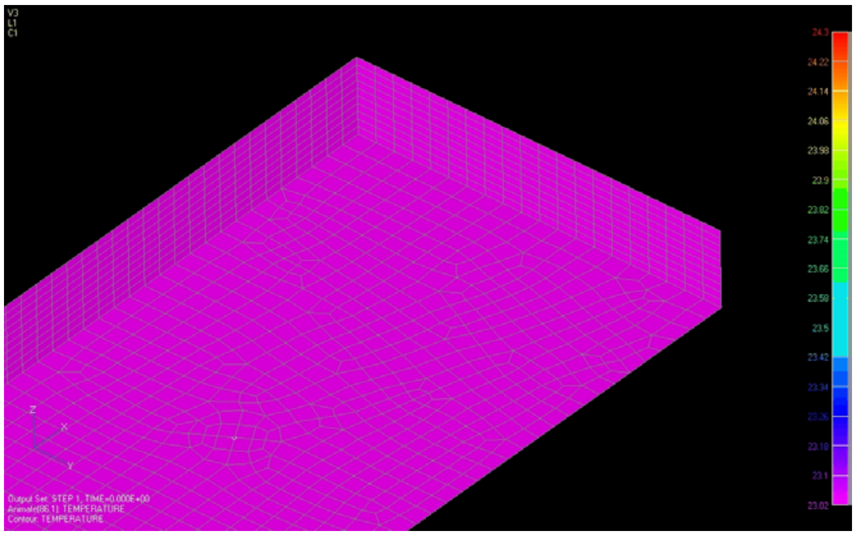
V3
L1
C1
24.3
24.22
24.14
24.06
23.98
23.9
23.82
23.74
23.66
23.58
23.5
23.42
23.34
23.1
23.02
Z
X
Y
Output Set: STEP 1, TIME=0.000E+00
Animate(86.1): TEMPERATURE
Contour: TEMPERATURE

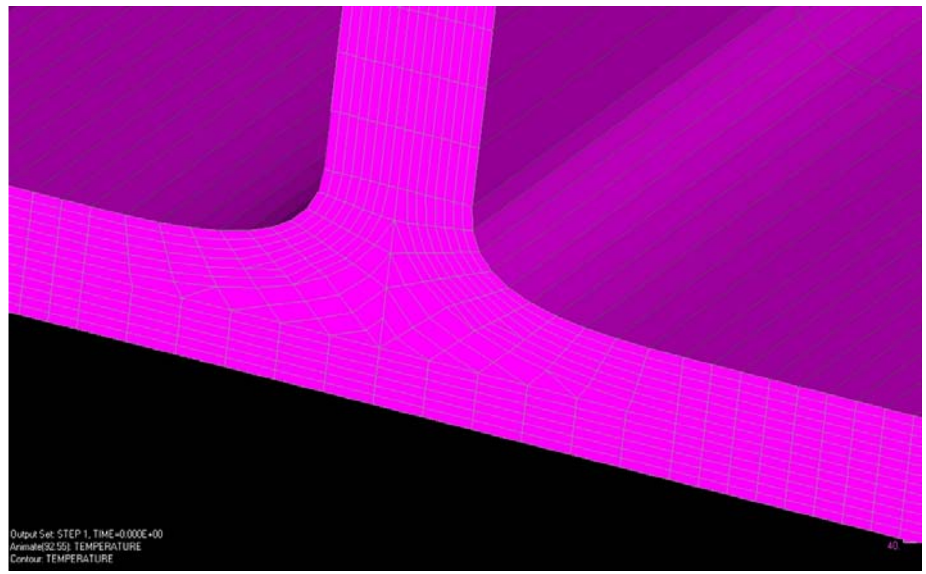
Output Set: STEP 1, TIME=0.000E+00
Animate(92.55): TEMPERATURE
Contour: TEMPERATURE

- Finite Element solution behaves as it should but the thermal response must be calibrated.
- Heat capacity and conductivity are the thermal properties that can be altered.
- Coupled they are considered thermal diffusivity.
- So by obtaining correct diffusivity a calibrated model could be assumed and prediction capabilities implemented in models.

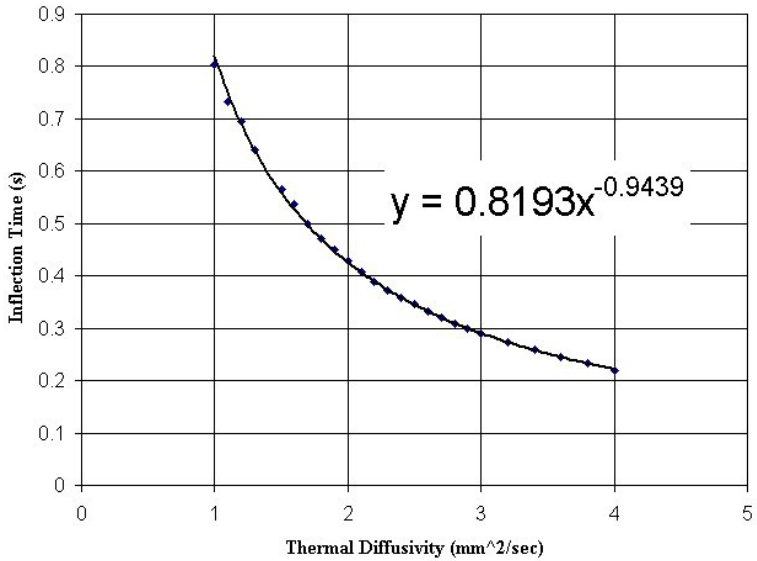
Inflection Time (s)
Thermal Diffusivity (mm^2/sec)
y = 0.8193x^-0.9439

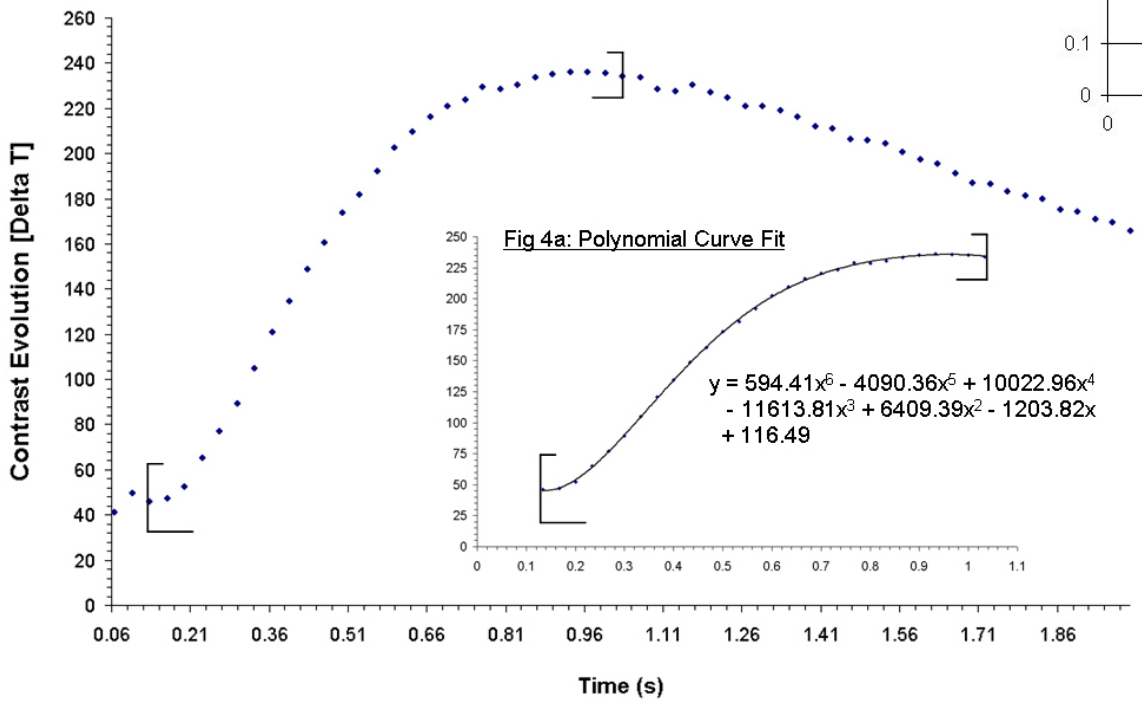
Contrast Evolution [Delta T]
Time (s)
Fig 4a: Polynomial Curve Fit
y = 594.41x^6 - 4090.36x^5 + 10022.96x^4 - 11613.81x^3 + 6409.39x^2 - 1203.82x + 116.49

[illegible]

[illegible]

- Inclusion of lateral heat flow
- No through thickness heat flow.
- No ‘around thickness’ heat flow.
- How much do these factors affect a delamination model?

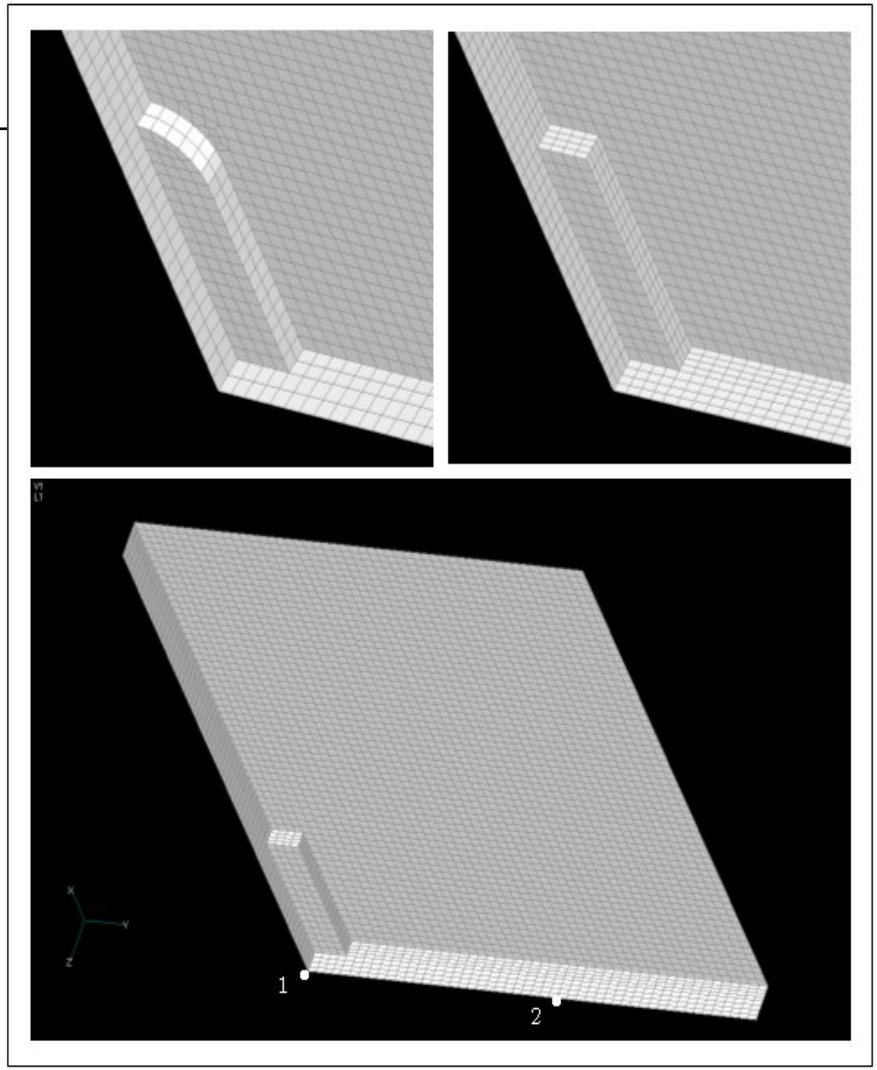

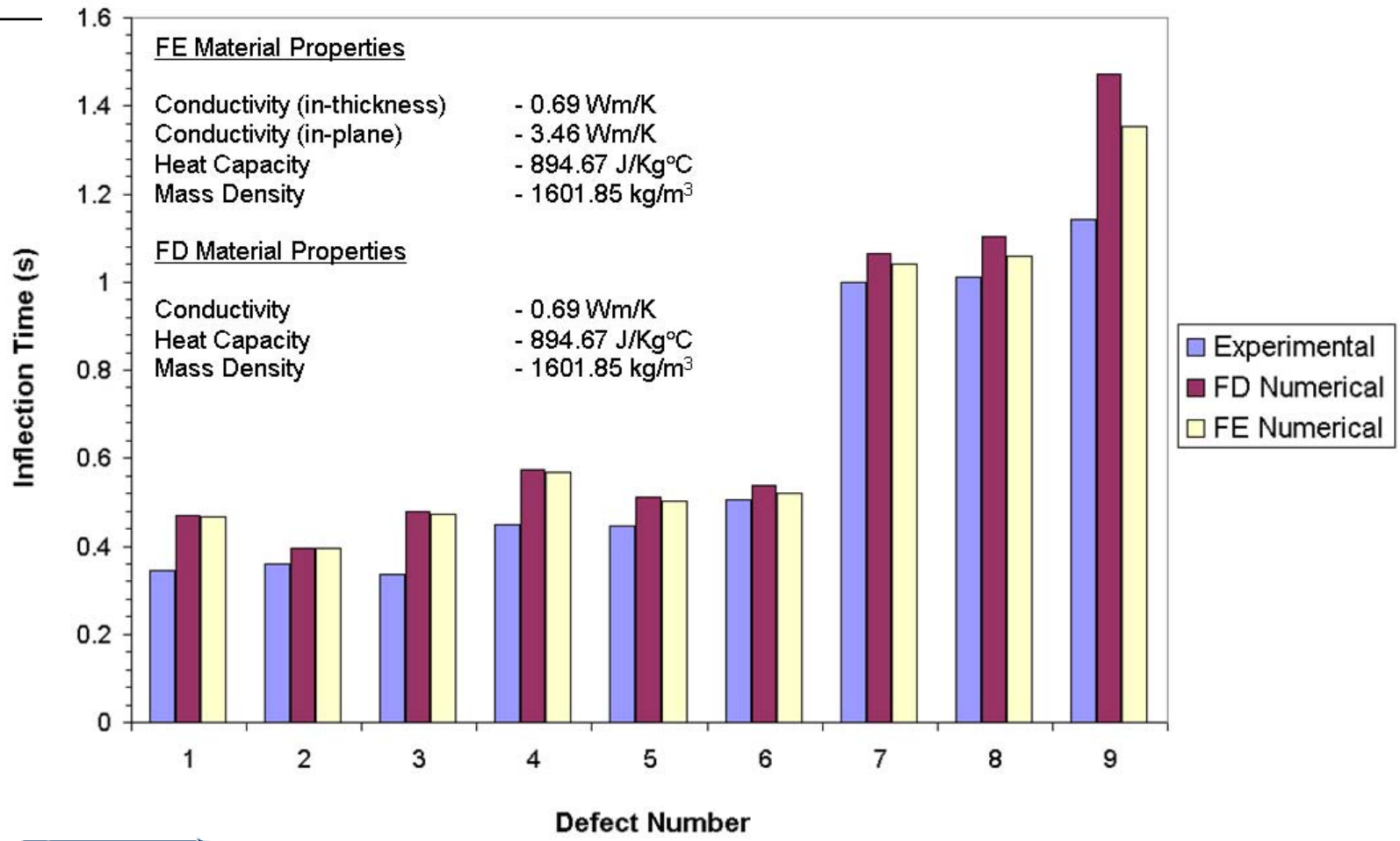
FE Material Properties
Conductivity (in-thickness) - 0.69 Wm/K
Conductivity (in-plane) - 3.46 Wm/K
Heat Capacity - 894.67 J/Kg°C
Mass Density - 1601.85 kg/m3
FD Material Properties
Conductivity - 0.69 Wm/K
Heat Capacity - 894.67 J/Kg°C
Mass Density - 1601.85 kg/m3
Inflection Time (s)
Defect Number
Experimental
FD Numerical
FE Numerical
0
0.2
0.4
0.6
0.8
1
1.2
1.4
1.6
1
2
3
4
5
6
7
8
9

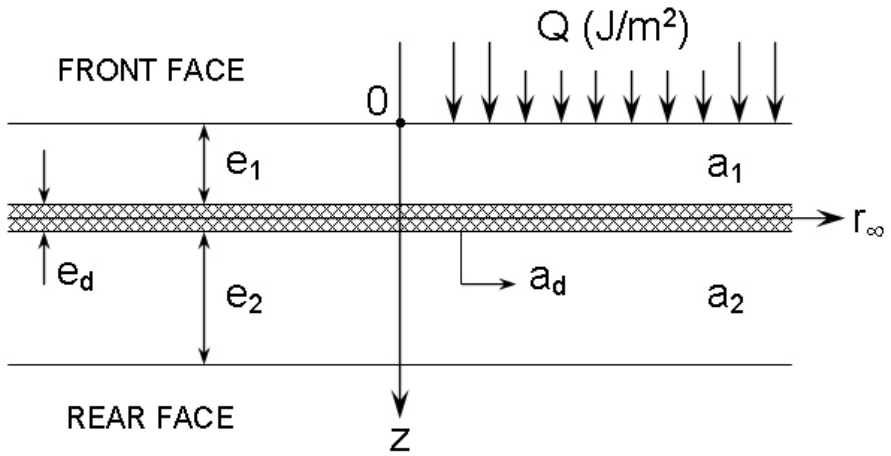

Q	Thermal Flux
a	Diffusivity
e	Thickness
r_∞	Infinite Radial Extent

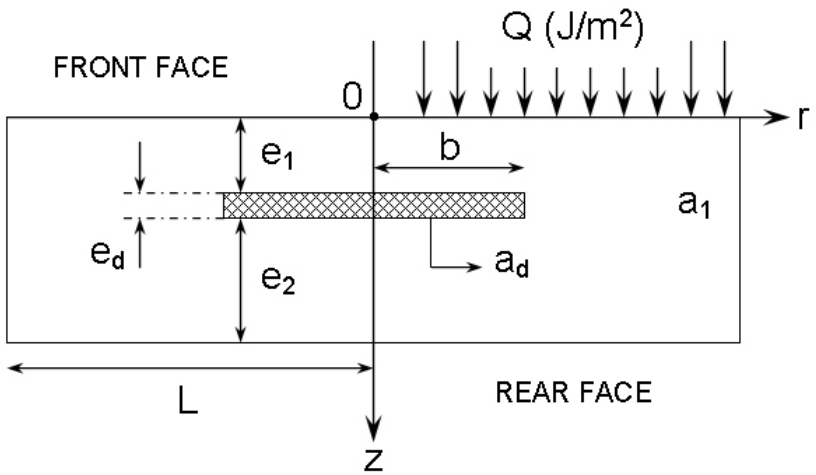

Q	Thermal Flux
a	Diffusivity
e	Thickness
r	Radial Extent
b	Defect Radius
L	Laminate Radius

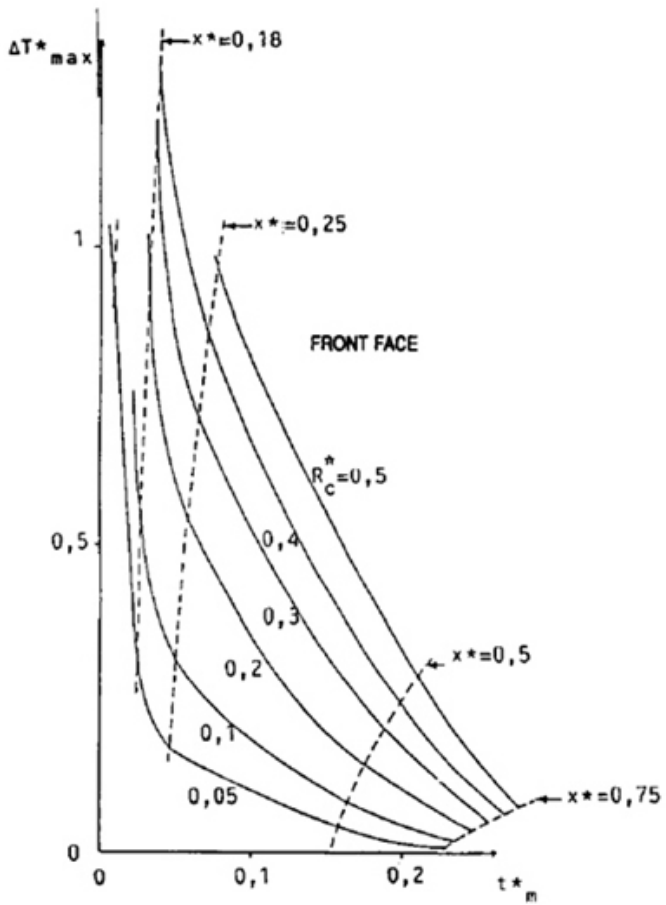

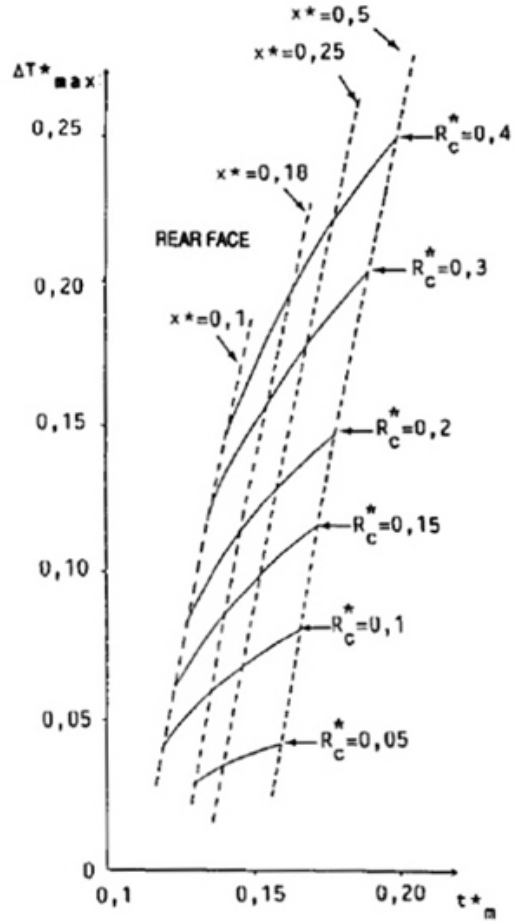

x^* = e_1 / e
R_c^* = R_c / (e / λ)
R_c = (e_d / λ_d)

where:
x^* = reduced depth
e_1 = defect depth
e = slab thickness
e_d = defect thickness
R_c^* = reduced resistance
R_c = contact resistance
λ = slab conductivity
λ_d = defect conductivity

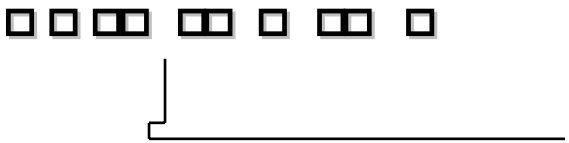

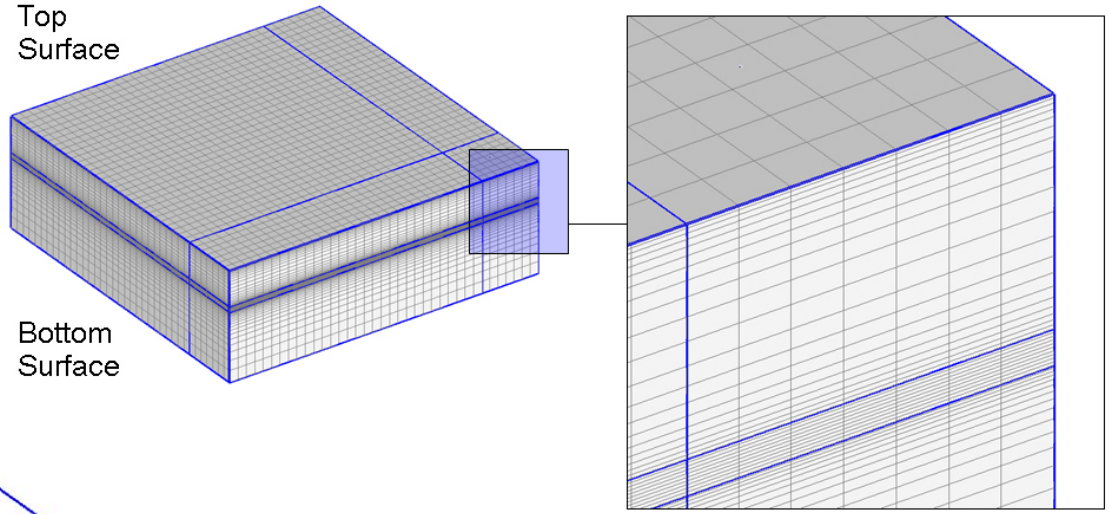
Top
Surface
Bottom
Surface

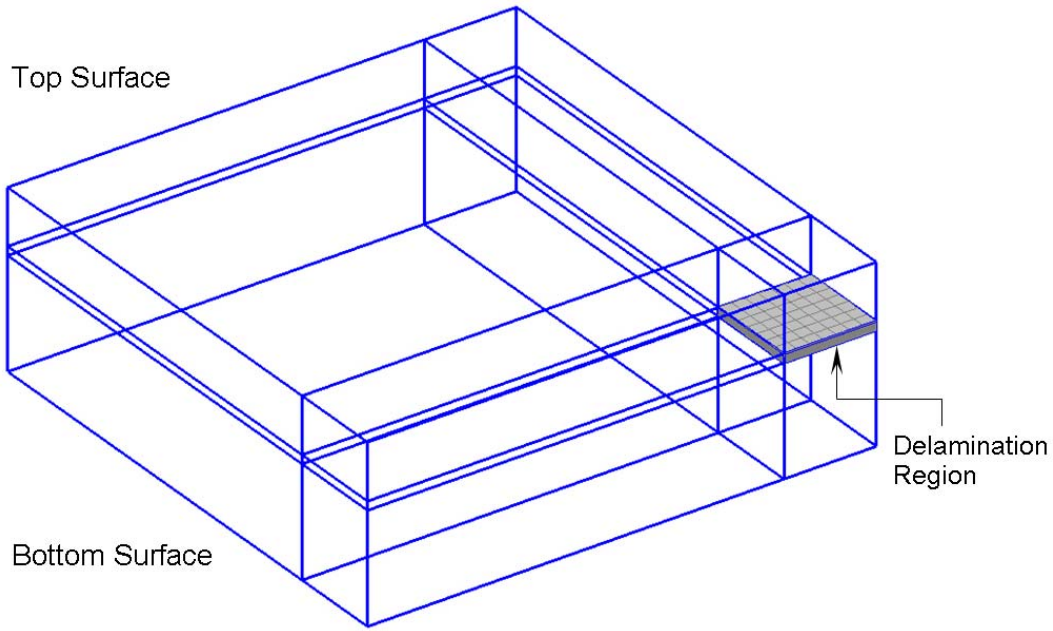
Top Surface
Delamination
Region
Bottom Surface

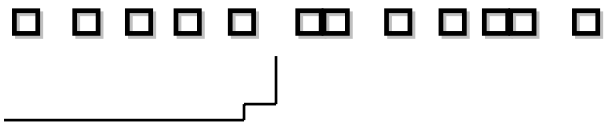

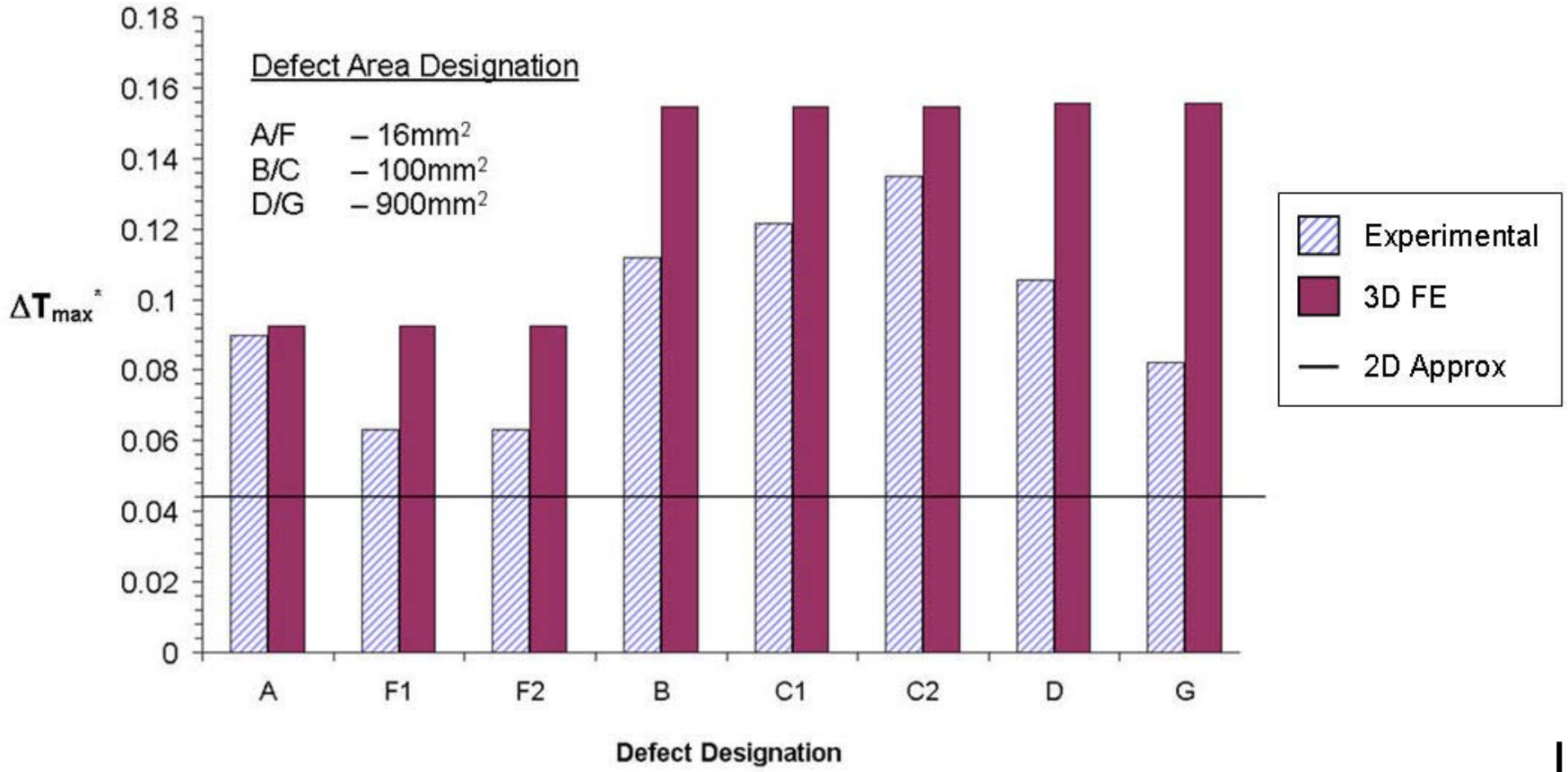
Defect Area Designation
A/F – 16mm²
B/C – 100mm²
D/G – 900mm²
ΔTmax*
0.18
0.16
0.14
0.12
0.1
0.08
0.06
0.04
0.02
0
A
F1
F2
B
C1
C2
D
G
Defect Designation
Experimental
3D FE
2D Approx

[illegible]

[illegible]

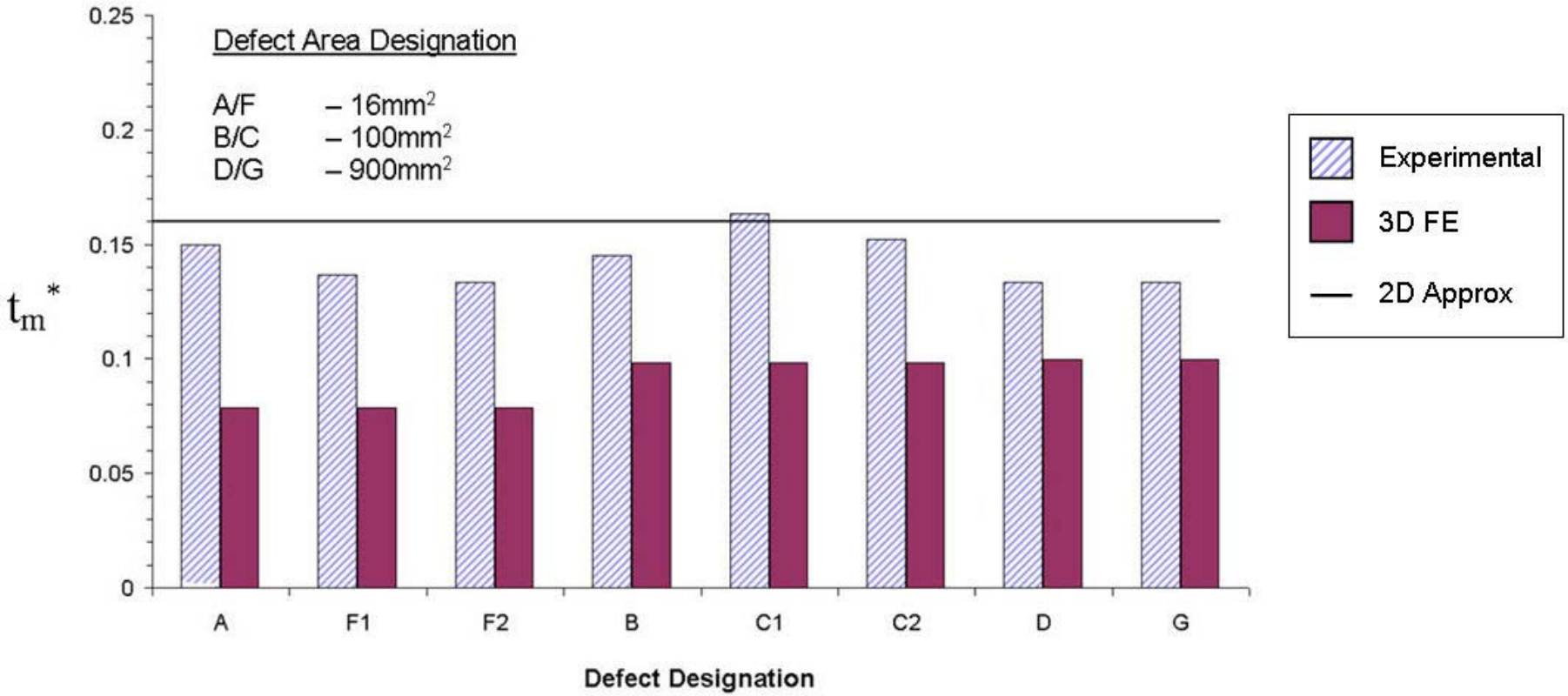
Defect Area Designation
A/F – 16mm²
B/C – 100mm²
D/G – 900mm²
0.25
0.2
0.15
0.1
0.05
0
t_m*
A
F1
F2
B
C1
C2
D
G
Defect Designation
Experimental
3D FE
2D Approx

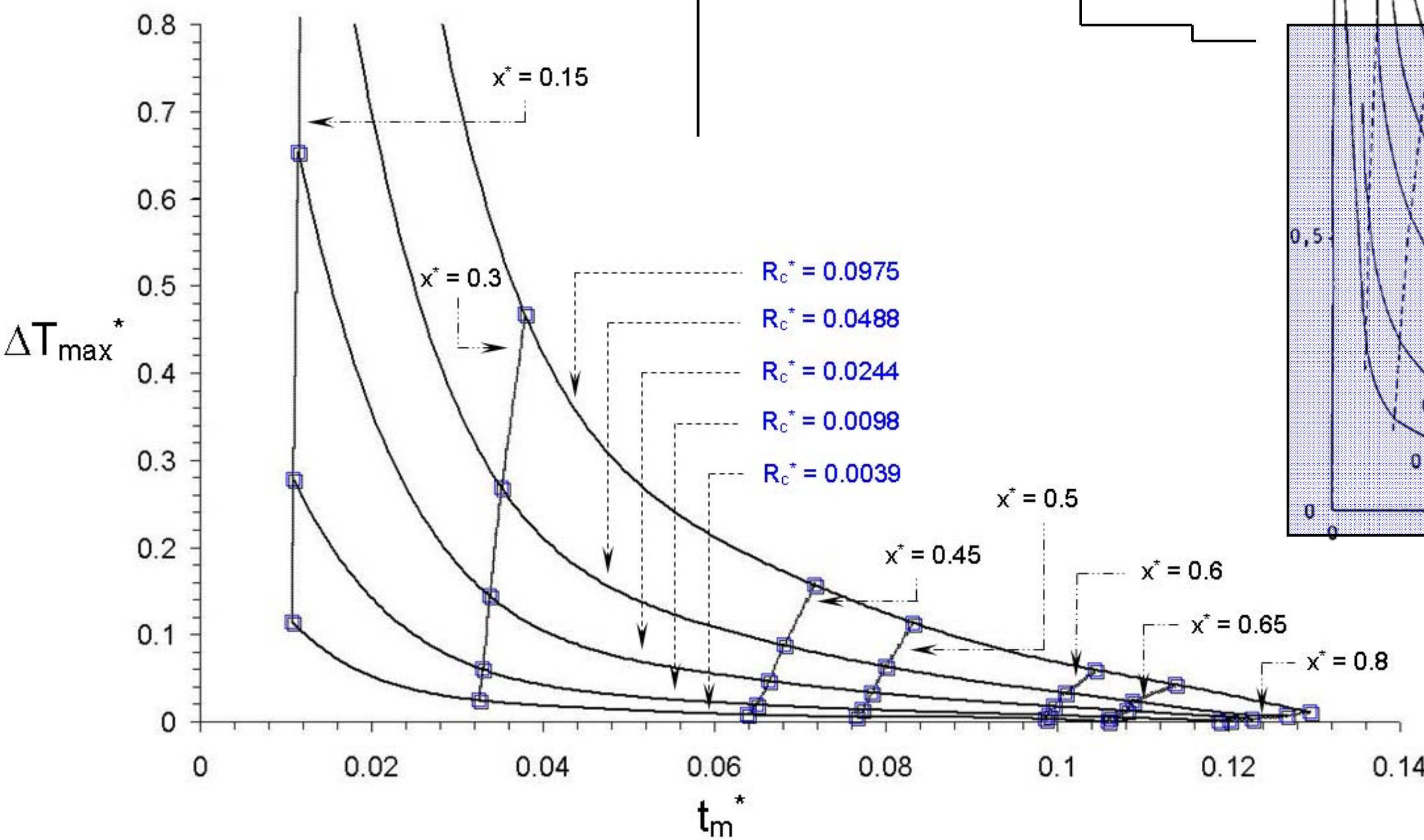

ΔT*max
x* = 0.15
x* = 0.3
Rc* = 0.0975
Rc* = 0.0488
Rc* = 0.0244
Rc* = 0.0098
Rc* = 0.0039
x* = 0.5
x* = 0.45
x* = 0.6
x* = 0.65
x* = 0.8
tm*

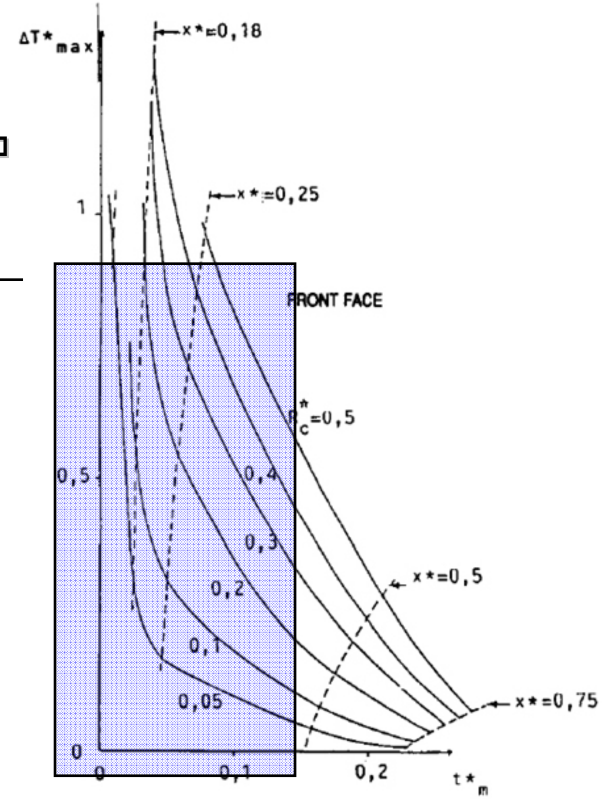

ΔT*max
x*=0,18
x*=0,25
FRONT FACE
Rc*=0,5
0,4
0,3
0,2
0,1
0,05
x*=0,5
x*=0,75
t*m

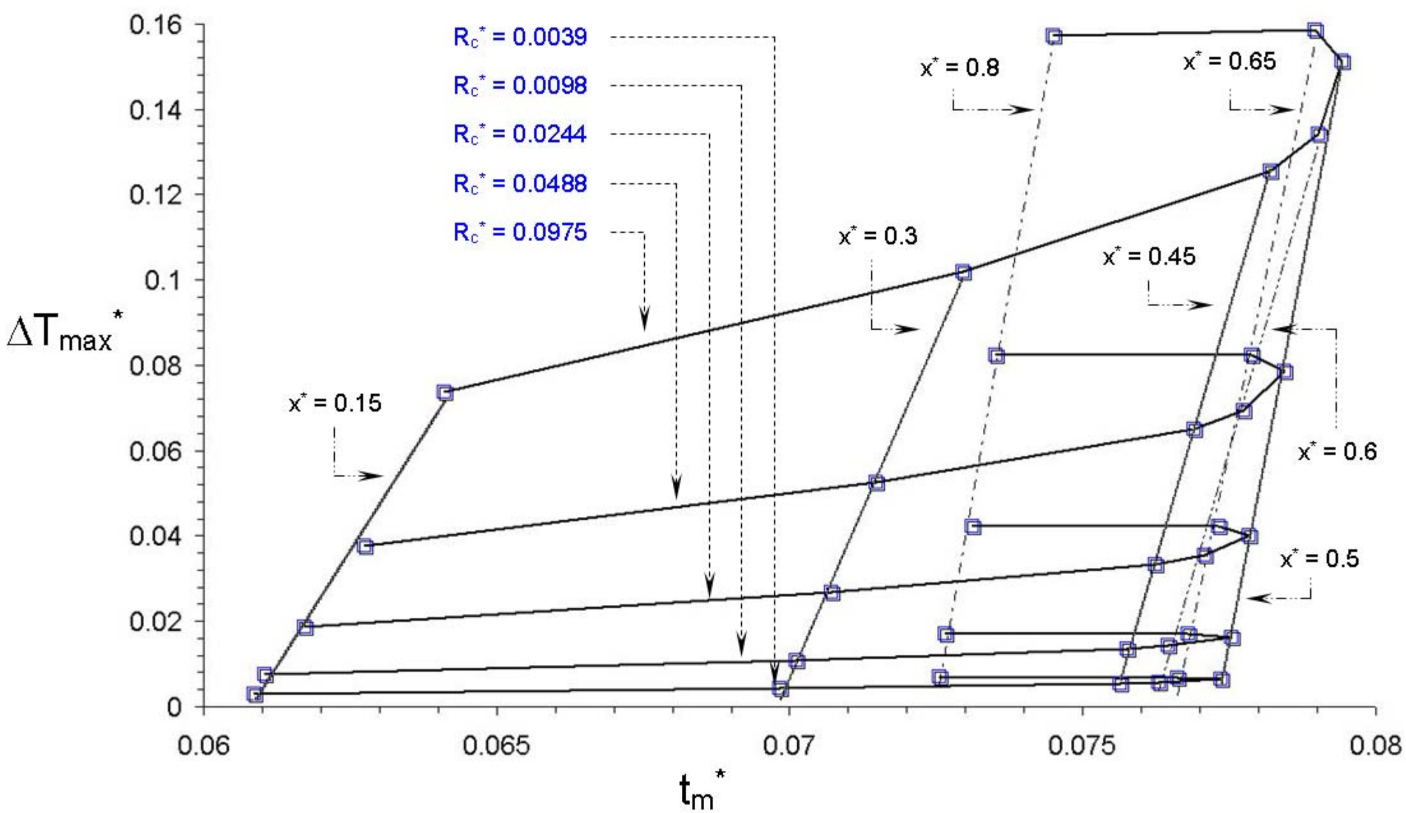
0.16
0.14
0.12
0.1
0.08
0.06
0.04
0.02
0
ΔTmax*
0.06
0.065
0.07
0.075
0.08
tm*
Rc* = 0.0039
Rc* = 0.0098
Rc* = 0.0244
Rc* = 0.0488
Rc* = 0.0975
x* = 0.15
x* = 0.3
x* = 0.8
x* = 0.65
x* = 0.45
x* = 0.6
x* = 0.5

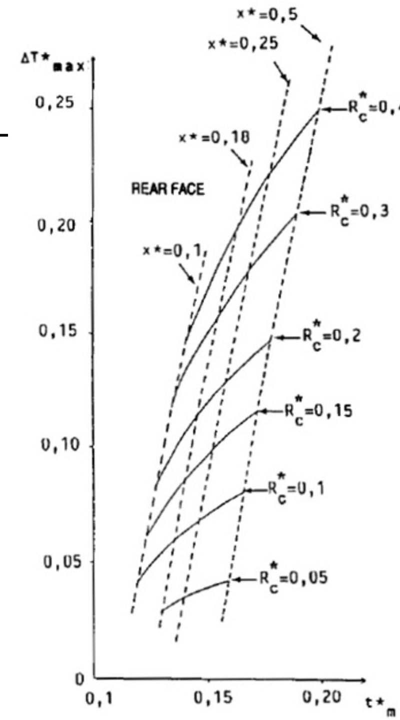
x*=0,5
x*=0,25
x*=0,18
x*=0,1
ΔT*max
0,25
0,20
0,15
0,10
0,05
0
REAR FACE
Rc*=0,4
Rc*=0,3
Rc*=0,2
Rc*=0,15
Rc*=0,1
Rc*=0,05
0,1
0,15
0,20
t*m

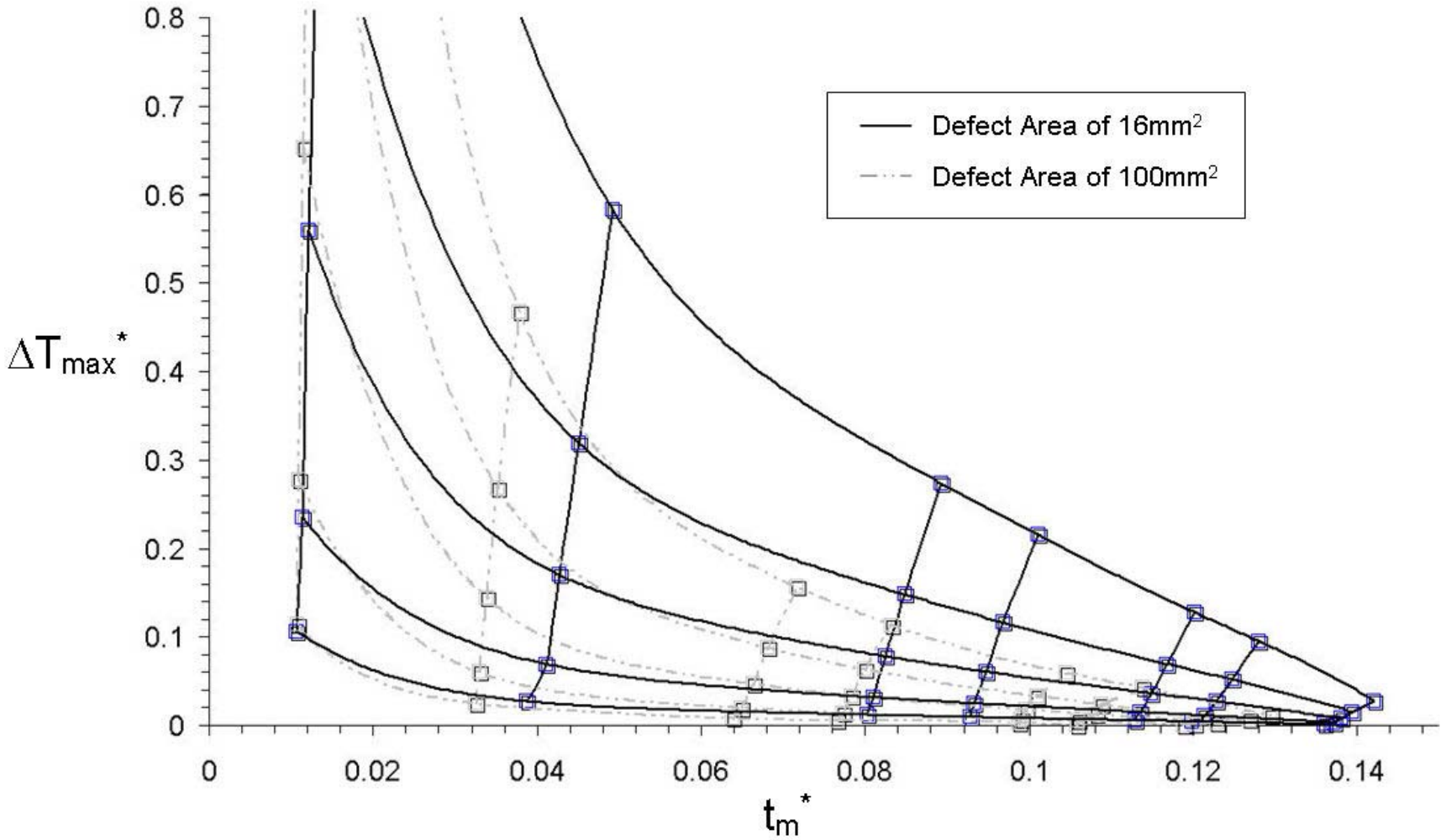
Defect Area of 16mm2
Defect Area of 100mm2
ΔTmax*
tm*
0.8
0.7
0.6
0.5
0.4
0.3
0.2
0.1
0
0.02
0.04
0.06
0.08
0.1
0.12
0.14

[illegible]

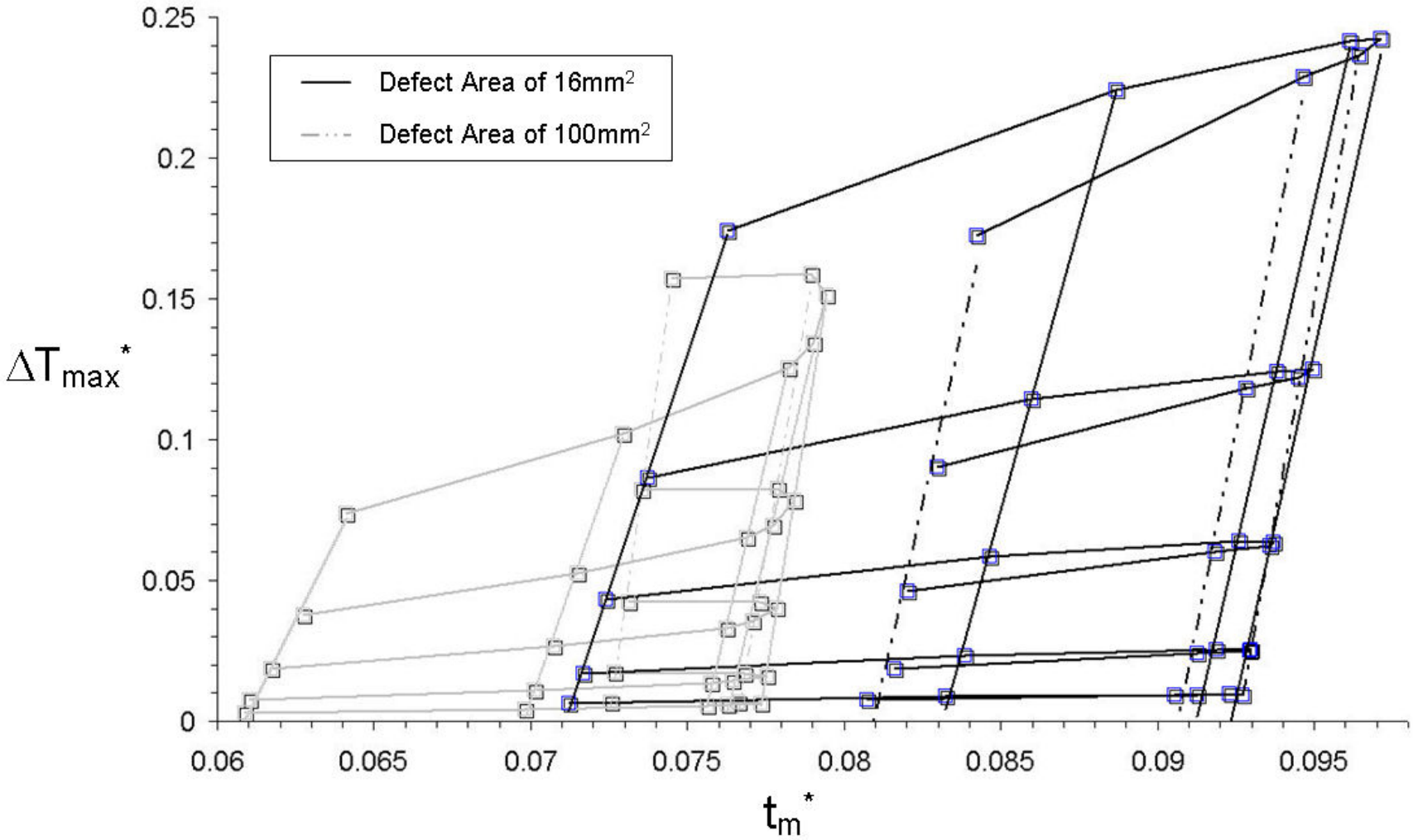
Defect Area of 16mm2
Defect Area of 100mm2
0.25
0.2
0.15
0.1
0.05
0
ΔTmax*
0.06
0.065
0.07
0.075
0.08
0.085
0.09
0.095
tm*

□ □ □ □ □ □□ □ □ □□ □ □ □ □ □ □□□ □ □ □ □ □ □

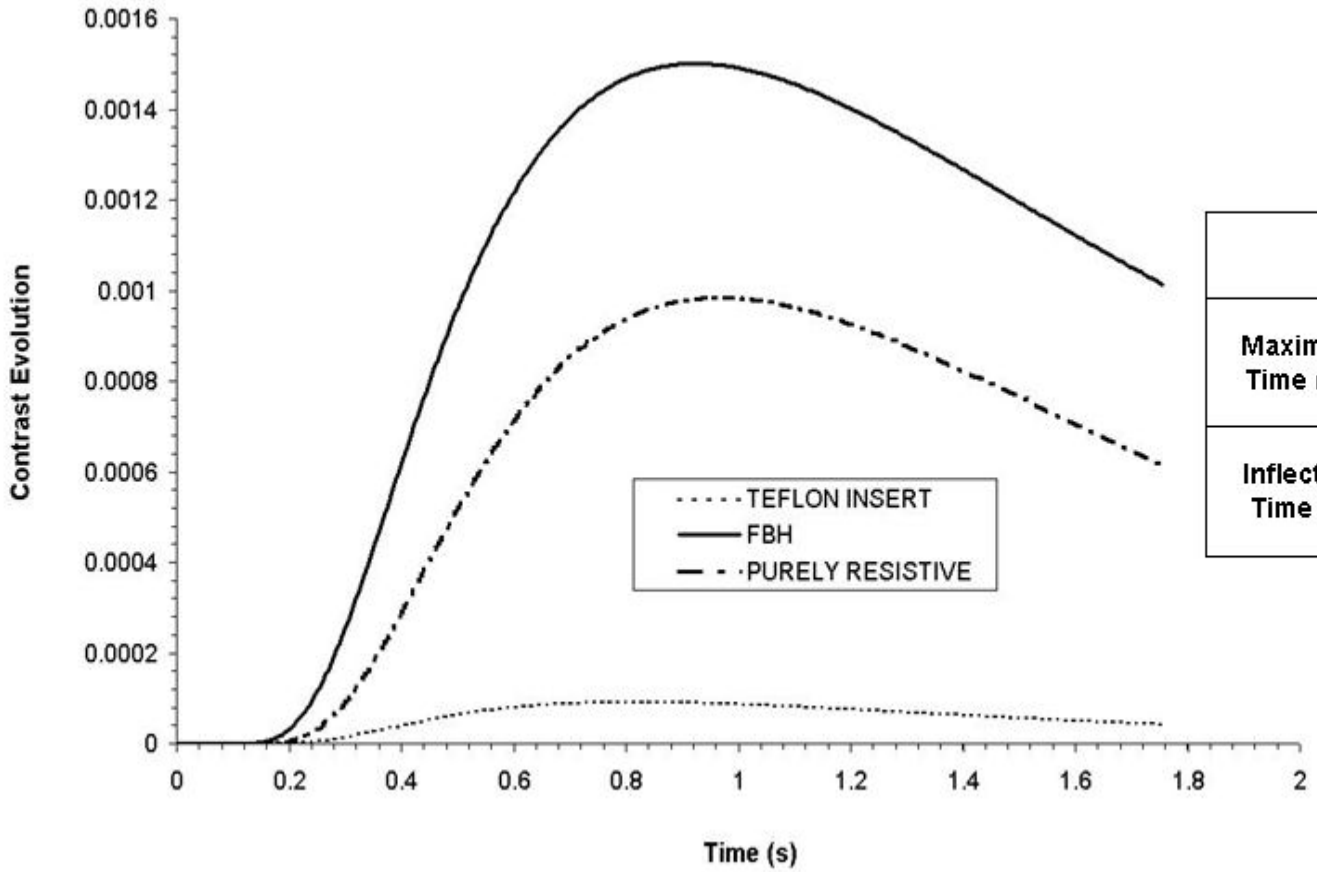

	TEF	FBH	PR
Maximum Time (t_m)	0.805	0.925	0.967
Inflection Time (t_i)	0.383	0.382	0.435

CRC-ACS

- Accurate representation of the lateral component is possible with the use of FE.
- This component cannot be ignored if prediction schemes are derived.
- The FBH assumption for delaminations is misguided.
- 2 point identification using inflection and maximum point will reduce experimental error.
- Studies into the nature of delaminations from a thermal perspective is required.

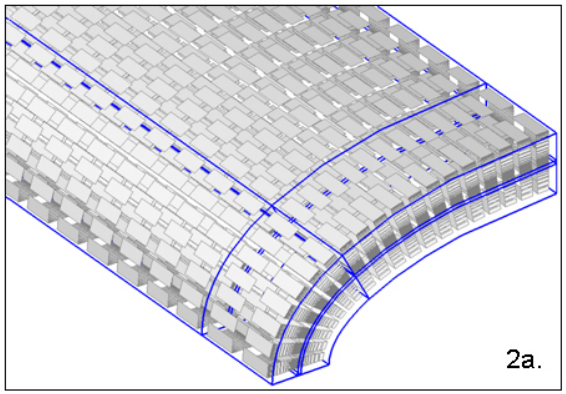
2a.

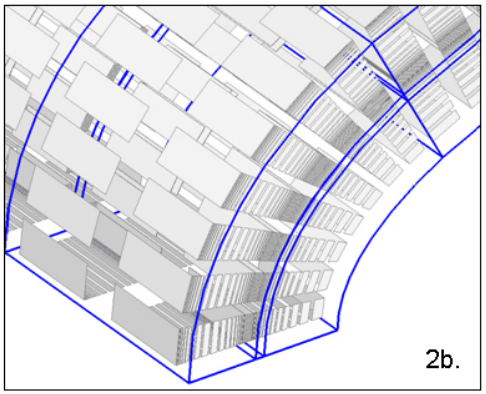
2b.

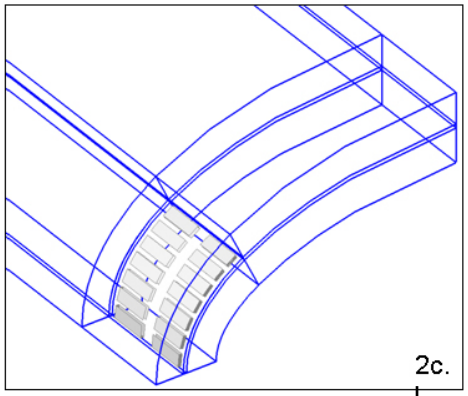
2c.

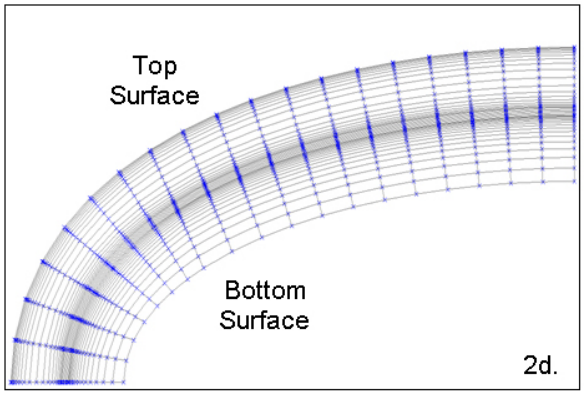
Top
Surface
Bottom
Surface
2d.

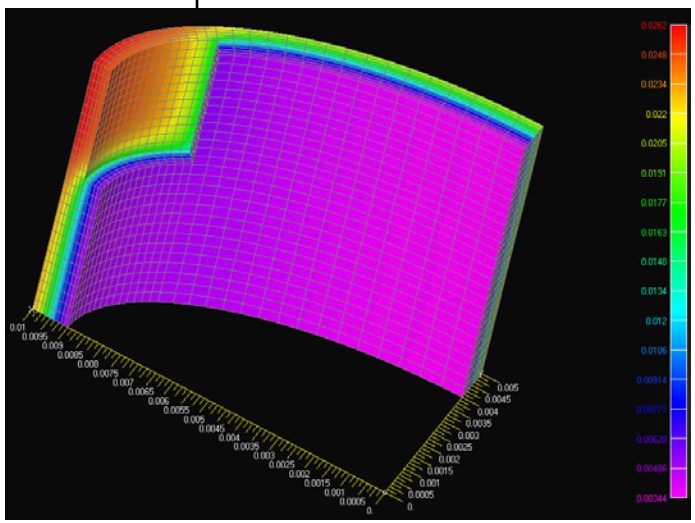

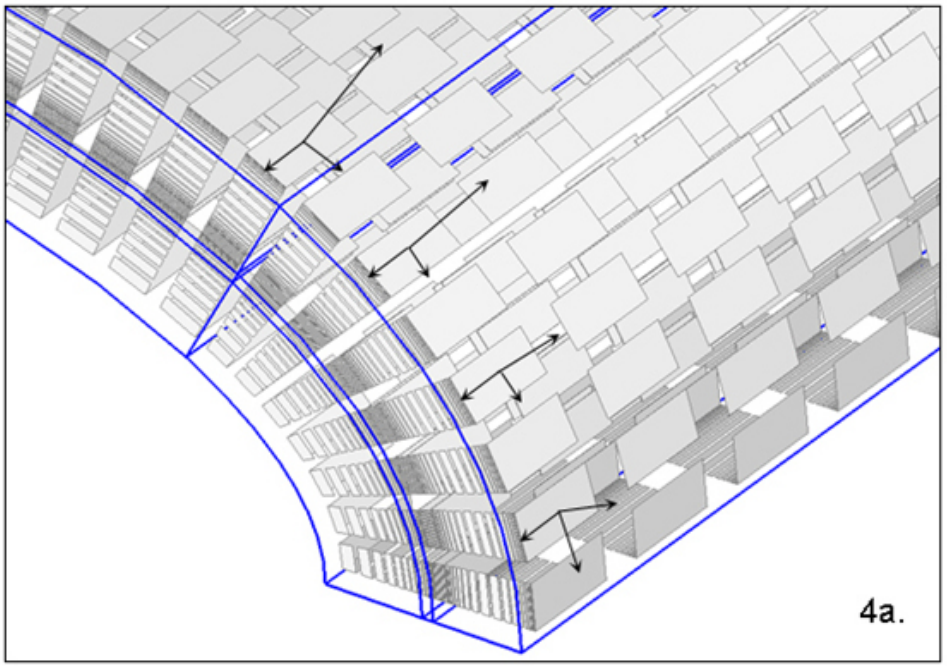
4a.

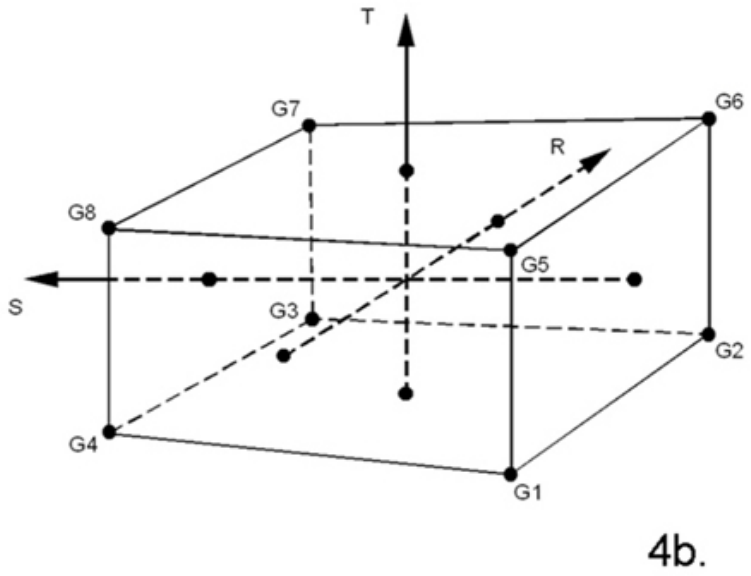
T
G7
G6
R
G8
G5
S
G3
G2
G4
G1
4b.

□ □ □ □ □ □ □ □ □ □ □ □ □ □ □ □ □

- □ □ □ □ □ □ □ □ □ □□□ □ □ □ □□□ □ □ □ □
- □ □ □ □ □□□□ □□□ □
- □ □ □□□ □□□ □□□ □ □ □□□
- □ □ □□□ □□□ □ □ □ □ □□□ □ □ □ □
- □ □ □□□□ □ □□□ □ □ □ □ □ □ □
- □ □ □□□ □□□ □ □ □ □ □□□ □ □ □ □□□ □ □ □